ISTANBUL TECHNICAL UNIVERSITY ★ GRADUATE SCHOOL

# IMPACT OF USING OBSERVED LAND-USE PROPERTIES ON THE REPRESENTATION OF HEATWAVES IN ALARO-SURFEX IN BELGIUM

M.Sc. THESIS

SAJJAD RIYADH SHINJAR ALGHEZI

Department of Geomatics Engineering

Geomatics Engineering Programme

SEPTEMBER 2025

**ISTANBUL TECHNICAL UNIVERSITY ⋆ GRADUATE SCHOOL**

# IMPACT OF USING OBSERVED LAND-USE PROPERTIES ON THE REPRESENTATION OF HEATWAVES IN ALARO-SURFEX IN BELGIUM

**M.Sc. THESIS**


**SAJJAD RIYADH SHINJAR ALGHEZI**
**(501211658)**

**Department of Geomatics Engineering**

**Geomatics Engineering Program**


**Thesis Advisor: Asst. Prof. Dr. Muhammed Oğuzhan METE**

**SEPTEMBER 2025**

ISTANBUL TEKNİK ÜNİVERSİTESİ ★ LİSANSÜSTÜ EĞİTİM ENSTİTÜSÜ

# GÖZLEMLENEN ARAZİ KULLANIM ÖZELLİKLERİNİN KULLANILMASININ BELÇİKA'DAKİ ALARO-SURFEX'TE ISI DALGALARININ TEMSİLİ ÜZERİNDEKİ ETKİSİ

**YÜKSEK LİSANS TEZİ**

**SAJJAD RIYADH SHINJAR ALGHEZI**
**(501211658)**

**Geomatik Mühendisliği Anabilim Dalı**

**Geomatik Mühendisliği Programı**

**Tez Danışmanı: Dr. Ögr. Üyesi Muhammed Oğuzhan METE**

**EYLÜL 2025**

Sajjad Riyadh Shinjar Alghezi, a M.Sc. student of ITU Graduate School student ID 501211658 successfully defended the thesis entitled “IMPACT OF USING OBSERVED LAND-USE PROPERTIES ON THE REPRESENTATION OF HEATWAVES IN ALARO-SURFEX IN BELGIUM”, which he prepared after fulfilling the requirements specified in the associated legislations, before the jury whose signatures are below.

| | | |
|---|---|---|
| **Thesis Advisor:** | **Asst. Prof. Dr. Muhammed Oğuzhan METE**<br>Istanbul Technical University | ........................... |
| **Jury Members:** | **Prof. Dr. Hande Demirel**<br>Istanbul Technical University | ............................. |
| | **Prof. Dr. Tim Van de Voorde**<br>Ghent University | .............................. |

**Date of Submission:** **10 July 2025**
**Date of Defense:** **11 September 202**

**FOREWORD**

To my beloved family who never stop believing in me to achieve all my dreams. And most especially, to ALLAH (s.w.a) who gives me the opportunity to achieve who I am and what I have today.

I would like to extend my sincere gratitude to my supervisor, Assist. Prof. Dr. Muhammed Oguzhan METE, for his invaluable support during the tough times and his guidance that made this research possible.

I am also deeply thankful to Prof. Dr. Tim Van de Voorde and Prof. Dr. Kwinten Van Weverberg for their valuable support and contributions to this research.

It must be clearly stated that it is impossible to make reference to everybody whom I got support during this research.

September 2025

Sajjad Riyadh Shinjar Alghezi
(Civil Engineer)

**TABLE OF CONTENTS**

**Page**

## ABBREVIATIONS

**ALARO** : A regional climate model used for high-resolution simulations
**SURFEX** : Surface Externalisée
**CORDEX** : Coordinated Regional Climate Downscaling Experiment
**RCM** : Regional Climate Model
**ERA5** : The fifth-generation reanalysis dataset from ECMWF
**ECMWF** : European Centre for Medium-Range Weather Forecasts
**LAI** : Leaf Area Index
**MODIS** : Moderate Resolution Imaging Spectroradiometer
**ICOS** : Integrated Carbon Observation System
**TEMP_AVG** : Average temperature simulated by the model
**TEMP_MAX** : Maximum temperature simulated by the model
**TEMP_MIN** : Minimum temperature simulated by the model
**MAE** : Mean Absolute Error
**MAB** : Mean Absolute Bias
**SW_absorbed**: Absorbed shortwave radiation at the surface
**SHF** : Sensible Heat Flux
**LHF** : Latent Heat Flux
**NR** : Net Radiation
**SRD** : Shortwave Radiation Downward
**SM_1** : Soil moisture at 1 cm depth
**SM_3** : Degree of saturation
**GEE** : Google Earth Engine
**NDVI** : Normalized Difference Vegetation Index
**SST** : Sea Surface Temperature
**ALADIN** : Aire Limitee Adaptation Dynamique d ´ eveloppement INterna-tional
**C** : Degree Celsius
**m2** : Square metre
**w** : Watts

**LIST OF TABLES**

**Page**

## LIST OF FIGURES

**Page**

**IMPACT OF USING OBSERVED LAND-USE PROPERTIES ON THE REPRESENTATION OF HEATWAVES IN ALARO-SURFEX IN BELGIUM**

**SUMMARY**


Accurate simulation of the thermal characteristics of heatwaves forms the basis of climate adaptation and risk management, particularly because heat extremes are increasing under global warming. This thesis analyzes the impact of refreshing land-use property values—more specifically Leaf Area Index (LAI), albedo, and surface roughness—on the performance of the ALARO-Surfex regional climate model in simulating heatwaves over Belgium for the summers of 2018 and 2019. Two versions of the model were compared: a reference setup using default Ecoclimap-I inputs and an updated setup using observationally based, spatially distributed parameters obtained from MODIS remote sensing data products.

The analysis used both model output and gridded observational climate data regridded onto a 5 km common resolution. Surface energy fluxes and temperature variables (Average temperature, Maximum temperature, Minimum temperature) of main interest were evaluated using Mean Absolute Error (MAE) and Mean Absolute Bias (MAB) over the entire domain and within dominant cropland classes (Ecoclimap-I land covers 166 and 182). Results showed that the updated model improved the simulation of mean and minimum temperature, particularly for the 2018 heatwave, by reducing MAB by up to 1.44 °C for Minimum temperature over cropland surfaces. These improvements are crucial for accurately representing nighttime cooling processes, which play a vital role in mitigating heat stress during extreme heat events.

However, the updated model exhibited challenges in simulating maximum temperatures, with MAB increasing by more than 1 °C in both years. Surface energy balance analysis revealed that reductions in albedo and LAI led to increased net radiation and sensible heat fluxes, enhancing daytime heating. At the same time, reduced latent heat fluxes limited evaporative cooling, contributing to the overestimation of maximum temperatures. Evaluation against surface energy balance measurements from eddy covariance data within the domain further supported these findings: the novel model improved Minimum temperature simulation but degraded Maximum temperature performance significantly.

These results highlight the complex trade-offs introduced by newer land surface characteristics and the importance of land-atmosphere interactions for regional heatwave simulations. The study concludes that while the incorporation of observational land-use updates enhances model realism and improves the simulation of certain temperature components, further improvements, perhaps through land-cover-specific parameterizations, are required to introduce a more balanced energy flux representation and avoid unintentional biases in extreme temperature simulations. This research contributes to the ongoing refinement of regional climate modeling approaches and identifies the need for improved model accuracy to enhance confidence in climate projections. By improving the accuracy of heatwave simulations,

this study supports disaster risk reduction efforts and informs climate adaptation strategies, such as urban planning, agricultural optimization, and early warning systems. Ultimately, the findings emphasize the need for continued advancements in regional climate modeling to better anticipate and mitigate the impacts of future heatwave events.

The findings of this study have significant implications for climate adaptation policy and disaster risk management, particularly in nations like Belgium, which are increasingly exposed to heatwaves due to climate change. Heatwaves are a multi-dimensional threat that impacts human health, agricultural production, energy systems, and urban infrastructure. Realistic modeling of heatwave behavior, as demonstrated in the current study, is thus essential to develop early warning systems and targeted interventions to mitigate related risks. For instance, the advanced simulation of nighttime thermal cooling processes (minimums) can be applied to inform public health policy, e.g., to ascertain locales where vulnerable populations may be placed at higher risk under prolonged heat episodes. Similarly, the traded-off simulations of daytime highs suggest the need for further parameterized improvements in an effort to better simulate daytime heating trends, which are critical to urban planning strategy aimed at reducing exposure to extreme heat. Urban heat island effect, wherein cities, particularly, are subject to the exaggeration of temperature extremes in urban cities, is minimized by incorporating observationally derived land-use data into regional climate models. Urban planners are then able to design heat-resilient cities through augmenting vegetation cover, applying reflective surfaces, and optimizing water consumption. These measures not only enhance urban heatwave resilience but also contribute to wider sustainability goals such as reducing carbon emissions and conserving water resources. Furthermore, the study emphasizes the importance of integrating climate science with disaster risk reduction programs like the Sendai Framework for Disaster Risk Reduction (2015–2030), which emphasizes upgraded risk analysis, early warning, and interventions in community resilience development. By bridging the gap between technological innovation and real-world applications, this research opens doors to stronger societies and ecosystems when it comes to increasing climate challenges.

Although this study demonstrates potential from employing satellite-derived land-use properties, further research needs to be done to enhance the accuracy of the model. Significant areas consist of parameterizing land cover to adjust biases in the simulation of maximum temperature and timescales and climatic zones. Incorporating regional climate models with hydrological and socioeconomic models would also be a more complete method of appreciating heatwave impacts. Besides, mitigating uncertainties with sensitivity analyses and ensemble modeling is still crucial. These tasks can capitalize on this thesis for enhancing the representation of heatwaves in climate models and facilitating evidence-based decision-making for a sustainable future.

Beyond the Belgian case study, the methodological insights from this thesis hold broader relevance for regions facing recurrent or intensifying heatwaves. By demonstrating how satellite-derived land-use properties can improve regional climate model performance, this research provides a transferable framework that can be applied in other European contexts and globally. Integrating high-resolution land surface data into climate modeling not only enhances hazard assessment but also strengthens the foundation for transboundary adaptation initiatives, such as those coordinated under the European Green Deal and international disaster risk frameworks. Thus, the outcomes of this study extend beyond academic advancement to inform practical strategies for climate resilience, aligning scientific innovation with urgent policy needs in an era of accelerating climate extremes.

# GÖZLEMLENEN ARAZİ KULLANIM ÖZELLİKLERİNİN KULLANILMASININ BELÇİKA'DAKİ ALARO-SURFEX'TE ISI DALGALARININ TEMSİLİ ÜZERİNDEKİ ETKİSİ

## ÖZET

Sıcak dalgalarının termal özelliklerinin doğru simülasyonu, özellikle küresel ısınma nedeniyle aşırı sıcaklıkların artması nedeniyle, iklim adaptasyonu ve risk yönetiminin temelini oluşturmaktadır. Bu tez, arazi kullanım özelliklerinin değerlerinin (daha spesifik olarak Yaprak Alan İndeksi (LAI), albedo ve yüzey pürüzlülüğü) 2018 ve 2019 yazlarında Belçika üzerinde sıcak dalgalarını simüle eden ALARO-Surfex bölgesel iklim modelinin performansı üzerindeki etkisini analiz etmektedir. Modelin iki versiyonu karşılaştırılmıştır: varsayılan Ecoclimap-I girdilerini kullanan bir referans kurulum ve MODIS uzaktan algılama veri ürünlerinden elde edilen, gözlem tabanlı, uzamsal olarak dağılımlı parametreleri kullanan güncellenmiş bir kurulum.

Analizde, hem model çıktısı hem de 5 km ortak çözünürlüğe yeniden ızgaralanmış ızgaralı gözlem iklim verileri kullanılmıştır. Ana ilgi konusu olan yüzey enerji akışları ve sıcaklık değişkenleri (ortalama sıcaklık, maksimum sıcaklık, minimum sıcaklık), tüm alan ve baskın tarım arazisi sınıfları (Ecoclimap-I arazi örtüsü 166 ve 182) üzerinde Ortalama Mutlak Hata (MAE) ve Ortalama Mutlak Sapma (MAB) kullanılarak değerlendirildi. Sonuçlar, güncellenen modelin, özellikle 2018 sıcak dalgası için, tarım arazileri üzerindeki minimum sıcaklık için MAB'yi 1,44 °C'ye kadar azaltarak ortalama ve minimum sıcaklık simülasyonunu iyileştirdiğini göstermiştir. Bu iyileştirmeler, aşırı sıcak olaylar sırasında ısı stresini hafifletmede hayati bir rol oynayan gece soğuma süreçlerini doğru bir şekilde temsil etmek için çok önemlidir.

Ancak, güncellenen model, her iki yılda da MAB'nin 1 °C'den fazla artmasıyla maksimum sıcaklıkların simülasyonunda zorluklar sergiledi. Yüzey enerji dengesi analizi, albedo ve LAI'deki azalmaların net radyasyon ve hissedilebilir ısı akışlarının artmasına yol açarak gündüz ısınmasını artırdığını ortaya koydu. Aynı zamanda, azalan gizli ısı akışları buharlaşmalı soğutmayı sınırlayarak maksimum sıcaklıkların fazla tahmin edilmesine katkıda bulundu. Alan içindeki girdap kovaryans verilerinden elde edilen yüzey enerji dengesi ölçümlerine göre yapılan değerlendirme, bu bulguları daha da destekledi: yeni model, minimum sıcaklık simülasyonunu iyileştirdi, ancak maksimum sıcaklık performansını önemli ölçüde düşürdü.

Bu sonuçlar, yeni kara yüzeyi özelliklerinin getirdiği karmaşık ödünleşimleri ve bölgesel sıcak dalgası simülasyonları için kara-atmosfer etkileşimlerinin önemini vurgulamaktadır. Çalışma, gözlemsel arazi kullanımı güncellemelerinin dahil edilmesinin model gerçekçiliğini artırdığı ve belirli sıcaklık bileşenlerinin simülasyonunu iyileştirdiği, ancak daha dengeli bir enerji akışı temsili sunmak ve aşırı sıcaklık simülasyonlarında istenmeyen önyargıları önlemek için, belki de arazi örtüsüne özgü parametrelemeler yoluyla daha fazla iyileştirme yapılması gerektiği sonucuna varmıştır. Bu araştırma, bölgesel iklim modelleme yaklaşımlarının sürekli iyileştirilmesine katkıda bulunmakta ve iklim tahminlerine olan güveni artırmak için model doğruluğunun iyileştirilmesi gerektiğini ortaya koymaktadır. Sıcak dalgası simülasyonlarının doğruluğunu artırarak, bu çalışma afet riskini azaltma çabalarını desteklemekte ve kentsel planlama, tarımsal optimizasyon ve erken uyarı sistemleri

gibi iklim adaptasyon stratejilerine bilgi sağlamaktadır. Sonuç olarak, bulgular gelecekteki sıcak dalgası olaylarının etkilerini daha iyi tahmin etmek ve hafifletmek için bölgesel iklim modellemesinde sürekli ilerlemelerin gerekliliğini vurgulamaktadır.

Bu çalışmanın bulguları, özellikle iklim değişikliği nedeniyle sıcak dalgalarına giderek daha fazla maruz kalan Belçika gibi ülkelerde, iklim adaptasyon politikası ve afet risk yönetimi için önemli sonuçlar doğurmaktadır. Sıcak dalgaları, insan sağlığını, tarımsal üretimi, enerji sistemlerini ve kentsel altyapıyı etkileyen çok boyutlu bir tehdittir. Dolayısıyla, mevcut çalışmada gösterildiği gibi, sıcak dalgalarının davranışının gerçekçi bir şekilde modellenmesi, ilgili riskleri azaltmak için erken uyarı sistemleri ve hedefli müdahaleler geliştirmek açısından çok önemlidir. Örneğin, gece termal soğuma süreçlerinin (minimumlar) gelişmiş simülasyonu, halk sağlığı politikasına bilgi sağlamak için kullanılabilir, örneğin, uzun süreli sıcaklık dalgaları sırasında savunmasız nüfusların daha yüksek risk altında olabileceği yerleri belirlemek için. Benzer şekilde, gündüz yüksek sıcaklıklarının simülasyonları, aşırı sıcağa maruz kalmayı azaltmayı amaçlayan kentsel planlama stratejisi için kritik öneme sahip gündüz ısınma eğilimlerini daha iyi simüle etmek için parametrelerin daha da iyileştirilmesi gerektiğini göstermektedir. Özellikle şehirlerin aşırı sıcaklıkların etkisine maruz kaldığı kentsel ısı adası etkisi, gözlemlerden elde edilen arazi kullanım verilerinin bölgesel iklim modellerine dahil edilmesiyle en aza indirgenir. Böylece şehir planlamacıları, bitki örtüsünü artırarak, yansıtıcı yüzeyler uygulayarak ve su tüketimini optimize ederek ısıya dayanıklı şehirler tasarlayabilirler. Bu önlemler, kentsel sıcak dalgalarına karşı dayanıklılığı artırmakla kalmaz, aynı zamanda karbon emisyonlarının azaltılması ve su kaynaklarının korunması gibi daha geniş sürdürülebilirlik hedeflerine de katkıda bulunur. Ayrıca, çalışma, iklim biliminin, risk analizinin iyileştirilmesi, erken uyarı ve topluluk direncinin geliştirilmesine yönelik müdahaleleri vurgulayan Sendai Afet Riskini Azaltma Çerçevesi (2015-2030) gibi afet riskini azaltma programlarıyla entegre edilmesinin önemini vurgulamaktadır. Teknolojik yenilikler ile gerçek dünya uygulamaları arasındaki boşluğu dolduran bu araştırma, artan iklim sorunları karşısında daha güçlü toplumlar ve ekosistemler için yeni kapılar açmaktadır.

Bu çalışma, uydu verilerinden elde edilen arazi kullanım özelliklerinin kullanımının potansiyelini gösterse de, modelin doğruluğunu artırmak için daha fazla araştırma yapılması gerekmektedir. Önemli alanlar, maksimum sıcaklık ve zaman ölçekleri ile iklim bölgelerinin simülasyonundaki sapmaları düzeltmek için arazi örtüsünün parametrelendirilmesinden oluşmaktadır. Bölgesel iklim modellerini hidrolojik ve sosyoekonomik modellerle birleştirmek de sıcak dalgalarının etkilerini değerlendirmek için daha eksiksiz bir yöntem olacaktır. Ayrıca, duyarlılık analizleri ve topluluk modellemesi ile belirsizlikleri azaltmak hala çok önemlidir. Bu görevler, iklim modellerinde sıcak dalgalarının temsilini geliştirmek ve sürdürülebilir bir gelecek için kanıta dayalı karar vermeyi kolaylaştırmak için bu tezden yararlanabilir.

Belçika vaka çalışmasının ötesinde, bu tezden elde edilen metodolojik bilgiler, tekrarlayan veya yoğunlaşan sıcak dalgalarıyla karşı karşıya olan bölgeler için daha geniş bir öneme sahiptir. Uydu verilerinden elde edilen arazi kullanım özelliklerinin bölgesel iklim modeli performansını nasıl iyileştirebileceğini gösteren bu araştırma, diğer Avrupa bağlamlarında ve küresel olarak uygulanabilecek aktarılabilir bir çerçeve sunmaktadır. Yüksek çözünürlüklü arazi yüzeyi verilerinin iklim modellemesine entegre edilmesi, sadece tehlike değerlendirmesini iyileştirmekle kalmaz, aynı zamanda Avrupa Yeşil Anlaşması ve uluslararası afet riski çerçeveleri kapsamında koordine edilenler gibi sınır ötesi uyum girişimlerinin temelini de güçlendirir. Bu nedenle, bu çalışmanın sonuçları akademik ilerlemenin ötesine geçerek, iklim direncine yönelik pratik stratejilere bilgi sağlar ve iklim aşırılıklarının hızlandığı bir dönemde bilimsel yenilikleri acil politika ihtiyaçlarıyla uyumlu hale getirir.

# 1. INTRODUCTION

## 1.1 Background and Motivation

Heatwaves are among the most intense climate hazards to impact Europe, with extensive effects on public health, agriculture, energy use, and infrastructure. The past decades have witnessed the rising frequency, persistence, and intensity of anthropogenic climatic change-induced heatwaves (Giorgi & Gutowski, 2015; IPCC, 2021). These heatwaves are increasingly menacing densely populated cities and densely productive farming regions like Belgium, worsening pre-existing water resource, crop yield, and human health vulnerabilities (Caluwaerts et al., 2020). It is therefore essential to understand and well model heatwave behavior in order to inform adaptation, enhance climate resilience, and facilitate evidence-based policy-making.

From a disaster management perspective, heatwaves represent a significant natural hazard with cascading impacts on ecosystems, economies, and societies. The Sendai Framework for Disaster Risk Reduction (2015–2030) emphasizes the importance of understanding and addressing risks posed by climate-related disasters, including heatwaves, through improved risk assessments, early warning systems, and community resilience-building measures (UNDRR, 2015). Accurate simulations of heatwaves play a pivotal role in this context, as they enable stakeholders to develop targeted strategies for prevention, preparedness, response, and recovery. For instance, high-resolution temperature projections can support urban planning decisions, such as increasing vegetation cover or implementing cool roofs, to mitigate urban heat island effects and reduce exposure to extreme heat (Oleson et al., 2015).

Regional Climate Models (RCMs) such as ALARO in conjunction with

SURFEX land surface scheme are capable of downscaling global climate data to higher resolution suitable for local scale analysis (Berckmans et al., 2017; Giot et al., 2014). Simulation of heatwaves by RCMs relies, however, on their description of land surface processes. A group of most important parameters such as albedo, Leaf Area Index (LAI), and surface roughness control the energy, water, and momentum exchanges between the Earth's surface and atmosphere. These variables directly influence the surface energy budget, which in turn modulates near-surface temperatures during extreme heat events (Seneviratne et al., 2010; Napoly et al., 2017).

Despite their importance, most RCMs use static or climatological land surface conditions that do not properly account for interannual or seasonal variability of land cover and vegetation. These might create significant climate simulation biases, especially for heatwaves during those instances of maximal land-atmosphere interactions (Berckmans et al., 2017; Giot et al., 2014). To address this gap, recent advancements have explored the integration of satellite-derived observations—such as those from the MODIS platform—to update model input parameters (Didan, 2015; Myneni et al., 2015; Schaaf & Wang, 2015). By combining measured LAI, albedo, and roughness values, models can realistically simulate the dynamic characteristic of land surface properties and reduce temperature-simulation uncertainty (Berckmans, 2018; Cui et al., 2023).

Incorporating observed land-use properties into regional climate models not only enhances the accuracy of heatwave simulations but also supports disaster management efforts by providing actionable insights for policymakers and practitioners. For example, improved simulations can inform agricultural adaptation strategies, such as optimizing irrigation practices and adjusting planting cycles, to mitigate the impacts of heatwaves on crop yields (Lobell et al., 2014). Similarly, urban planners can use these findings to design heat-resilient cities by prioritizing green infrastructure and reflective surfaces. By bridging the gap between technical modeling advancements and real-world applications, this study contributes to building more resilient societies and ecosystems in the face of escalating climate risks.

## 1.2 Research Problem and Thesis Context

The fundamental challenge in regional climate modeling is the inadequate representation of extreme temperature conditions, especially during heat waves—due to outdated or overly simplified surface parameterizations (Christensen et al., 2007; Kotlarski et al., 2014). Traditional model settings are often based on coarse or outdated land surface parameterizations that fail to reflect the high-resolution temporal and spatial variation of vegetation and surface characteristics. This may lead to extreme simulated temperature errors, undermining climate forecast accuracy and hampering effective decision-making.

This thesis analyzes the impact of land surface parameter updates on ALARO-Surfex regional climate model performance in simulating heatwave dynamics across Belgium in July 2018 and July 2019. The study region comprises Belgium and the surrounding areas, with a concentrated focus on cropland regions, which are ubiquitous in the terrain and exhibit distinct thermal responses to alterations in surface characteristics.

This study addresses the problem of inadequate heatwave representation by examining whether the addition of observed, time-varying land-use properties—such as LAI, albedo, and roughness—can enhance the simulation of heatwave events in Belgium. The primary objective of this study is to ascertain whether the updating of land-use properties improves the model's ability to simulate heatwave conditions for different land cover classes. Specifically, we examine how such updates impact temperature biases (Average temperature, Maximum temperature, Minimum temperature) during two critical heatwave seasons, July 2018 and July 2019, and evaluate land cover-specific responses, specifically agricultural croplands.

The new parameters were derived from satellite data (MODIS) and were used to overwrite the default land surface properties in the model. We conducted several experiments with the ALARO-Surfex model driven by

ERA5 reanalysis data, which provides high-resolution initial and lateral boundary conditions (Hersbach et al., 2020). A comparison was made with gridded observation-based climate datasets to measure the performance of the baseline (default) and updated model settings, allowing an overall evaluation of the improvements within the models. Independent verification has also been made with high-resolution ground-based weather observations from ICOS station at Lonzée. This approach allows a detailed assessment of how observed land surface characteristics affect temperature simulations during extreme heat events, providing insights into model sensitivity to surface energy balance processes.

## 1.3 Objectives

This study investigates the impact of incorporating satellite-derived land-use features into the ALARO-Surfex model on heatwave simulation over Belgium. The research objectives are to:

1) Enhance the reliability of regional climate models for disaster management and adaptation strategies.
2) Evaluate the effect of updating Leaf Area Index (LAI), albedo, and roughness with satellite-derived information on temperature biases in the ALARO-Surfex model.
3) Evaluate the influence of these revisions of land-use on average, maximum, and minimum temperature simulation across heatwave conditions.
4) To examine the spatial patterns of temperature biases over prevailing land cover categories, particularly agricultural cropland (Ecoclimap-I classes 166 and 182).
5) Explain how differences in land surface parameters affect surface energy fluxes and soil moisture processes.

## 1.4 Importance of Study

This study contributes to the enhanced understanding of dynamic surface properties and their influence on the performance of regional climate models by simulating intense heatwaves. Through the comparison of model behavior for various years with contrasting heatwave intensity (2018 and 2019) and the attribution of effects to land cover, the study addresses the substantial uncertainties involved in heatwave simulation. The findings are of more direct relevance for improving simulation of land-atmosphere exchange in climate models to make more precise predictions of the impacts of heatwaves on cities, agriculture, and public health.

Accurate simulation of heatwave behavior is not only crucial to Belgium but also of global interest, particularly to densely populated urban areas and intensely agricultural regions. By reducing the biases of land-use features, this research aids in laying the groundwork for improved climate resilience and policy-making choice in city expansion, water planning, and environmentally friendly agriculture. Furthermore, these advancements support disaster management frameworks by enhancing the reliability of early warning systems, risk assessments, and adaptation strategies tailored to heatwave vulnerabilities.

Lastly, the research lingers on the demand for observational data use of top quality to promote regional climate forecasting precision within schemes in climate models. While accurate heatwave simulations are crucial for scientific understanding, their integration into disaster management frameworks is equally important for mitigating risks and enhancing resilience. The following chapter explores heatwaves as a climate-related disaster and discusses their implications for disaster risk reduction and climate adaptation strategies

### 1.5 Structure of The Thesis

The remaining parts of this thesis follow the pattern as below:

Chapter 2 – Disaster Management and Heatwaves : Provides a conceptual framework for disaster management and positions heatwaves as a climate-related disaster, highlighting the role of climate models in preparedness.

Chapter 3 – Literature Review: Provides an inclusive review of relevant literature of regional climate modeling, land surface depiction, and how land surface renewal influences regional climate simulations.

Chapter 4 – Methodology: Describes study area, sources of data, model configuration, preprocessing techniques, and analytic methodology used.

Chapter 5 – Results: Displays the model performance, spatial and temporal bias diagnostics, energy balance diagnostics, and correlation studies.

Chapter 6 – Discussion: Describes the results in terms of model sensitivity and land surface feedback.

Chapter 7 – Conclusion and Future Work: Summarizes findings and suggests recommendations for future improvements in regional climate modeling

# 2. DISASTER MANAGEMENT AND HEATWAVES

## 2.1 Introduction to Disaster Management

Disaster management consists of a procedure of managing the risks of natural and man-made hazards. It is typically divided into four stages: prevention, preparedness, response, and recovery (UNDRR, 2015). Prevention involves measures to reduce or terminate the causes of disasters, whereas preparedness deals with planning and capacity development to prevent their effects. Response is the immediate response in and following a disaster to save lives and reduce suffering, and recovery is the reconstruction of infrastructure, livelihoods, and communities to pre-disaster levels or better.

Heatwaves are being increasingly recognized as a significant natural hazard, affecting human health, agriculture, infrastructure, and energy production (Caluwaerts et al., 2020; IPCC, 2021). Heatwave duration, intensity, and frequency have grown exponentially due to anthropogenic climate change and are therefore a significant issue for disaster management policy (Giorgi & Gutowski, 2015). Accurate prediction of heat event occurrences is essential in providing early warning systems, emergency planning, and resource management. For instance, simulations of high-resolution heatwaves can be employed to inform public health intervention, including setting cooling centers within urban areas, and farming practices to avoid crop damage.

The use of future-generation regional climate models, such as ALARO-Surfex, in disaster risk management has the potential to increase greenhouse gas emissions-driven heatwave projection accuracy. The models allow for high-spatial and temporal resolution examination of hot-weather extremes, which empowers actors with the respective information to tailor adaptation and mitigation actions (Seneviratne et al., 2010). With the enhancement of land-use parameterization, such as Leaf Area Index (LAI) and albedo, these models become better equipped to accurately represent the intricate interdependencies between land surface properties and atmospheric processes and hence become more valuable tools for disaster planning.

### 2.2 Heatwaves as a Climate-Related Disaster

Heatwaves are not merely extreme weather events but also disasters with cascading effects that threaten ecosystems, economies, and societies. They are characterized by prolonged spells of unusually high temperatures, typically with high humidity, which enhance their impact (Perkins-Kirkpatrick & Lewis, 2020). The impacts of heatwaves are diverse and range from high mortality rates, particularly among vulnerable populations such as the elderly and people with underlying medical conditions (WHO, 2023). In addition, heatwaves are enormous agricultural threats in the guise of reducing crop yields, stressing livestock, and depleting water supplies (Lobell et al., 2011). Heatwaves also lead to a rise in energy consumption from enhanced air-conditioning usage, which consequently puts additional pressures on power grids and potential blackouts (Davis & Gertler, 2015).

At the international level, frameworks such as the Sendai Framework for Disaster Risk Reduction (2015–2030) demand a more effective understanding and addressing of climate-related disaster risks, including heatwaves (UNDRR, 2015). The framework refers to the needs for improved risk analysis, early warning systems, and community resilience building. At the regional level, initiatives such as the European Climate Adaptation Platform (Climate-ADAPT) work to enhance preparedness for heatwaves through the provision of toolkits and policy guidance to policymakers and practitioners (EEA, 2021). Despite these efforts, significant gaps remain in our ability to anticipate and mitigate the effects of heatwaves, particularly at the local scales at which their effects are most keenly felt.

It is essential to comprehend the dynamics of heatwaves to mitigate risks and enhance resilience. For example, densely populated cities and productive agricultural areas, such as those in Belgium, are particularly vulnerable to heatwaves due to underlying problems with water availability, crop yields, and human health (Caluwaerts et al., 2020). By integrating high-resolution climate modeling into disaster management systems, decision-makers are able to prepare for and respond to the cascading effects of heatwaves, thus reducing their social and economic fallout.

### 2.3 Role of Regional Climate Models in Disaster Management

Regional climate models (RCMs), such as ALARO-Surfex, play a significant role in disaster management by providing high-resolution simulations of heatwaves and other extreme weather events. As opposed to global climate models, which employ coarse resolutions, RCMs can simulate fine-scale processes, as well as local variations in temperature, precipitation, and other meteorological variables (Giorgi & Gutowski, 2015). This capability is particularly valuable in assessing heatwave risk in specific places, such as Belgium, where site-specific features such as land cover, terrain, and urban heat islands significantly influence temperature extremes.

One of the greatest strengths of RCMs is the fact that they can be run with observed land-use parameters, e.g., LAI, albedo, and soil moisture. These are necessary in order to accurately simulate land-atmosphere interactions, which are the ones that determine the heatwave intensity and duration (Seneviratne et al., 2010). For example, vegetation cover variability (e.g., reduced LAI) can influence sensible to latent heat flux partitioning and hence modulate surface temperatures. Similarly, albedo variability can dictate the magnitude of solar radiation absorption by the Earth's surface and further condition heatwave processes.

Accurate parameterization of land use is particularly useful for disaster preparedness because it enables stakeholders to identify where vulnerability is high and direct interventions there. As an example, simulations conducted using updated land-use data can help urban planners design heat-resilient cities by optimizing vegetation cover, surface reflectance, and irrigation schemes (Oleson et al., 2015). In agricultural regions, such models may inform adaptive measures such as altering planting dates, cultivating drought-tolerant varieties, and optimizing water use in order to minimize the impact of heatwaves on crops (Lobell et al., 2011).

Though promising, RCMs have fallen behind in representing heatwaves as accurately as possible because of various issues such as representation uncertainties of land surfaces and dynamical modeling techniques (Seneviratne et al., 2010). Overcoming these requires further model parameterization improvement and verification against observation. For example, this study shows how employing satellite-retrieved land-use properties improves the modeling of two important heatwave events in Belgium and highlights thereby the importance of realistic representation of the land surface for disaster management. As such, improving the representation of land surface properties in RCMs not only promotes scientific understanding but also lays the groundwork for the application of disaster risk reduction strategies.

### 2.4 Risk Analysis Frameworks

Risk analysis is a central component of disaster management, providing a structured process for risk identification, estimation, and prioritization. Heatwave risk may be conceptualized in terms of three primary components: hazard, exposure, and vulnerability (IPCC, 2021). Hazard defines the heat extreme event, and exposure encompasses the population, infrastructure, and ecosystems exposed to the hazard. Vulnerability takes place through age structures, socioeconomic situations, and substandard cooling facilities.

Within heatwaves, risk assessment models can be employed to identify populations and locations that are at greatest risk. For example, urban areas with high levels of impervious cover, such as asphalt and concrete, are susceptible to the urban heat island effect, which prolongs the impact of heatwaves (Oleson et al., 2015). Similarly, agricultural regions may have higher risks from diminished soil moisture and enhanced evapotranspiration during heatwaves (Seneviratne et al., 2010). High-resolution climate model results can be incorporated into risk assessment schemes to provide more accurate and localized estimates of heatwave risks, enabling interventions in targeted areas.

### 2.5 Adaptation and Mitigation Strategies

Adaptation and mitigation are central aspects of managing disasters, whose purpose is to reduce populations' and ecosystems' exposure to heatwaves. Adaptation is reacting to occurring and predicted impacts of heatwaves, while mitigation seeks to address the reasons for climate change through reducing the emissions of greenhouse gases.

Among the promising adaptation measures is the embracing of nature-based solutions, such as increasing green cover in urban areas to mitigate the urban heat island effect (Oleson et al., 2015). Vegetation is a canopy provider that also enhances evaporative cooling, hence reducing surface temperatures and thermal comfort. Similarly, efficient irrigation in agricultural regions can maintain soil water content, reducing the impact of heatwaves on agriculture production (Lobell et al., 2011).

Mitigation measures, though, seek to reduce greenhouse gases from policy interventions, technology, and behavior change. An example is a transition to clean energy, which reduces the carbon intensity of energy-consuming operations, for example, air conditioners causing the urban heat island effect (Davis & Gertler, 2015). International agreements, like the Paris Agreement, also have an important role to play in coordinating global actions towards climate change adaptation and mitigation.

The value of regional climate models such as ALARO-Surfex in informing adaptation and mitigation planning has been highlighted by this study. Through the improvement of heatwave simulation credibility, these models are able to enable evidence-based decision-making and therefore contribute to more resilient ecosystems and societies.

### 2.6 Urban Planning and the Effects of Heatwaves

Urban planning is key in mitigating heatwave impacts, particularly in densely populated urban areas where the urban heat island (UHI) phenomenon increases temperature extremes. Urban heat island (UHI) effect, meaning higher temperatures over urbanized spaces compared to the surrounding rural spaces, results from human activities, reduced vegetation cover, and the high utilization of heat-conductive materials such as asphalt and concrete (Stewart & Oke, 2012; Redon et al., 2020). With the growing frequency and intensity of heatwaves due to climate change, integrating heatwave resilience into city planning is now a necessary requirement.

Integrating green infrastructure in the form of parks, green roofs, and tree-lined avenues is one of the most critical steps to mitigate heatwave impacts in cities. These features not only reduce surface and air temperatures through shading and evapotranspiration but also partake in the quality of urban living overall by cleaning the air and providing recreational spaces (Oleson et al., 2015). For example, studies have determined that increased Leaf Area Index (LAI) values in cities can significantly reduce surface temperatures, thereby relieving the UHI effect and mitigating the health hazards due to heat (Caluwaerts et al., 2020).

Another important urban planning aspect is the use of reflective materials, which are generally referred to as "cool roofs" and "cool pavements." These materials are specifically designed to maximize surface albedo and reduce solar radiation absorption by urban structures (Wang et al., 2021). Detailed land cover data, as seen in the case of Ghent, Belgium, has been important to model the effect of such interventions on UHI processes (Top, 2018). By the integration of observed land-use features within regional climate models (RCMs), planners are able to better estimate the possible returns for these approaches and direct investments accordingly.

Besides physical measures, urban planning must address the social exposure to heatwaves as well. Low-income communities, older adults, and people with pre-existing medical conditions are disproportionately affected by heat stress due to limited availability of cooling centers and access to healthcare (WHO, 2023). Urban planning systems must therefore incorporate equitable strategies, such as the establishment of cooling centers in at-risk neighborhoods and promoting energy-efficient building design.

The integration of dynamic land surface data in RCMs provides a strong potential to enhance urban planning processes. Studies like Sara Top (2018) have emphasized the real benefits of using high-resolution simulations to inform heat risk management policies. For instance, by identifying urban grids with greater sensible heat flux (SHF) during heatwaves, planners can target those specific areas selectively for intervention, such as increased vegetation cover or cool roof initiatives. This approach not just enhances the resilience of urban areas but also advances broader sustainability goals, such as reducing carbon emissions and safeguarding water resources.

Forward, urban development has to take into account projected changes in land cover, vegetation patterns, and anthropogenic utilization under different climate change conditions. This calls for a transdisciplinary effort that combines results from climatology, urban development, and public health to develop adaptive actions optimized for local environments. Urban planners can be at the forefront in reducing the social and economic impacts of heatwaves, thereby producing more sustainable and resilient cities.

The next chapter synthesizes recent literature on regional climate modeling and land-surface coupling, which is the foundation of the technical work of this research.

# 3. LITERATURE REVIEW

## 3.1 Heatwaves, Energy Balance, and Land-Atmosphere Feedback

Heatwaves—defined as prolonged periods of highly elevated temperature relative to climatological norms—are one of the most important climate extremes to affect Europe (Perkins-Kirkpatrick & Lewis, 2020). When coupled with droughts, heatwaves produce compound extremes that can severely strain ecosystems, agriculture, and human health (Zscheischler et al., 2018). These compound events are characterized by feedback among high temperatures, deficient rainfall, and dry ground.

The balance of surface energy is key in the onset and intensity of heatwaves. Incoming shortwave radiation is partitioned into ground heat flux, latent heat flux (LHF), sensible heat flux (SHF), and longwave radiation. Vegetation dictates this partitioning by regulating evapotranspiration, surface albedo, and roughness (Seneviratne et al., 2010; Teuling et al., 2010). During droughts, soil moisture limitations reduce LHF, which enhances SHF and leads to increased conditions—a concept referred to as soil moisture-temperature coupling.

These processes must be replicated in climate models by means of physically meaningful representations of land surface characteristics. Regional Climate Models (RCMs) are capable of delivering the spatial resolution required to resolve heterogeneity in vegetation physics, topography, and land cover. Coupled extremes are however still hard to simulate, especially under future climate projection. State-of-the-art modeling frameworks currently more and more examine multi-model ensembles and data assimilation approaches in order to better constrain simulations (Kornhuber et al., 2019; Seneviratne et al., 2021).

This study builds on earlier studies focused on enhancing RCM heatwave simulations by including satellite-retrieved observations of those key land surface properties—albedo, LAI, and roughness—in the ALARO-Surfex model, a widely used high-resolution RCM for Europe.

### 3.2 Regional Climate Modeling and Downscaling

Simulation of regional climate, especially the frequency of extreme events like heatwaves, has significantly been enhanced with the development of dynamical downscaling techniques. Dynamical downscaling enables high-resolution simulation by nesting Regional Climate Models (RCMs) into Global Climate Models (GCMs) or reanalysis data (Giorgi & Gutowski, 2015; Xue et al., 2014). Such a strategy is required for the simulation of fine-scale atmospheric processes such as land-atmosphere coupling and local topography effects, which cannot be resolved by low-resolution GCMs. Particularly the ALARO model, developed in the ALADIN-HIRLAM consortium and coupled with the SURFEX surface scheme land surface model, has been widely used in Europe and Belgium to perform dynamical downscaling analyses (Berckmans et al., 2017; Termonia et al., 2018). This combined model simulates in high fidelity the interaction of exchanges of energy, water, and carbon across land surface and atmosphere, thereby enhancing the realism of regional climate simulation.

The most notable upgrade in boundary condition quality is the use of reanalysis data such as ERA-Interim (Dee et al., 2011) and its successor ERA5 (Hersbach et al., 2020). ERA5 has higher temporal and spatial resolution than ERA-Interim and incorporates a broader array of observational data using better data assimilation schemes. It delivers hourly outputs at a horizontal resolution of approximately 31 km, which enables RCMs to simulate historic events in a realistic manner. These sorts of "perfect boundary conditions" are required for studies that aim to isolate model response to actual weather conditions, as in the present analysis of the July 2018 and 2019 heatwaves over Belgium.

Large-scale initiatives such as the Coordinated Regional Downscaling Experiment (CORDEX) and projects like PRUDENCE have resulted in standardized protocols for regional modeling and model inter-comparison (Christensen et al., 2007). Evaluation studies, such as Kotlarski et al. (2014) for EURO-CORDEX, demonstrated that while RCMs in general simulate the seasonal temperature cycle extremely well, systematic biases remain, for example, in the simulation of precipitation patterns. Such projects highlight the pressing necessity for continued improvements in model physical schemes, including surface representations.

### 3.3 Land Surface Representation and Land-Atmosphere Feedback

One of the most important sources of uncertainty in regional climate simulations arises from the representation of land surface processes. Parameters such as albedo, Leaf Area Index (LAI), surface roughness, and soil moisture availability have large effects on surface energy fluxes and near-surface temperatures (Seneviratne et al., 2010). Land-atmosphere interactions are particularly important during heatwaves, where partitioning between sensible and latent heat flux is critical. For instance, in the 2003 European heatwave, Fischer et al. (2007) found that low soil moisture considerably amplified near-surface temperatures by enhancing them through feedback processes, demonstrating that surface properties can profoundly alter the scale of extreme events.

Despite the recognized importance of land surface properties, the majority of RCMs, including ALARO-Surfex, in the past have relied on static information such as Ecoclimap-I. While such information is comprehensive, it may not capture the interannual or seasonal range of surface conditions. As a means of overcoming this deficiency, satellite-derived dynamic surface parameters, such as those from the MODIS platform, have been increasingly investigated (e.g., Schaaf et al., 2002; Jin et al., 2003; Román et al., 2010). Observational information such as MODIS LAI, broadband albedo, and NDVI products enables models to mimic actual vegetation processes, improving simulation of surface energy balances and climate feedback (Berckmans, 2018).

### 3.4 Impact of Land Surface Updates on Regional Simulations

Several studies have identified satellite-derived land surface parameter updating—especially using MODIS LAI and albedo—as a decisive factor in improving regional climate model performance (Li et al., 2016; Napoly et al., 2017; Wilson et al., 2012). LAI changes affect evapotranspiration rates and surface cooling, while surface albedo changes regulate the fraction of absorbed solar radiation, both directly altering surface energy balance components such as sensible heat, latent heat, and ground heat fluxes (Wilson et al., 2012; Li et al., 2016). These, in turn, affect the temperature and humidity simulations.

Wilson et al. (2012) demonstrated that surface litter and vegetation cover can have a substantial impact on the partitioning of energy fluxes between sensible and latent heat and on local climate conditions. Napoly et al. (2017) also demonstrated that improved soil and canopy parameterizations in the SURFEX model enhanced the simulation of ground heat fluxes and total energy partitioning. Validation of these land surface parameters remains demanding, involving high-quality observation data sets, e.g., flux tower observations and remote sensing products, to undergo rigorous model testing.

Urban settings present unique challenges to climate modeling. Studies by Zsebeházi et al. (2020) and Zsebeházi & Mahó (2021) emphasized the importance of accurate urban surface representation in SURFEX. Improved urban parameterizations, typically with the use of urban canopy models (UCMs), more accurately represent urban heat islands (UHI) and temperature extremes in cities like Budapest. UCMs play a crucial role in capturing the distinctive energy and water balance characteristics of cities (Stewart & Oke, 2012; Redon et al., 2020; Wang et al., 2021). The same has been found in the case of Ghent, Belgium, where high-resolution land cover data had a substantial effect on UHI simulations (Caluwaerts et al., 2020; Top, 2018). This recent Beijing study by Cui et al. (2023) further underscores the character of urban expansion and land cover change interactions with the dynamics of heatwaves, and the necessity of integrating observed land-use features into RCM configurations.

### 3.5 Challenges and Opportunities for Improving Heatwave Simulations

In general, more accurate simulation of heatwaves in RCMs such as ALARO-Surfex requires both boundary conditions refreshed with newer reanalysis datasets (e.g., ERA5) and dynamically observation-guided updates of land surface parameters. Satellite product-based observational constraints improve better representation of significant drivers such as LAI, albedo, and roughness, reducing biases in surface energy budgets. Furthermore, knowledge of land-atmosphere feedback, e.g., soil moisture (Seneviratne et al., 2010; Fischer et al., 2007), is central to the realistic simulation of heatwave persistence and intensity.

Given the growing exposure of European regions to the impacts of heatwaves, particularly in urban and agricultural land, the addition of dynamic land surface data to RCMs is an important step forward. Studies like Sara Top (2018), have shown the practical benefits of such improvements for urban planning and heat risk management.

In summary, while major progress has been made, the simulation of heatwaves in regional climate models remains a complex challenge that must be continually refined by both land surface representation and dynamical modeling techniques. This thesis contributes to this field of research by thoroughly examining the impact of newly observed land surface characteristics on the simulation of two major heatwave events in Belgium.

# 4. MATERIALS AND METHODS

## 4.1 Study Area and Period

This study focuses on Belgium and its surrounding area, spanning the geographic region of approximately 49.35°N to 52.105°N latitude and 2.0°E to 6.6°E longitude (Figure 4.1). The model domain was selected so that the regional atmospheric processes and land processes governing Belgium are included in its entirety, leaving a suitable buffer region to prevent boundary condition impacts. The experiments were carried out at 1.5 km horizontal resolution, enabling high-fidelity simulation of fine land cover structures, topography, and neighborhood-scale land-atmosphere interactions.

Belgium, which is situated in Western Europe, has a temperate maritime climate with quite mild summers, moderate total annual precipitation, and regular weather variability due to Atlantic influences. The area is characterized by a diverse landscape like agricultural croplands, urban areas, and mixed forests, and all of these contribute differently to surface energy fluxes and heatwave behavior.

The selected study time frame includes two significant heatwaves in July 2018 and July 2019. These two months witnessed extreme temperature departures, both with widespread influences on agriculture, public health, and energy supply systems. During July 2018, it was dominated by a persistent drought and high temperatures, while record-breaking maximum temperature values were reached in the majority of Belgian territories during July 2019. These contrasting but extreme occurrences offer an ideal laboratory for the evaluation of the sensitivity of the ALARO-Surfex model to new land surface parameters and for assessing the model ability to reproduce observed heatwave behavior under various climatic conditions.


**Figure 4.1:** Study area, the Map taking from mapsofworld.com.

### 4.1.1 Water bodies in Belgium

Water bodies are a contributing factor in local climate mechanisms due to their high heat capacity, thermal inertia, and contribution to regional humidity through evaporation. The Scheldt and the Meuse rivers, reservoirs, canals, and numerous small lakes are all substantial hydrological features in Belgium that are able to influence mesoscale atmospheric processes (Batelaan et al., 2003), figure 4.2 shows the water bodies of Belgium. The presence of such water bodies is generally thought to moderate temperatures by bringing localized cooling during heatwaves through enhanced latent heat fluxes (van Heerwaarden et al., 2010). In regional climate models such as ALARO-Surfex, surface waters are simulated as an extra category of land cover within Ecoclimap-I with specific surface energy balance characteristics compared to vegetated or urban surfaces (Masson et al., 2013).

However, because of the relatively limited geographical coverage of Belgian inland water bodies compared to arable land and urbanization, their impact would most likely be localized, with a particular concentration on the microclimate of adjacent grid cells. Nevertheless, they have to be represented correctly to ensure correct surface–atmosphere coupling and especially so over densely hydrologically networked regions such as Flanders.


**Figure 4.2:** Water bodies map of Belgium.

### 4.2 Model Data

Regional climate simulations in the current study were performed using the ALARO-Surfex model, whose atmospheric scheme is the ALARO atmospheric scheme (default configuration of the ALADIN system) and SURFEX land surface model. ALARO is part of the ALADIN-HIRLAM consortium for numerical weather prediction and has been widely used to perform limited-area climate modeling over Europe (Termonia et al., 2018). It is especially designed to resolve fine-scale atmospheric processes such as convection, radiation, and turbulence, hence suitable for high-resolution regional climate modeling.

SURFEX (Surface Externalisée) is the land surface model coupled with ALARO. It has been developed by Météo-France along with the ALADIN consortium and is capable of simulating exchanges of energy, water, carbon, and momentum between the atmosphere and ground surface (Masson et al., 2013). SURFEX operates on a tiling scheme that splits the ground surface into four main components: nature, town, inland water, and sea. Each cell of the grid is a mosaic of such tiles, and each tile is given specific physical and biophysical characteristics.

Under the nature tile, vegetation is also simulated through 19 Plant Functional Types (PFTs) with prescribed seasonal profiles for surface albedo, Leaf Area Index (LAI), surface roughness, and root depth. These parameters regulate the partitioning of net radiation into ground heat flux, sensible heat flux (SHF), and latent heat flux (LHF), and so play a critical role in regulating surface temperature and evapotranspiration. SURFEX possesses a climatological seasonal cycle for all PFTs in the default case, which may not capture interannual variability such as vegetation drought stress.

The baseline simulations used the Ecoclimap-I land cover database (Masson et al., 2003), which provides fractional cover of the 19 PFTs per grid cell at 1 km resolution over Europe. This static land cover map is used to assign fixed biophysical parameter values to each tile based on dominant vegetation type and associated seasonal profiles. In the control configuration of this study, LAI, albedo, and roughness were thus prescribed using default monthly climatologies defined by Ecoclimap-I for each vegetation class.

To isolate the impact of dynamic vegetation properties, experiment configuration was conducted in which satellite-derived MODIS data were used to update LAI, white- and black-sky albedo, and roughness for July 2018 and July 2019. These replaced the default Ecoclimap-I values and allowed the model to reflect observed surface changes during heatwave events. Figure 4.3 shows the methodology flowchart.

Both model configurations were driven by ERA5 reanalysis data, which provides hourly atmospheric initial and boundary conditions at 0.25° resolution (Hersbach et al., 2020). ERA5 combines a broad spectrum of atmospheric observations using an advanced 4D-Var data assimilation system, and as a result, it is a high-quality data source to evaluate the responses of regional models to realistic weather conditions.

Simulations began on April 1st for 2018 and 2019, and the first three months (April–June) were considered a spin-up period. Spin-up is extremely crucial for regional climate modeling to allow the coupled land-atmosphere system to reach thermodynamic and hydrologic balance, thereby minimizing the impact of arbitrary initial conditions. A three-month period is also applied in similar studies and has been sufficient in achieving balance between the atmosphere and land surface, particularly in high-resolution models driven with realistic boundary conditions (Giorgi & Mearns, 1999; Lucas-Picher et al., 2013; Rummukainen, 2010).

The decision to start simulations in April was taken so that the model would be able to simulate the spring replenishment of soil moisture following the winter dormant season. This is a critical time to represent the land-atmosphere coupling under following heatwave conditions in Belgium, where spring soil moisture strongly controls summer temperature extremes (Hirschi et al., 2018; Seneviratne et al., 2010). Initiating the simulations in April ensures that the soil and vegetation states are well stabilized and realistic prior to the assessment period in July.

In baseline configuration, the model operated with default land surface parameters of the Ecoclimap-I database, which provides climatological fractional cover of vegetation types. In the updated configuration, the default parameters were replaced with satellite-retrieved Leaf Area Index (LAI), albedo, and surface roughness. MODIS datasets were used to obtain new parameters, which were aggregated to monthly means for July 2018 and July 2019 to simulate realistic land surface conditions for the corresponding heatwave episodes.

The model was constrained with ERA5 reanalysis data, where lateral and initial boundary conditions were continuously updated for the atmospheric state realism. Daily sea surface temperature (SST) was also updated to incorporate large-scale interactions among the atmosphere and the ocean. Model output was regridded to a 5 km resolution using Climate Data Operators (CDO) for spatial compatibility with the observational climate grid to compare with observational data.

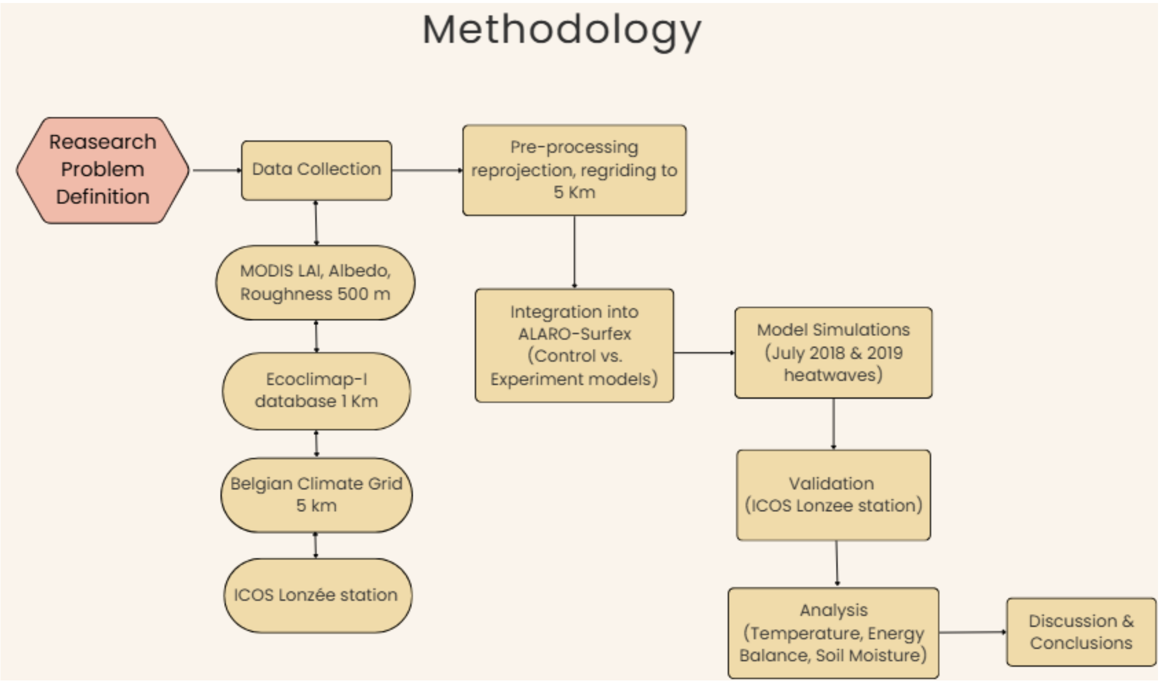


**Figure 4.3:** Methodology flow chart.

### 4.3 Satellite-Derived Land Surface Parameters

To improve the representation of land surface processes in the ALARO-Surfex model, new land-use parameters—including leaf area index (LAI), surface albedo (visible and near-infrared), and roughness length—were derived from MODIS satellite products using the Google Earth Engine (GEE) platform (Table 4.1). MODIS data offer high temporal resolution (8-day composites for LAI and 8-day or 16-day for albedo) and a native spatial resolution of 500 meters.

Monthly mean values of LAI were computed by averaging the available 8-day composite images for each month from April to August for the years 2018 and 2019. Similarly, the surface albedo was calculated as the weighted average of MODIS black-sky and white-sky albedo in the visible and near-infrared bands, also aggregated to monthly means. Roughness length was estimated indirectly based on vegetation type and structure inferred from MODIS vegetation indices.

After downloading monthly composites as GeoTIFFs, the data were preprocessed and regridded to meet the resolution of the ALARO-Surfex model grid (5 km) through bilinear interpolation, which provides a smoother representation of subgrid variability. MODIS's native sinusoidal projection was first reprojected to WGS84 (EPSG:4326) to meet the model's coordinate system. Then, the spatial resampling was conducted, and the values were reformatted into ASCII, according to the model's required input format.

Through ensuring consistent spatial and temporal co-alignment, and through applying appropriate resampling techniques, we aimed to remove biases introduced during translation of satellite-derived parameters into model-input. These pre-processed land surface parameters are now substitutes for the default climatological values used in the original ALARO-Surfex configuration and allow for more realistic heatwave mechanism simulations in Belgium.

**Table 4.1:** MODIS Data Products Used.

| Dataset | MODIS Product | Description |
|---|---|---|
| Blue-Sky Albedo VIS | MODIS/006/MCD43A3 | Surface Albedo (Visible Band) derived using black-sky and white-sky albedo in the visible spectrum. |
| Blue-Sky Albedo NIR | MODIS/006/MCD43A3 | Surface Albedo (Near-Infrared Band) derived using black-sky and white-sky albedo in the NIR spectrum. |
| Leaf Area Index (LAI) | MODIS/006/MOD15A3H | Leaf Area Index (8-day LAI composites) |
| Roughness | MODIS/006/MOD13A2 | Vegetation Indices (16-day composite, 1 km resolution. |

### 4.3.1 MODIS lai dataset (MODIS/006/MCD15A3H)

The Moderate Resolution Imaging Spectroradiometer (MODIS) MODIS/006/MCD15A3H product was utilised in order to extract Leaf Area Index (LAI) data for input into the ALARO-Surfex model. The data set provides global 500 m LAI and Fraction of Photosynthetically Active Radiation (FPAR) 4-day interval estimates, from an 8-day composite period.

To depict the vegetation conditions over the heatwaves, the data for April through August of 2018 and 2019 were processed. For every month, all the 8-day LAI composites available were included in the analysis. The invalid-flagged pixels were screened out to ensure data reliability. However, explicit filtering using the MODIS quality assurance (QA) flags was not performed.

Monthly average LAI values were computed as the mean of all 8-day composites available in each month. This contrasts with the default maximum FPAR compositing technique in MODIS Collection 6, which prioritizes the highest quality retrievals (Myneni et al., 2015; Didan, 2015). While this method sacrifices temporal resolution in order to get improved quality data, it might be capable of smoothing the fast vegetation variations within heatwaves (Fang et al., 2013; Ma et al., 2024).

The resulting monthly composites were exported as GeoTIFF and converted to ASCII format to match the Surfex model input format. These new maps of LAI replace the prescribed default values in the control simulations, in an effort to more realistically represent surface processes in the model for heatwave events. Visual inspection bore witness to the realism of the derived LAI fields (Figure 4.2).

**Table 4.2:** Monthly spatial averages, minimum, and maximum values of MODIS LAI (MCD15A3H) over Belgium for April–July of 2018 and 2019. April–June are spin-up months, July is the simulation month.

| Date | Average Value | Minimum Value | Maximum Value |
|---|---|---|---|
| 2018-04 | 1.415 | 0.071 | 6.071 |
| 2018-05 | 2.413 | 0.1 | 6.562 |
| 2018-06 | 2.161 | 0.087 | 6.562 |
| 2018-07 | 1.769 | 0.1 | 6.542 |
| 2019-04 | 1.619 | 0.085 | 6.585 |
| 2019-05 | 1.869 | 0.087 | 6.437 |
| 2019-06 | 2.324 | 0.075 | 6.637 |
| 2019-07 | 1.759 | 0.1 | 6.614 |

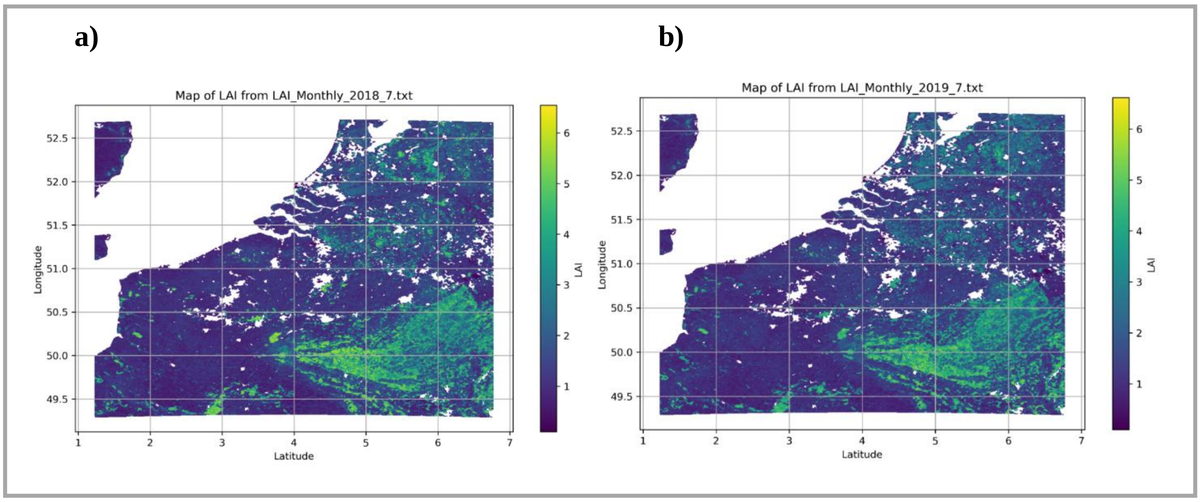


**Figure 4. 4: a)** Leaf Area Index dataset distribution monthly average 2018_July and b**)** Leaf Area Index dataset distribution monthly average 2019_ July

### 4.3.2 MODIS albedo dataset (MODIS/006/MCD43A3)

Albedo, as a surface reflectivity parameter, plays a key role in the energy balance of Earth. Albedo data was obtained from MODIS/006/MCD43A3. It provides Black-sky albedo and white-sky albedo bands across different ranges of spectral measures such as VIS and NIR wavelengths. Similar to LAI data, the region of interest (ROI) was set to encompass Belgium and its environment, and the time of interest was April-August for 2018 and 2019 (Tables 4.3 and 4.4).

Surface albedo, or the fraction of reflected solar to incident solar radiation, is a simple surface energy balance parameter with significant influences on atmospheric processes and near-surface temperature (Ma et al., 2024; Andres-Anaya et al., 2024). In regional climate models such as ALARO-Surfex, the accurate modeling of albedo is essential to reproduce the surface-atmosphere energy exchanges and to simulate temperature extremes such as heatwaves (Napoly et al., 2017; Berckmans et al., 2017).

The total surface albedo under actual sky conditions—referred to as blue-sky albedo—is influenced by both the directional reflectance properties of the surface and the angular distribution of incoming solar radiation. This radiation consists of direct beam and diffuses skylight components. Accordingly, blue-sky albedo ($\alpha\_bs$) can be expressed as a weighted average of black-sky albedo ($\alpha\_bsa$) and white-sky albedo ($\alpha\_wsa$), using the equation:

$$\alpha bs(\lambda) = (1 - fdiff) \cdot \alpha bsa(\lambda) + fdiff \cdot \alpha wsa(\lambda) \tag{4.1}$$

where $fdiff$ represents the diffuse skylight fraction and λ denotes the spectral band (visible or near-infrared).

Black-sky albedo (directional-hemispherical reflectance) is for exclusively direct solar illumination at the given solar zenith angle, and white-sky albedo (bi-hemispherical reflectance) is for albedo under completely diffuse illumination. Both are provided by the MODIS BRDF/Albedo product (MCD43A3), which uses a kernel-driven BRDF model in order to determine spectrally resolved albedo estimates (Schaaf et al., 2002; Jin et al., 2003).

Although $fdiff$ varies dynamically with aerosol optical depth, cloud cover, and solar geometry (Román et al., 2010), this study applies a fixed diffuse fraction of 0.15—reflecting typical summer sky conditions in Belgium, where direct sunlight dominates with intermittent diffuse radiation. This corresponds to a white-sky weight of 0.15 and black-sky weight of 0.85. The broadband blue-sky albedo in the ALARO-Surfex simulations was therefore calculated for every spectral band as:

$$Blue - Sky\ Albedo\ (VIS)$$
$$= 0.85 \times Black - Sky\ Albedo\ (VIS) + 0.15 \times White - Sky\ Albedo\ (VIS) \quad (4.2)$$

$$Blue - Sky\ Albedo\ (NIR)$$
$$= 0.85 \times Black - Sky\ Albedo\ (NIR) + 0.15 \times White - Sky\ Albedo\ (NIR) \quad (4.3)$$

The Blue-Sky Albedo for VIS and NIR for each month was exported separately as GeoTIFF files to further analyze. Visualization of the data are shown in figures 4.3 and 4.4.

This approach offers a practical balance between computational simplicity and physical realism for the heatwave-focused simulations in this study. While more dynamic aerosol- or time-specific weightings could further improve accuracy, the adopted scheme is consistent with methods used in similar land surface and remote sensing studies (Román et al., 2010; Ma et al., 2024). Future work may consider applying location-specific diffuse fractions using available atmospheric radiation products to refine this parameterization.

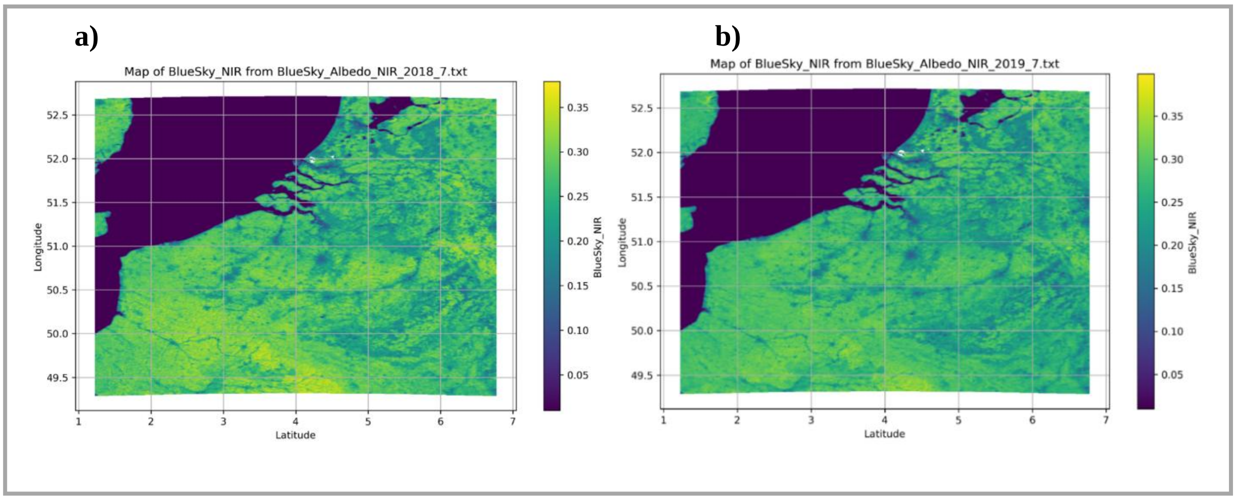


**Figure 4.5: a)** BlueSky NIR dataset distribution monthly average 2018_ July and **b)** BlueSky Albedo NIR dataset distribution monthly average 2019_ July.

**Table 4.3:** Monthly spatial mean, minimum, and maximum blue-sky albedo values in the near-infrared (NIR) band, derived from MODIS MCD43A3 over Belgium for April–July of 2018 and 2019. April–June are spin-up months, July is the simulation month.

| Date | Average Value | Minimum Value | Maximum Value |
|---|---|---|---|
| 2018-04 | 0.199 | 0.01 | 0.427 |
| 2018-05 | 0.213 | 0.01 | 0.405 |
| 2018-06 | 0.207 | 0.01 | 0.371 |
| 2018-07 | 0.202 | 0.01 | 0.378 |
| 2019-04 | 0.209 | 0.01 | 0.46 |
| 2019-05 | 0.209 | 0.01 | 0.419 |
| 2019-06 | 0.207 | 0.01 | 0.382 |
| 2019-07 | 0.203 | 0.01 | 0.399 |

**Table 4.4:** Monthly spatial mean, minimum, and maximum blue-sky albedo values in the near-infrared (VIS) band, derived from MODIS MCD43A3 over Belgium for April–July of 2018 and 2019. April–June are spin-up months, July is the simulation month.

| Date | Average Value | Minimum Value | Maximum Value |
|---|---|---|---|
| 2018-04 | 0.047 | 0.01 | 0.171 |
| 2018-05 | 0.045 | 0.01 | 0.181 |
| 2018-06 | 0.041 | 0.01 | 0.179 |
| 2018-07 | 0.05 | 0.01 | 0.175 |
| 2019-04 | 0.047 | 0.01 | 0.215 |
| 2019-05 | 0.043 | 0.01 | 0.306 |
| 2019-06 | 0.041 | 0.01 | 0.174 |
| 2019-07 | 0.048 | 0.01 | 0.174 |

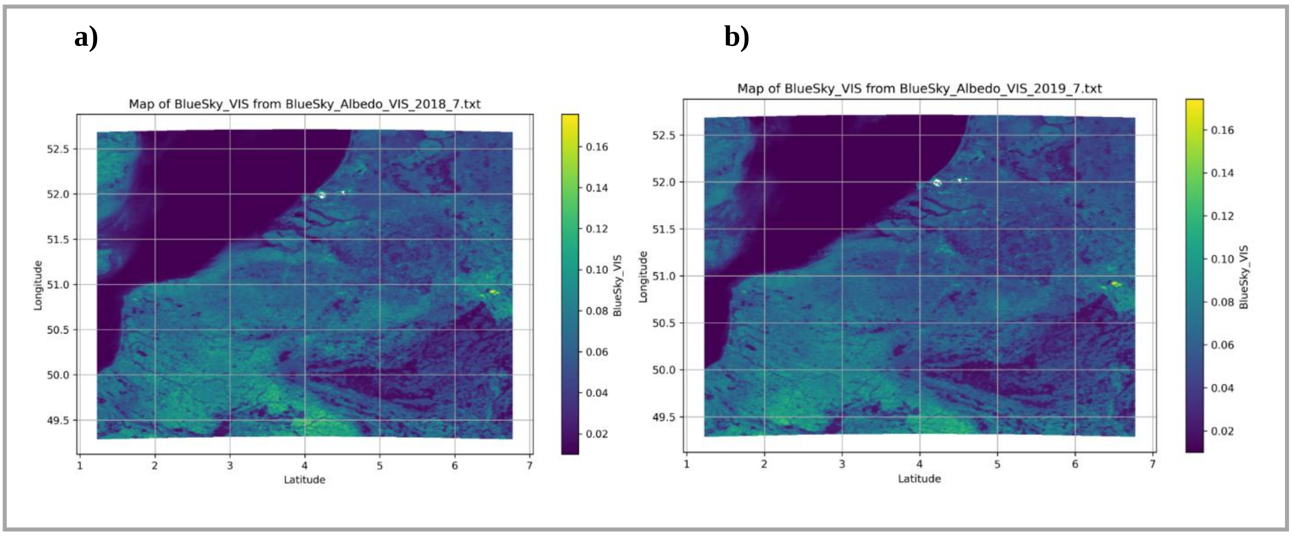


**Figure 4.6: a)** BlueSky Albedo VIS dataset distribution monthly average 2018_ July and **b)** BlueSky Albedo VIS dataset distribution monthly average 2019_ July.

### 4.3.3 MODIS NDVI dataset (MODIS/006/MOD13A2)

The Normalized Difference Vegetation Index (NDVI) is an index most commonly used to measure vegetation health, density, and greenness. It is a reflectance in the red and near-infrared (NIR) bands and can be calculated as:

$$NDVI = (NIR - RED) / (NIR + RED) \tag{4.4}$$

NDVI values are between -1 and 1, with greater values representing healthier and denser vegetation. For this research, the MODIS/006/MOD13A2 data product was utilized to retrieve NDVI composites for a 16-day period. The initial data storage NDVI as scaled integers (×10,000) to preserve precision; we therefore normalized values by dividing by 10,000 to gain actual NDVI values, as documented in the MODIS VI User Guide (Didan, 2015) and within LP DAAC documentation (NASA LP DAAC, 2023).

NDVI was used here as a vegetation structure surrogate, to provide an estimate of spatial variability in surface roughness length. While NDVI is not aerodynamic roughness ($z_0$) itself, it has previously been used as an estimator of relative surface roughness in other research when there are no high-resolution land surface data available (e.g., Ma et al., 2024).The rationale is that denser, taller vegetation typically corresponds to higher NDVI and greater aerodynamic resistance.

For each month from April to August in 2018 and 2019, NDVI data over Belgium and surrounding regions were averaged and resampled to the model domain (Table 4.5). The processed monthly roughness proxy layers were exported as GeoTIFF and ASCII files and subsequently used to update the roughness length parameter in the modified ALARO-Surfex simulations. Visualizations of these processed NDVI-derived layers are presented in figure 4.5.

**Table 4.5:** Monthly spatial statistics of NDVI-derived surface roughness proxy over Belgium for April–July in 2018 and 2019. Values represent average, minimum, and maximum proxy roughness lengths (unitless) estimated from MODIS MOD13A2 NDVI. April–June were spin-up months; July was used for the heatwave simulations.

| Date | Average Value | Minimum Value | Maximum Value |
|---|---|---|---|
| 2018-04 | 0.645 | 0.01 | 0.905 |
| 2018-05 | 0.701 | 0.01 | 0.93 |
| 2018-06 | 0.676 | 0.01 | 0.931 |
| 2018-07 | 0.574 | 0.01 | 0.91 |
| 2019-04 | 0.667 | 0.01 | 0.91 |
| 2019-05 | 0.698 | 0.01 | 0.917 |
| 2019-06 | 0.706 | 0.01 | 0.92 |
| 2019-07 | 0.612 | 0.01 | 0.915 |

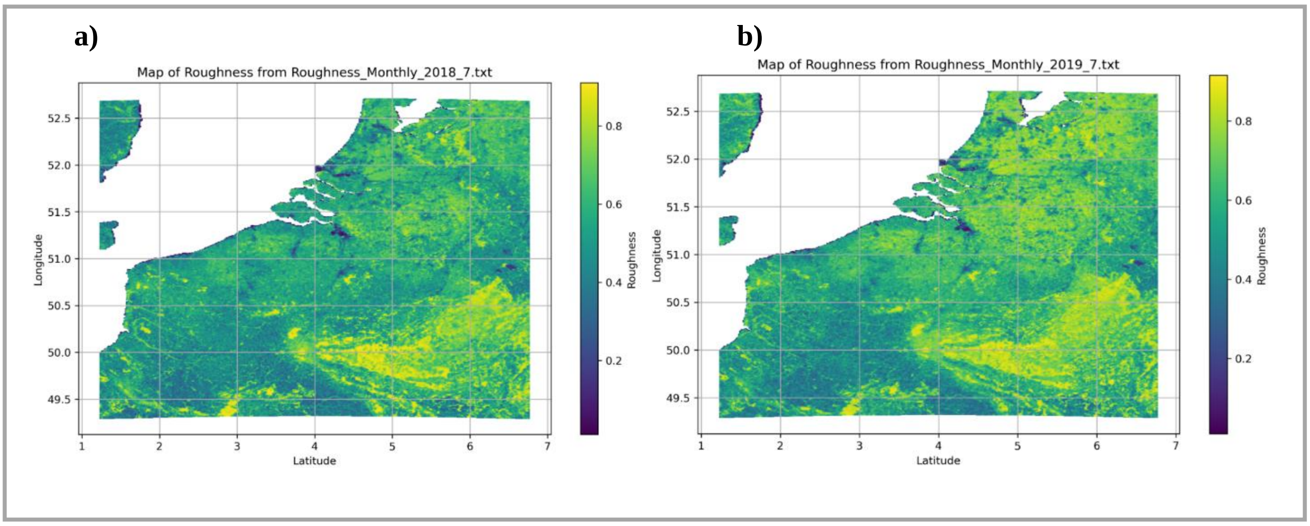


**Figure 4.7: a)** Roughness dataset distribution of July monthly average 2018 and **b)** Roughness dataset distribution of July monthly average 2019.

### 4.4 Land Cover Data

Land cover data were obtained from the Ecoclimap-I database, which provides global land surface classification at a spatial resolution of 1 km (figure 4.6). Ecoclimap-I is used within the SURFEX model to assign land surface parameter values for 19 plant functional types (PFTs), each with fixed seasonal cycles of LAI, albedo, and roughness length. For this study, two dominant vegetation types over Belgium were selected: type 166 (Temperate Crops) and type 182 (Temperate Pastures), based on the SURFEX land cover classification (SURFEX documentation, 2024).

The decision to focus on pasture and cropland was driven by their extensive coverage across the Belgian landscape and their known sensitivity to heat and drought extremes. Both land cover types possess distinct phenological and biophysical responses to climate stressors (Seneviratne et al., 2010) that make them well-suited to be used to examine the implications of dynamic Land Surface Parameter updates. Their thermal response throughout the 2018 and 2019 heatwaves also exhibited varying temperature responses in initial analyses.

To assess land cover-specific temperature biases, spatial masks were developed for each land cover type. These masks were applied to both model outputs and gridded observational datasets to isolate areas dominated by each type (figure 4.7). This approach enabled a more targeted comparison between the control configuration (default SURFEX parameters from Ecoclimap-I) and the experiment configuration (updated LAI, albedo, and roughness from MODIS). The spatial masks facilitated quantification of how land surface updates affected heatwave simulation performance across different vegetation regimes.

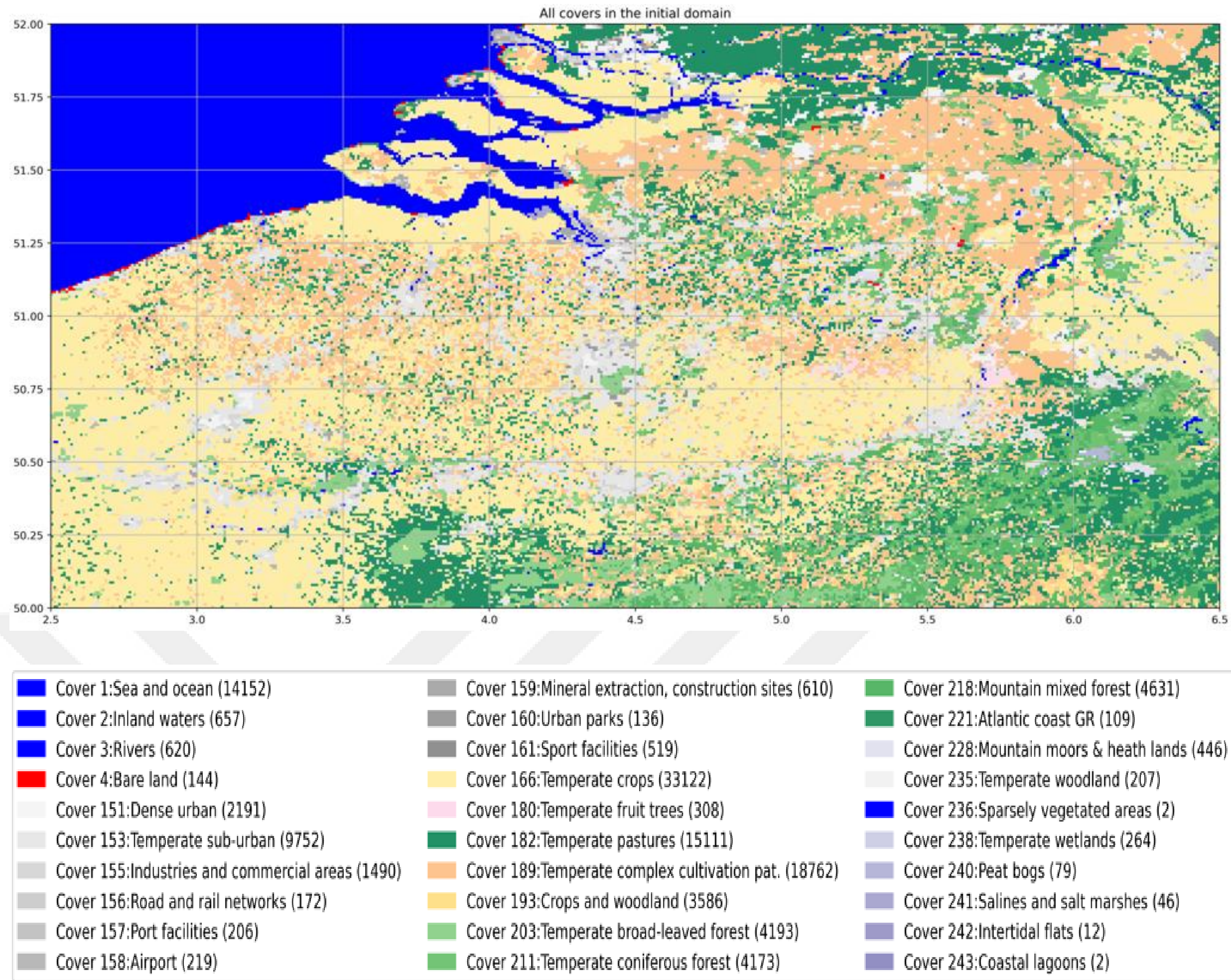


**Figure 4.8:** ECOCLIMAP-I Land Cove classes for the study area.

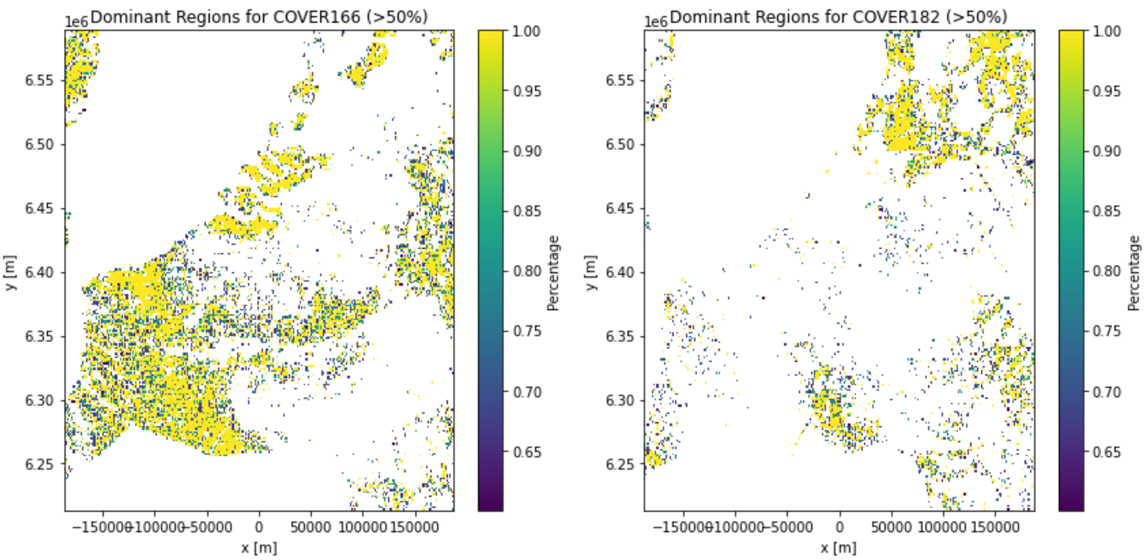


**Figure 4.9:** Dominant Regions for Land Cover Type 166 and 182 (>50%)

### 4.5 Observational Data

To evaluate the performance of the ALARO-Surfex model configurations, we used two independent observational datasets: the Belgian Climate Grid and in-situ measurements from the Integrated Carbon Observation System (ICOS) station at Lonzée.

The Belgian Climate Grid is a high-resolution gridded observational dataset produced by the Royal Meteorological Institute of Belgium (RMI), originally described in Smet et al. (2012). It provides hourly values of average temperature (TEMP_AVG), maximum temperature (TEMP_MAX), and minimum temperature (TEMP_MIN) at a spatial resolution of 5 km, covering the territory of Belgium. The dataset is constructed by spatial interpolation of observations from an extensive network of automatic and synoptic weather stations operated by RMI and spans multiple decades (Figure 3.8). In this study, gridded temperature data from April to July of 2018 and 2019 were used to evaluate surface temperature outputs from both the control configuration and the experiment configuration of the ALARO-Surfex simulations.

Additionally, we employed local-scale data from the ICOS station at Lonzée, part of the Integrated Carbon Observation System (ICOS), a European research infrastructure that provides high-precision, long-term greenhouse gas and meteorological measurements (ICOS RI, 2023), (Figure 4.9). The Lonzée site is a Class-1 eddy covariance flux tower, located in a mixed cropland region, and is equipped with sensors that record air temperature, humidity, radiation, wind, and $CO_2$ fluxes. The station provides hourly data, which were aggregated to daily averages to match the model output. This local dataset was used to complement the gridded evaluation and assess the model’s ability to reproduce the observed surface energy balance dynamics at a representative agricultural site.

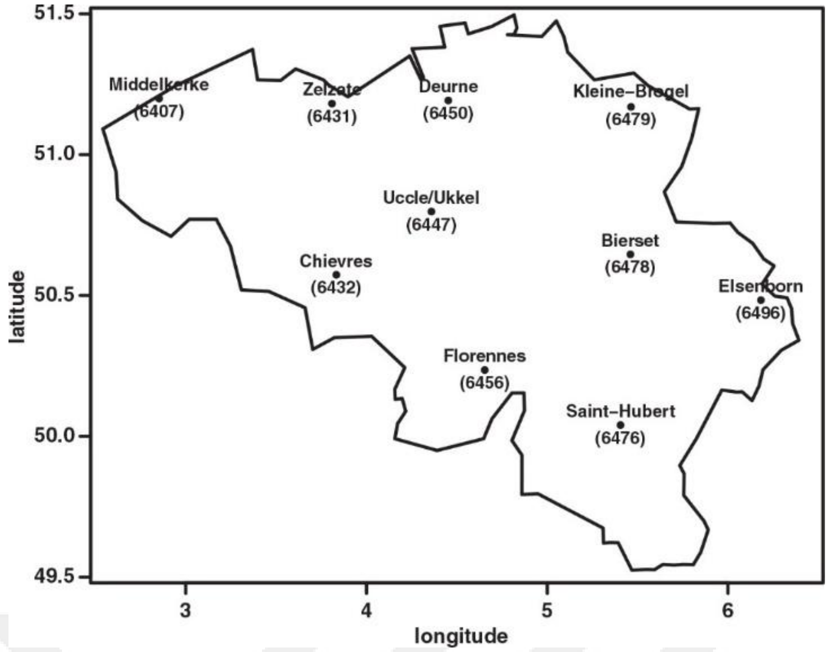


**Figure 4.10**: Belgian weather stations used in this study are denoted with a dot, together with their place name and their WMO number in parentheses. (Adapted from Smat et al.,2012).

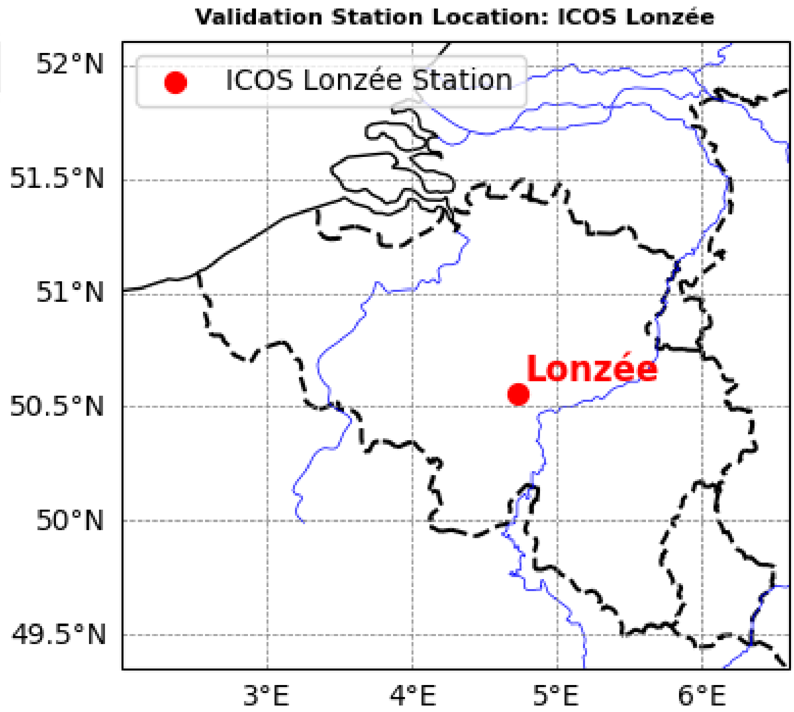


**Figure 4.11:** Validation Station : ICOS Lonzée

### 4.6 Statistical analysis and bias assessment

Several statistical techniques were employed in the research to evaluate the performance of the model, as well as the impact of the new land surface properties.

#### 4.6.1 Mean absolute error (MAE)

Mean Absolute Error (MAE) was employed to estimate the average size of the model simulation-observation errors. It gives an estimate of the general accuracy of the model, without regard to the direction of the errors.

$$\mathrm{MAE} = (1/\mathrm{n}) * \Sigma\,|\mathrm{Yi} - \mathrm{Xi}| \qquad (4.5)$$

where:

- n is the number of data points
- Yi is the model-simulated temperature.
- Xi is the observed temperature.

#### 4.6.2 Mean absolute bias (MAB)

The Mean Absolute Bias (MAB) was used to quantify the systematic bias of the model runs. It informs us whether the model overestimates or underestimates the temperature.

$$\mathrm{MAB} = (1/\mathrm{n}) * \Sigma\,(\mathrm{Yi} - \mathrm{Xi}) \qquad (4.6)$$

where:

- n is the number of data points
- Yi is the model-simulated temperature.
- Xi is the observed temperature.

#### 4.6.3 Albedo, LAI and Temperature change analysis

To investigate the interaction between temperature responses and surface property alterations during heatwaves, we conducted spatial regression analysis. We quantified, in specific terms, the extent to which changes in albedo and Leaf Area Index (LAI) from experiment and control conditions were associated with changes in the surface temperature variables TEMP_AVG, TEMP_MAX, and TEMP_MIN.

The July 2018 and July 2019 comparisons were performed pixel by pixel across all cropland grid cells defined as class 166 or class 182. For each pixel, the LAI difference and albedo difference (ΔLAI, Δalbedo) were calculated as:

$$\Delta Albedo = Albedo(experimental) - Albedo(control) \tag{4.7}$$

$$\Delta LAI = LAI\ (experimental) - LAI\ (control) \tag{4.8}$$

Similarly, changes in temperature were computed for each variable:

$$\Delta TEMP\_AVG = TEMP\_AVG\ (experimental) - TEMP\_AVG(control) \tag{4.9}$$

$$\Delta TEMP\_MAX = TEMP\_MAX\ (experimental) - TEMP\_MAX(control) \tag{4.10}$$

$$\Delta TEMP\_MIN = TEMP\_MIN\ (experimental) - TEMP\_MIN(control) \tag{4.11}$$

This regression approach allowed us to evaluate whether the observed surface parameter updates (from MODIS) explain systematic differences in modeled temperature behavior during heatwaves.

#### 4.6.4 Surface energy balance analysis

The components of the surface energy balance, including shortwaves radiation, net radiation, sensible heat flux, and latent heat flux, were analyzed to see how the new land-use characteristics affected the energy fluxes at the ground surface. Old (control simulation) model and new (experiment simulation) model setups comparisons were calculated and compared spatially and statistically.

#### 4.6.5 Soil moisture analysis

Soil moisture variations at 1 cm and 10 cm depths were analyzed to ascertain the impact of the new land-use characteristics on soil moisture dynamics. Differences in soil moisture between the old (control) and new (experiment) model configurations were calculated and compared.

#### 4.6.6 ICOS data validation

To evaluate the performance of the ALARO-Surfex model locally, model outputs were compared with ICOS ecosystem station data in Lonzée, Belgium. The station provides continuous high-resolution eddy covariance measurements of meteorological and surface energy balance parameters. It is classified as a Class 1 site in the European ICOS network and is located in an agricultural region representative of cropland-type surfaces.

Model near-surface temperature simulations were validated for TEMP_AVG, TEMP_MAX, and TEMP_MIN. Mean Absolute Error (MAE) and Mean Absolute Bias (MAB) for control and experiment runs were calculated in order to quantify systematic difference from the observed. These measurements provided a sense of the ability of the model to simulate day-to-day temperature variation under conditions of extreme heat.

# 5. RESULTS

## 5.1 Overview of Simulation Performance

The ALARO-Surfex model was applied to examine the impact of observed, spatially variable land-use parameters on heatwave simulations for July 2018 and 2019 over Belgium. The control setup based on default land surface properties from the Ecoclimap-I dataset and the experiment setup with satellite-derived parameters for albedo, Leaf Area Index (LAI), and roughness length were compared. The key goal was to see whether the new parameters had an added advantage on the capacity of the model in simulating the most relevant temperature indices—mean (TEMP_AVG), highest (TEMP_MAX), and lowest (TEMP_MIN) temperatures—across the different land cover classes as well as for the entire domain.

At the domain level, results showed distinct patterns in performance differences between the new and former model settings. The setup of the new model demonstrated better simulation of TEMP_MIN and biases were reduced significantly over all regions. Mean Absolute Bias (MAB) for TEMP_MIN decreased by about -1.67°C during 2018 and -1.23°C during 2019.

However, the new parameters initiated an increase in the biases for daytime warming (TEMP_MAX). MAB for TEMP_MAX declined by +0.74°C for 2018 and +0.67°C for 2019, meaning that the new configuration was not able to recover large daytime temperatures during heatwaves very well. This is more severe where crop type 166 had constrained areas because they suffered reduced LAI and greater soil drying enhanced sensible heat fluxes to cause daytime warming stronger.

Performance of the mean temperature (TEMP_AVG) was also mixed. While the new configuration of the model was better in some places, particularly over the central area of Belgium, global biases varied little from those in the original configuration. That suggests that offsetting effects of improved nighttime cooling and increased daytime warming partially nullified each other when averaged diurnally.

One of the dominant characteristics of the simulation output was variability in spatial model bias. Regions with dense vegetation cover were generally better impacted by the enhanced parameters, showing lower bias in both TEMP_AVG and TEMP_MIN (Table 5.1 and 5.3). In cases of sparse vegetation cover and arid conditions, the models had higher bias in TEMP_MAX, indicating land surface sensitivity for the model.

These findings emphasize the complexity of land-atmosphere interaction processes during heatwave events. While the updated land-use parameters improved some aspects of the simulation, they also introduced additional complexity in reproducing extreme daytime temperatures. The subsequent sections examine these findings in greater detail, exploring the role played by albedo, LAI, soil moisture, and surface energy fluxes in driving the observed biases.

## 5.2 Temperature Performance Evaluation

### 5.2.1 TEMP_AVG (Average Temperature)

#### 5.2.1.1 Overall model performance

In 2018, the new model shows a notable improvement over the old model, with MAE decreasing from 2.04°C to 1.74°C and MAB from 1.62°C to 1.24°C, indicating improved accuracy. In 2019, the improvements are smaller but still present (MAE reduced from 1.63°C to 1.56°C, MAB from 1.49°C to 1.40°C), showing marginal improvement. The Mean Absolute Error (MAE) and Mean Absolute Bias (MAB) for TEMP_AVG for the old model (control) and the new model (experiment) configurations are presented in table 5.1. Visual confirmation of these trends is presented in figures 5.1 and 5.2.

#### 5.2.1.2 Model performance by land cover

**Cropland 166**

For land cover type 166, the updated parameters improved the simulation of average temperature in both years. In 2018, the MAE decreased from 1.97 °C in the old model (control) to 1.67 °C in the new model (experiment), and the MAB decreased from 1.58 °C to 1.30 °C. In 2019, the MAE decreased from 1.49 °C to 1.43 °C, and the MAB decreased from 1.33 °C to 1.26 °C.

### Cropland 182

Similarly, for land cover type 182, the updated parameters improved the simulation of average temperature. In 2018, the MAE decreased from 2.08 °C in the old model (control) to 1.71 °C in the new model (experiment), and the MAB decreased from 1.38 °C to 0.81 °C. Notably, the reduction in MAB for land cover 182 in 2018 was substantial. In 2019, the MAE decreased from 1.67 °C to 1.60 °C, and the MAB decreased from 1.53 °C to 1.40 °C.

The new parameterizations (LAI, albedo, and roughness) lead to consistent improvements in TEMP_AVG across all land covers, especially in 2018. The more substantial performance gain in 2018 may be linked to more extreme heatwave events during that year, where model updates had greater impact.

**Table 5.1:** Mean Absolute Error (MAE) and Mean Absolute Bias (MAB) for average temperature (TEMP_AVG) in the ALARO-Surfex model for 2018 and 2019. The table compares the performance of the old model (control), and the new model (experiment) Values are presented for the overall model domain as well as for two dominant cropland types: cropland 166 (temperate crops) and cropland 182 (temperate pastures).

| Year | Land Cover | Model | MAE (°C) | MAB (°C) |
|---|---|---|---|---|
| 2018 | | Old Model | 2.04 | 1.62 |
| 2018 | | New Model | 1.74 | 1.24 |
| 2018 | 166 | Old Model | 1.97 | 1.58 |
| 2018 | 166 | New Model | 1.67 | 1.3 |
| 2018 | 182 | Old Model | 2.08 | 1.38 |
| 2018 | 182 | New Model | 1.71 | 0.81 |
| 2019 | | Old Model | 1.63 | 1.49 |
| 2019 | | New Model | 1.56 | 1.4 |
| 2019 | 166 | Old Model | 1.49 | 1.33 |
| 2019 | 166 | New Model | 1.43 | 1.26 |
| 2019 | 182 | Old Model | 1.67 | 1.53 |
| 2019 | 182 | New Model | 1.6 | 1.4 |

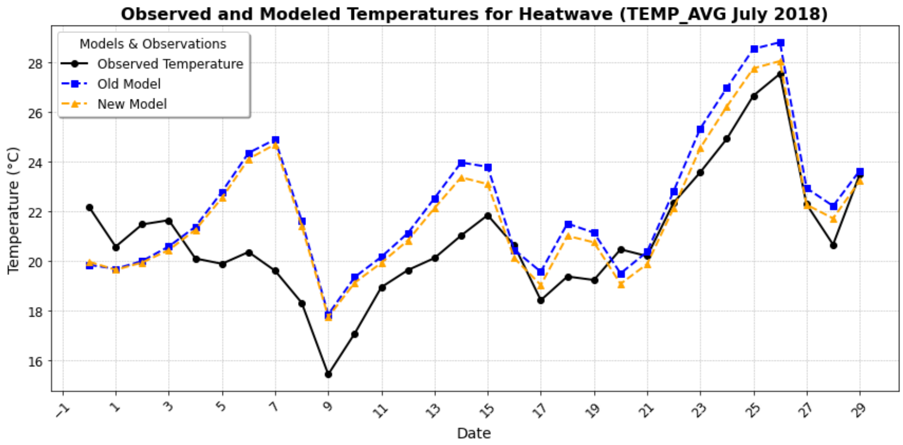


**Figure 5.1:** Domain-average Temperatures Time series for the Heatwave 2018.

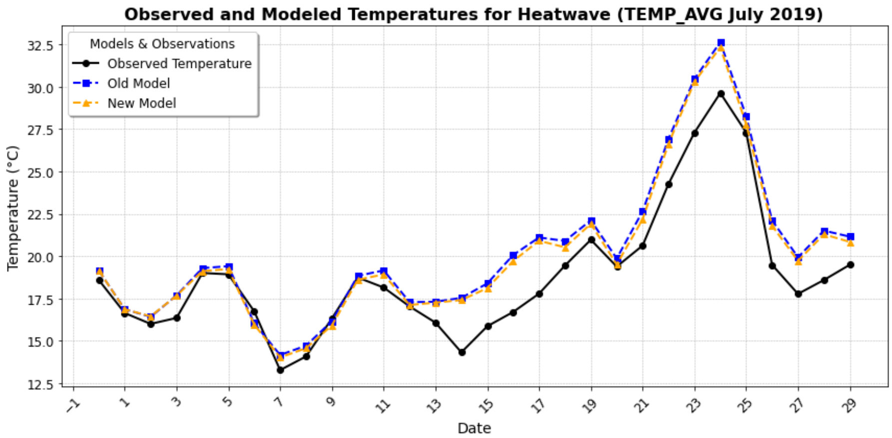


**Figure 5.2:** Domain-average Temperatures Time series for the Heatwave 2019.

### 5.2.2 TEMP_MAX (Maximum Temperature)

#### 5.2.2.1 Overall model performance

Contrary to TEMP_AVG, the new model worsens TEMP_MAX simulations. In 2018, MAE increases from 1.79°C to 2.07°C, and MAB shifts from a modest overestimation (0.22°C) to a substantial one (1.16°C) indicating a significant worsening of daytime heating biases. A similar trend is observed in 2019, with MAE increasing from 1.83°C to 2.23°C, and MAB from 0.51°C to 1.52°C, further exacerbating daytime warming biases. The Mean Absolute Error (MAE) and Mean Absolute Bias (MAB) for TEMP_MAX for the old model (control) and the new model (experiment) configurations are presented in table 5.2, and figures 5.3 and 5.4 provide visual confirmation of these trends.

#### 5.2.2.2 Model performance by land cover

**Cropland 166**

For land cover type 166, the simulation of maximum temperature worsened with the updated parameters, consistent with the overall model performance. In 2018, the MAE increased from 1.81 °C in the old model (control) to 2.11 °C in the new model (experiment), and the MAB increased from 0.30 °C to 1.37 °C. In 2019, the MAE increased from 1.60 °C to 2.07 °C, and the MAB increased from 0.43 °C to 1.46 °C.

**Cropland 182**

For land cover type 182, the MAE showed a slight increase in 2018 (from 1.99 °C to 2.04 °C) but a substantial increase in MAB (from -0.22 °C to 0.63 °C). In 2019, the MAE increased from 2.01 °C to 2.23 °C, and the MAB increased from 0.33 °C to 1.32 °C.

**Table 5.2:** Mean Absolute Error (MAE) and Mean Absolute Bias (MAB) for average temperature (TEMP_MAX) in the ALARO-Surfex model for 2018 and 2019. The table compares the performance of the old model (control), and the new model (experiment) Values are presented for the overall model domain as well as for two dominant cropland types: cropland 166 (temperate crops) and cropland 182 (temperate pastures).

| Year | Land Cover | Model | MAE (°C) | MAB (°C) |
|---|---|---|---|---|
| 2018 | | Old Model | 1.79 | 0.22 |
| 2018 | | New Model | 2.07 | 1.16 |
| 2018 | 166 | Old Model | 1.81 | 0.3 |
| 2018 | 166 | New Model | 2.11 | 1.37 |
| 2018 | 182 | Old Model | 1.99 | -0.22 |
| 2018 | 182 | New Model | 2.04 | 0.63 |
| 2019 | | Old Model | 1.83 | 0.51 |
| 2019 | | New Model | 2.23 | 1.52 |
| 2019 | 166 | Old Model | 1.6 | 0.43 |
| 2019 | 166 | New Model | 2.07 | 1.46 |
| 2019 | 182 | Old Model | 2.01 | 0.33 |
| 2019 | 182 | New Model | 2.23 | 1.32 |

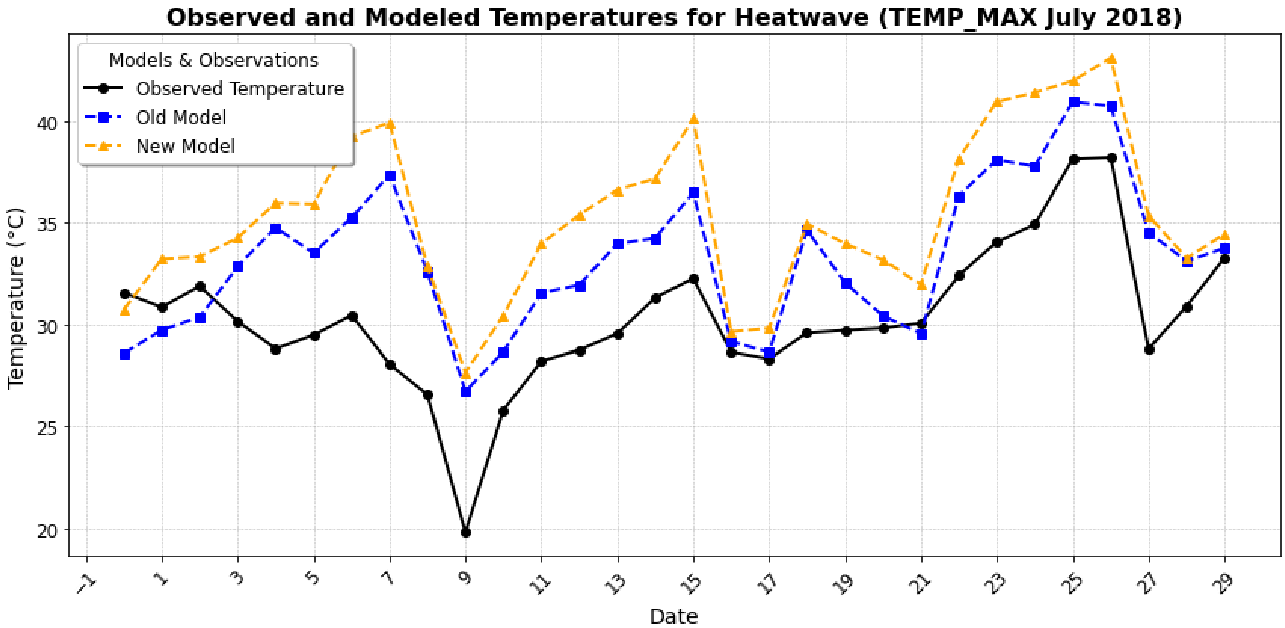


**Figure 5.3:** Maximum Temperatures Time series for the Heatwave 2018.

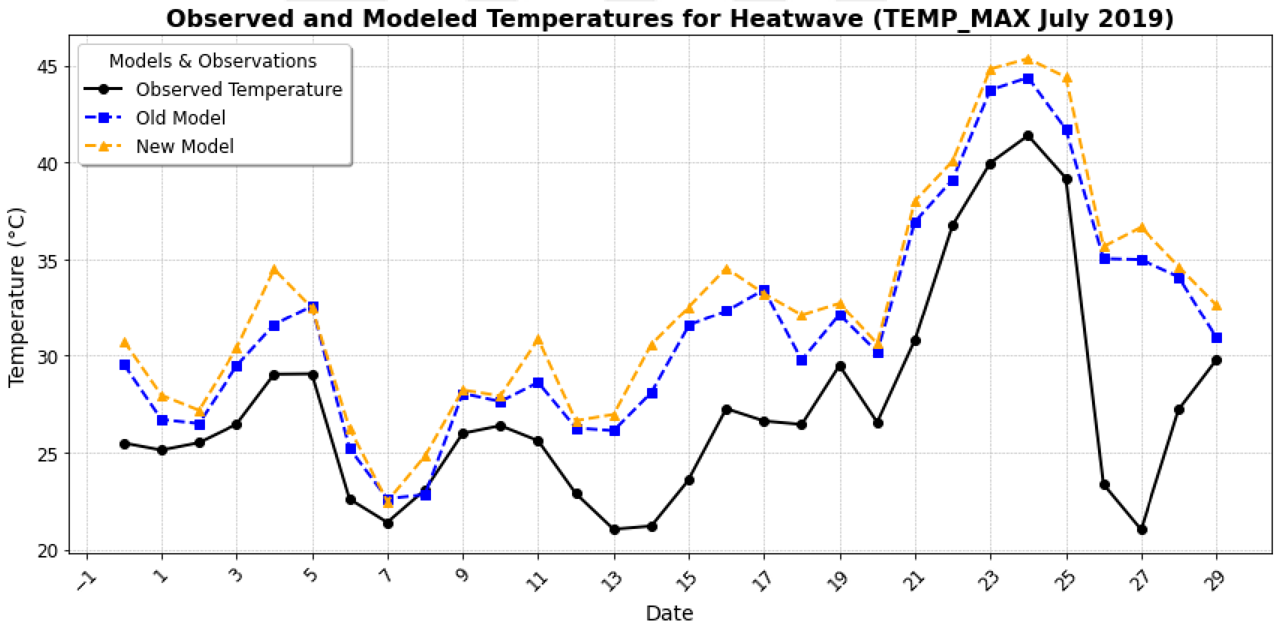


**Figure 5.4:** Maximum Temperatures Time series for the Heatwave 2019.

### 5.2.3 TEMP_MIN (Minimum Temperature)

#### 5.2.3.1 Overall model performance

The new model significantly improves TEMP_MIN simulations. In 2018, MAE is reduced from 2.52°C to 1.54°C, and MAB from 2.27°C to 0.33°C. In 2019, MAE drops from 2.21°C to 1.41°C, and MAB from 2.10°C to 0.74°C. The Mean Absolute Error (MAE) and Mean Absolute Bias (MAB) for TEMP_MIN for the old model (control) and the new model (experiment) configurations are presented table 5.3, and figures 5.5 and 5.6 provide visual confirmation of these trends.

#### 5.2.3.2 Model performance by land cover

**Cropland 166**

For land cover type 166, the updated parameters significantly improved the simulation of minimum temperature. In 2018, the MAE decreased from 2.33 °C in the old model (control) to 1.48 °C in the new model (experiment), and the MAB decreased from 2.10 °C to 0.28 °C. In 2019, the MAE decreased from 2.03 °C to 1.40 °C, and the MAB decreased from 1.81 °C to 0.50 °C.

**Cropland 182**

For land cover type 182, the simulation of minimum temperature also improved with the updated parameters. In 2018, the MAE decreased from 2.50 °C in the old model (control) to 1.55 °C in the new model (experiment), and the MAB decreased from 2.04 °C to -0.39 °C. The change in MAB from a positive to a negative value indicates a shift from overestimation to underestimation of minimum temperature for this land cover type. In 2019, the MAE decreased from 2.28 °C to 1.35 °C, and the MAB decreased from 2.22 °C to 0.63 °C.

**Table 5.3:** Mean Absolute Error (MAE) and Mean Absolute Bias (MAB) for average temperature (TEMP_MIN) in the ALARO-Surfex model for 2018 and 2019. The table compares the performance of the old model (control), and the new model (experiment) Values are presented for the overall model domain as well as for two dominant cropland types: cropland 166 (temperate crops) and cropland 182 (temperate pastures).

| Year | Land Cover | Model | MAE (°C) | MAB (°C) |
|---|---|---|---|---|
| 2018 | | Old Model | 2.52 | 2.27 |
| 2018 | | New Model | 1.54 | 0.33 |
| 2018 | 166 | Old Model | 2.33 | 2.1 |
| 2018 | 166 | New Model | 1.48 | 0.28 |
| 2018 | 182 | Old Model | 2.5 | 2.04 |
| 2018 | 182 | New Model | 1.55 | -0.39 |
| 2019 | | Old Model | 2.21 | 2.1 |
| 2019 | | New Model | 1.41 | 0.74 |
| 2019 | 166 | Old Model | 2.03 | 1.81 |
| 2019 | 166 | New Model | 1.4 | 0.5 |
| 2019 | 182 | Old Model | 2.28 | 2.22 |
| 2019 | 182 | New Model | 1.35 | 0.63 |

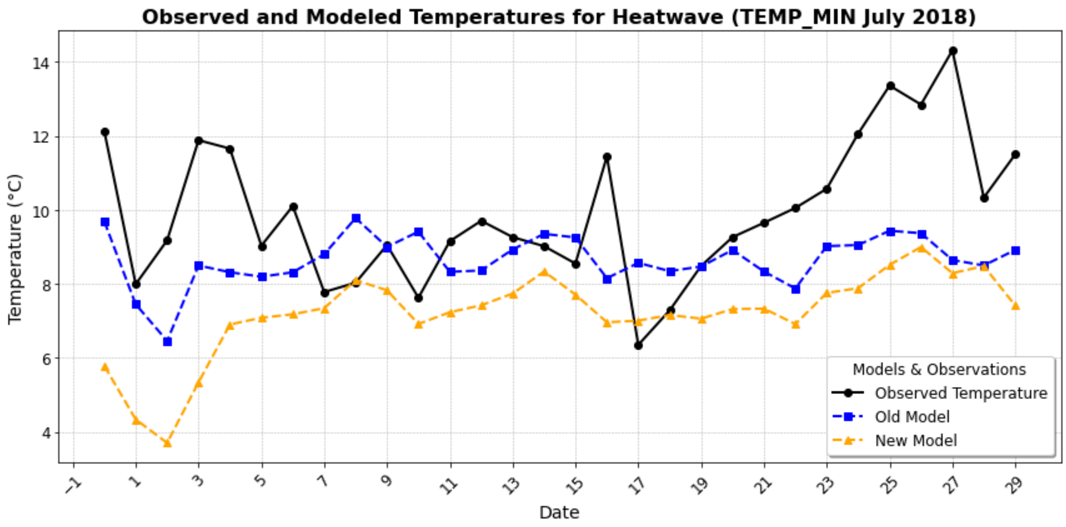


**Figure 5.5:** Minimum Temperatures Time series for the Heatwave 2018.

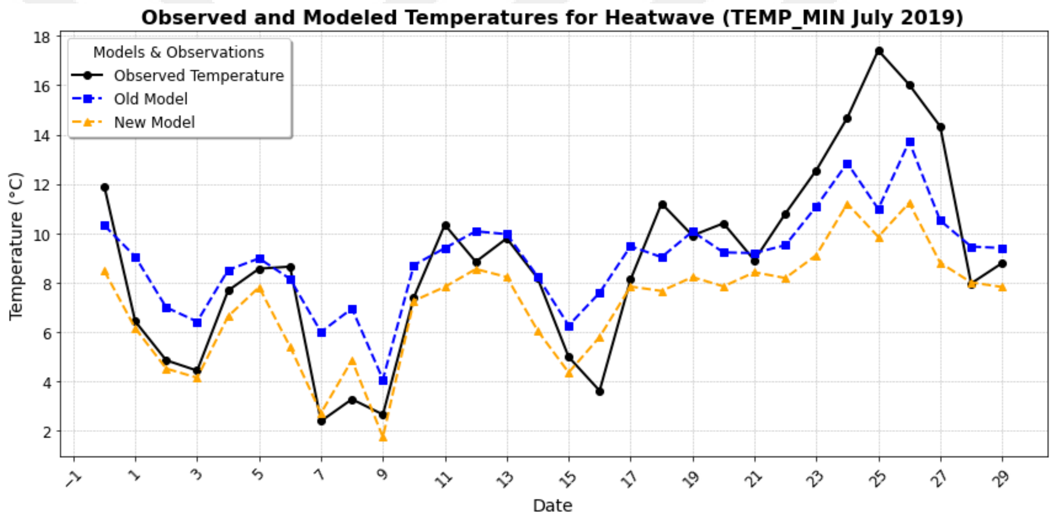


**Figure 5.6:** Minimum Temperatures Time series for the Heatwave 2019.

## 5.4 Model Validation Using ICOS Lonzée

To assess the performance of the model beyond the gridded domain analysis, an independent validation was conducted using observational data from the ICOS station at Lonzée for the month of July in 2018 and 2019. The validation focuses on comparing the performance of the old model (control) and the new model (experiment) configurations for three temperature metrics: Average Temperature (TEMP_AVG), Maximum Temperature (TEMP_MAX), and Minimum Temperature (TEMP_MIN). The validation was quantified using two standard metrics: Mean Absolute Error (MAE) and Mean Absolute Bias (MAB). The results are summarized in tables (5.4 to 5.6).

### 5.4.1 Interpretation of results for TEMP_AVG

For 2018, the new model (experiment) performs slightly better in MAE (2.11 °C vs. 2.15 °C) but performs worse in MAB (1.80 °C vs. 1.64 °C), which suggests an increase in systematic bias even though overall error is reduced. For 2019, both MAE and MAB are slightly worse with the new model, showing poorer performance. These results are opposite to the domain-wide test in which the new model consistently improved TEMP_AVG simulation. It would mean either that local circumstances at Lonzée could be non-representative of the larger model area, or that site-specific influences prevail. Figure 5.7 and 5.8 (Temperature Validation Against ICOS Lonzée Station – Daily Average Temperature) illustrates the time evolution of TEMP_AVG.

**Table 5.4:** Validation Results for TEMP_AVG - ICOS Lonzée Station.

| Year | Model | MAE (°C) | MAB (°C) |
|---|---|---|---|
| 2018 | Old Model | 2.15 | 1.64 |
| 2018 | New Model | 2.11 | 1.8 |
| 2019 | Old Model | 2.2 | 2.09 |
| 2019 | New Model | 2.33 | 2.21 |

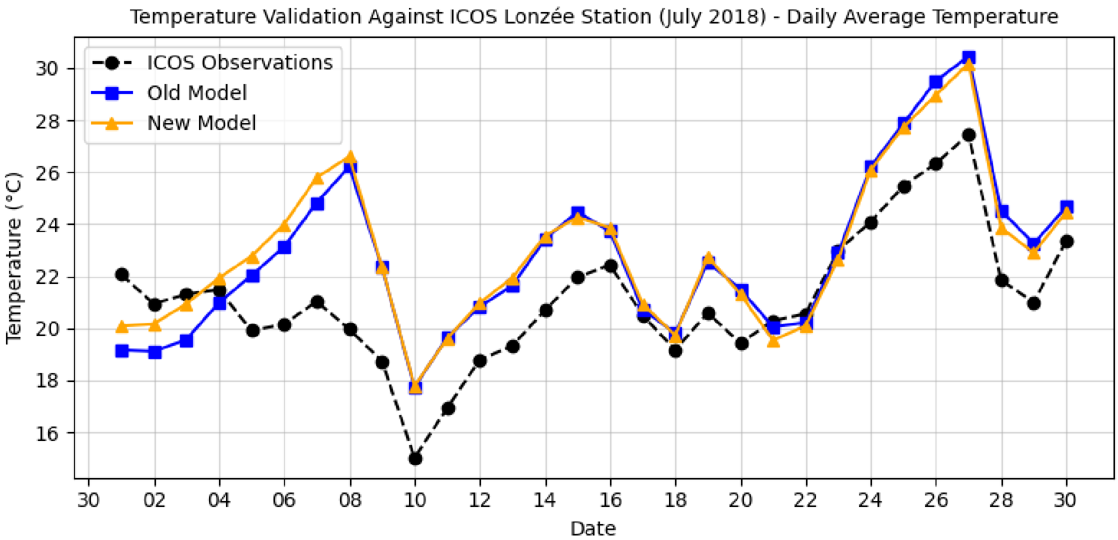


**Figure 5.7:** Temperature Validation Against ICOS Lonzée Station – Daily Average Temperature 2018.

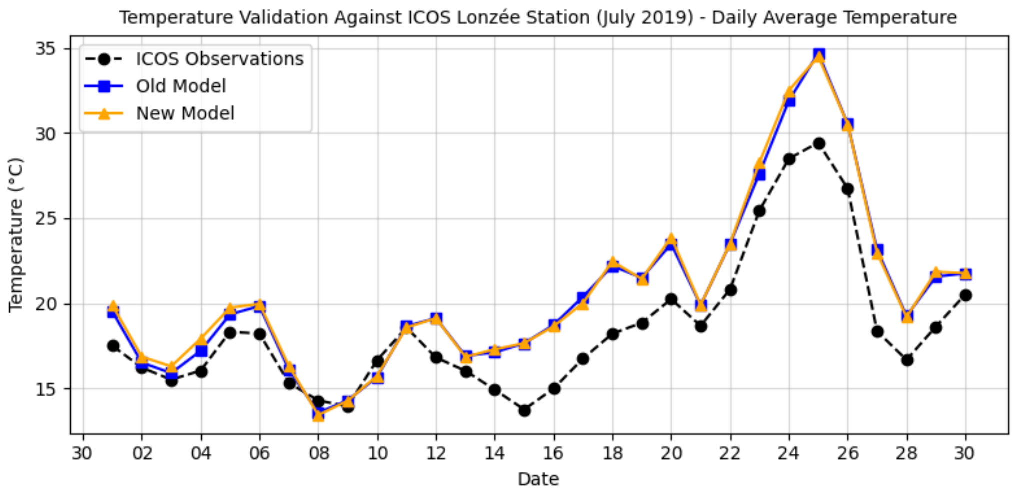


**Figure 5.8:** Temperature Validation Against ICOS Lonzée Station – Daily Average Temperature 2019.

### 5.4.2 Interpretation of results for TEMP_MAX

For maximum temperature, the validation clearly indicates performance deterioration with the new model (experiment) for both years. For 2018, MAE increased from 2.35 °C to 3.38 °C, and the MAB doubled, from 1.59 °C to 3.21 °C. This trend also occurred in 2019. These results support previous findings of the spatial bias analysis and confirm a systematic overestimation of maximum temperatures using the new model (experiment). This would mean that the new land surface parameters, most notably reduced albedo and LAI, most likely augmented the model's heat uptake and sensible heat flux and led to overheating during the day. Figure 5.9 and 5.10 (Temperature Validation with ICOS Lonzée Station – Daily MAX Temperature) shows the extreme daytime warming biases of the new model (experiment).

**Table 5.5:** Validation Results for TEMP_MAX - ICOS Lonzée Station.

| Year | Model | MAE (°C) | MAB (°C) |
|---|---|---|---|
| 2018 | Old Model | 2.35 | 1.59 |
| 2018 | New Model | 3.38 | 3.21 |
| 2019 | Old Model | 2.21 | 1.52 |
| 2019 | New Model | 3.16 | 2.83 |

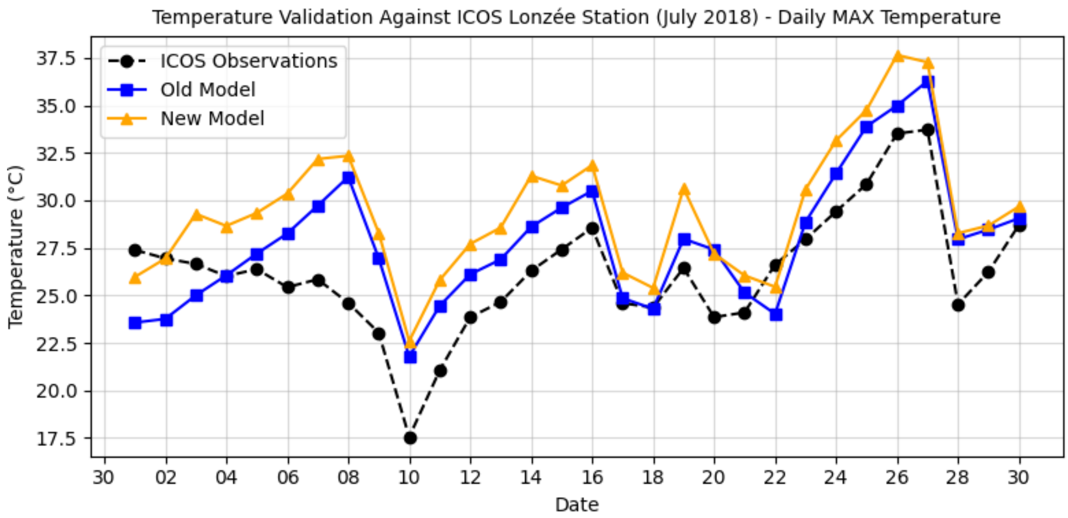


**Figure 5.9:** Temperature Validation Against ICOS Lonzée Station – Daily MAX Temperature 2018.

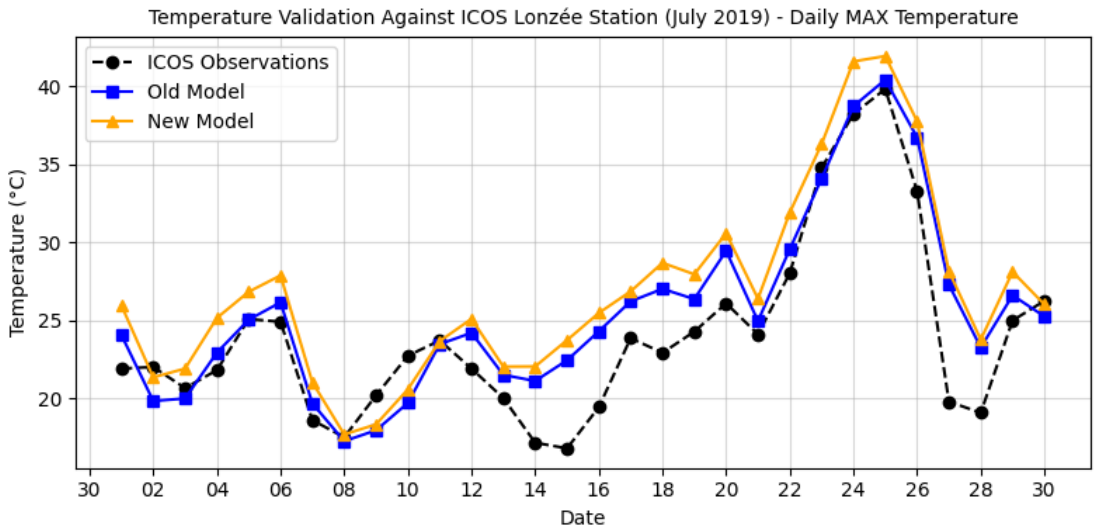


**Figure 5.10:** Temperature Validation Against ICOS Lonzée Station – Daily MAX Temperature 2019.

### 5.4.3 Interpretation of results for TEMP_ MIN

In contrast, minimum temperature performance was significantly improved by the new model (experiment). Both MAE and MAB decreased in both years. For instance, in 2018, MAE decreased from 2.28 °C to 1.77 °C, and MAB decreased significantly from 1.68 °C to 0.41 °C. This improvement is attributed to enhanced soil moisture dynamics, LAI-driven evapotranspiration, and increased night surface cooling processes in the new model (experiment) configuration. These results are totally in line with the domain-scale bias assessment, supporting the increased capture of nighttime temperature variability by the model. Figure 5.11 and 5.12 (Temperature Validation Against ICOS Lonzée Station – Daily MIN Temperature) shows that nighttime cooling processes were accurately represented by the new model, particularly during 2018. Differences did remain in 2019, which implies existing biases in evapotranspiration or soil moisture processes.

**Table 5.6:** Validation Results for TEMP_MIN - ICOS Lonzée Station.

| Year | Model | MAE (°C) | MAB (°C) |
|---|---|---|---|
| 2018 | Old Model | 2.28 | 1.68 |
| 2018 | New Model | 1.77 | 0.41 |
| 2019 | Old Model | 2.59 | 2.57 |
| 2019 | New Model | 1.91 | 1.67 |

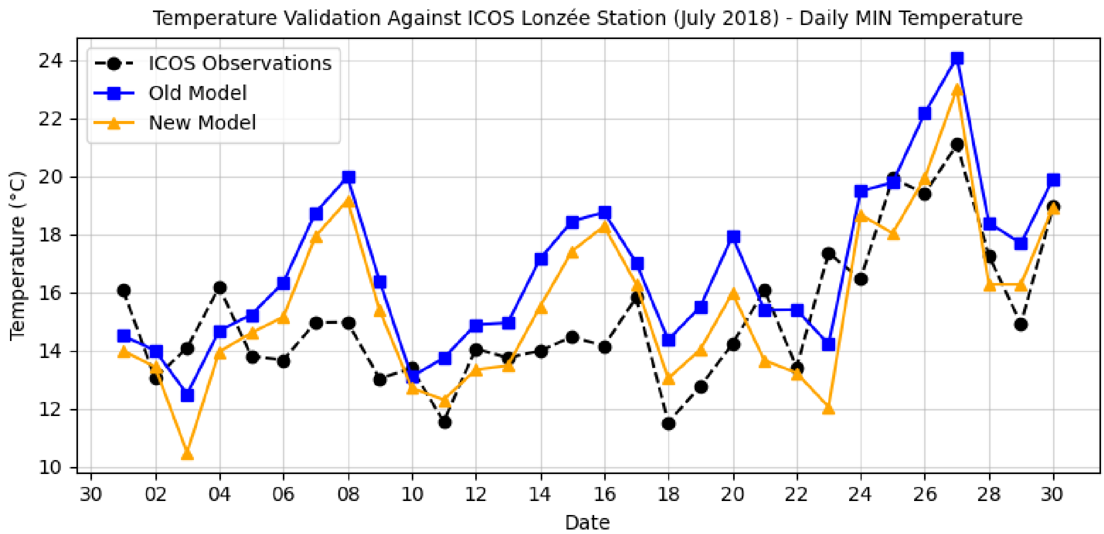


**Figure 5.11:** Temperature Validation Against ICOS Lonzée Station – Daily MIN Temperature 2018.

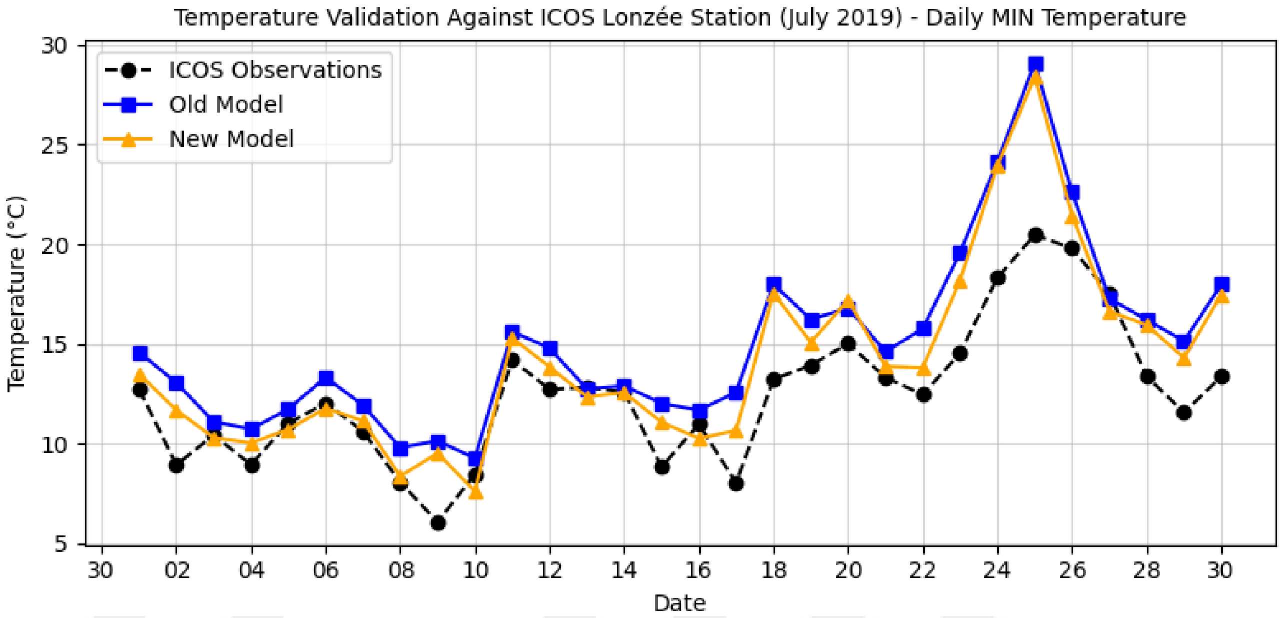


**Figure 5.12:** Temperature Validation Against ICOS Lonzée Station – Daily MIN Temperature 2019.

### 5.5 Albedo, LAI, and Temperature Relationships

This subsection presents the comparison of the differences in albedo and Leaf Area Index (LAI) changes under the old model (control) and the new model (experiment) configurations, and their relationship with changes in mean, maximum, and minimum temperatures. These relationships are necessary to interpret the implications of new land-use properties for the simulation of heatwave conditions by the model.

Table 5.7 summarizes the differences in albedo, LAI, and temperature (TEMP_AVG, TEMP_MAX, TEMP_MIN) between the new (experiment) and old model (control) configurations for the overall model domain and for land cover types 166 and 182, for both 2018 and 2019. Spatial patterns of temperature differences are illustrated from figure 5.13 through figure 5.15.

**Table 5.7:** Summary of differences between variables of Albedo, LAI and Temperatures.

| Variable Difference | Year | Overall Model | Land Cover 166 | Land Cover 182 |
|---|---|---|---|---|
| Albedo | 2018 | -0.019 | -0.024 | -0.012 |
| Albedo | 2019 | -0.004 | -0.012 | 0.016 |
| LAI | 2018 | -1.582 | -1.601 | -1.833 |
| LAI | 2019 | -1.022 | -0.824 | -1.878 |
| Temperature (AVG) | 2018 | -0.391 | -0.267 | -0.577 |
| Temperature (AVG) | 2019 | -0.211 | -0.152 | -0.184 |
| Temperature (MAX) | 2018 | 0.742 | 1.086 | 0.809 |
| Temperature (MAX) | 2019 | 0.67 | 0.887 | 0.798 |
| Temperature (MIN) | 2018 | -1.673 | -1.709 | -2.307 |
| Temperature (MIN) | 2019 | -1.227 | -1.296 | -1.487 |

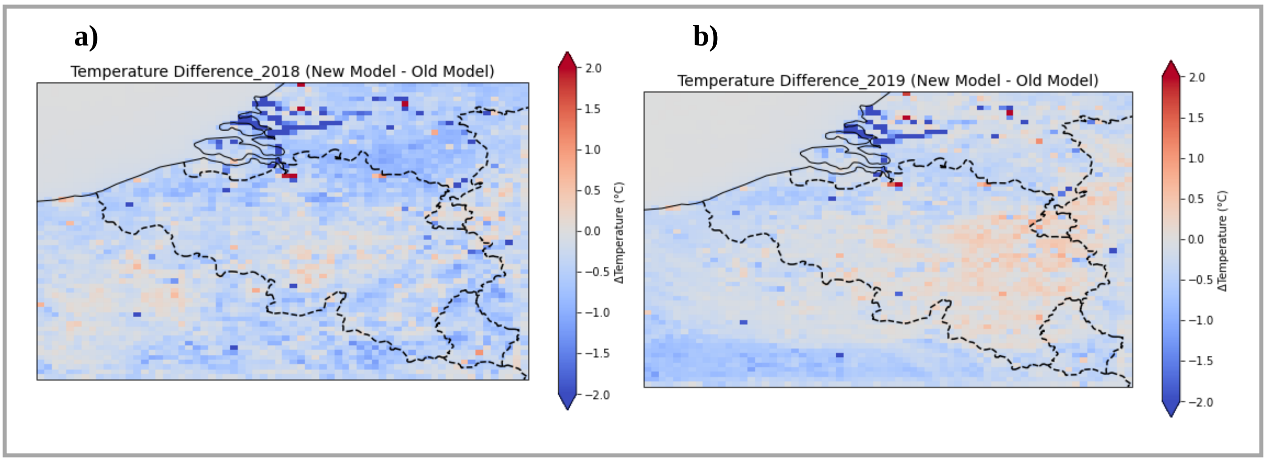


**Figure 5.13: a)** Average temperature difference July_2018 and **b)** Average temperature difference July_2019

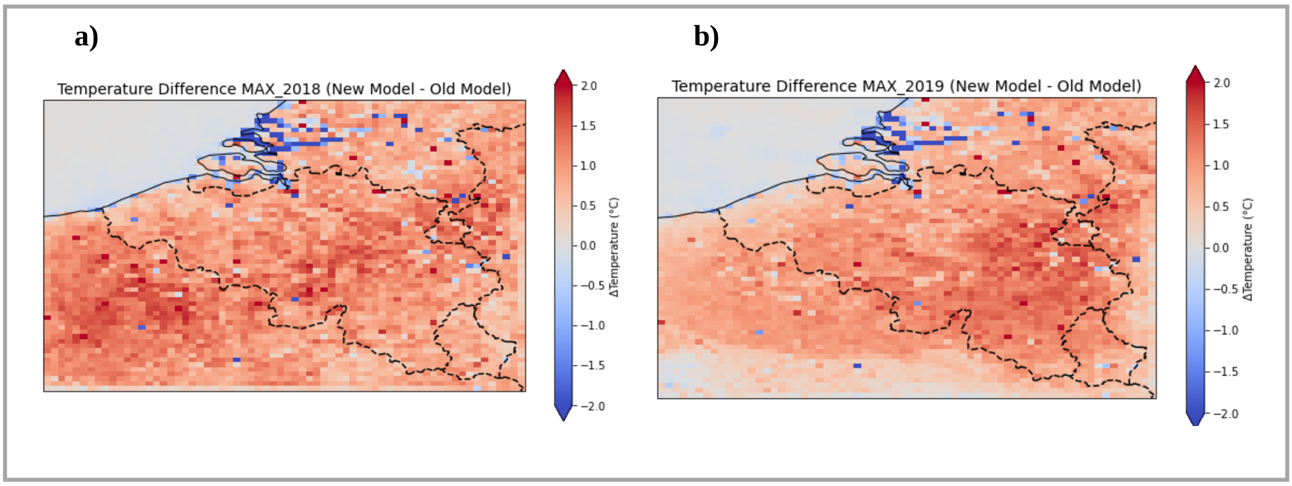


**Figure 5.14: a)** Maximum temperature difference 2018 for July and **b)** Maximum temperature difference 2019 for July.

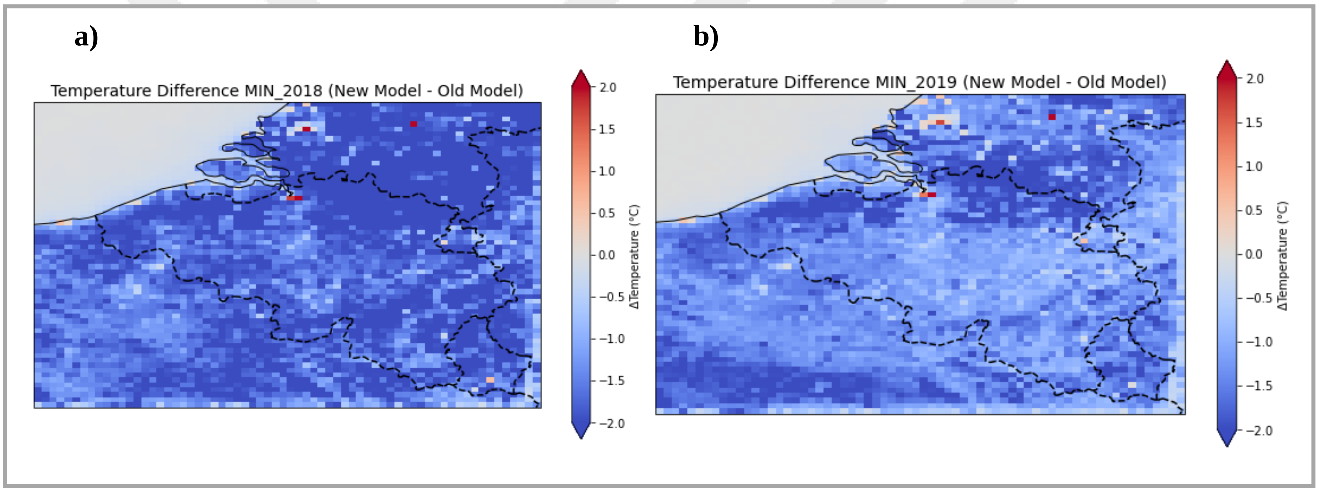


**Figure 5.15: a)** Minimum temperature difference 2018 for July and **b)** Minimum temperature difference 2019 for July.

### 5.5.1 Albedo–Temperature dynamics

Albedo, the fraction of solar radiation reflected by the surface, showed an overall decrease in 2018 (-0.019) and a smaller decline in 2019 (-0.004). These reductions suggest that more shortwave radiation was absorbed at the surface, likely contributing to daytime heating. This effect was especially evident for land cover 166, where albedo dropped significantly in both years (-0.024 in 2018 and -0.012 in 2019). Conversely, land cover 182 experienced a modest albedo decline in 2018 (-0.012), followed by an increase in 2019 (+0.016), reflecting year-to-year surface changes (Table 5.7).

Despite these reductions in reflectivity, the new model (experiment) results showed cooling in average temperature (TEMP_AVG): -0.391 °C in 2018 and -0.2112 °C in 2019 (Table 5.7). This pattern suggests that albedo alone does not fully explain the thermal response, especially since decreases in albedo would typically be expected to increase surface temperatures. The decoupling between albedo and TEMP_AVG implies that other processes (e.g., soil moisture retention, evaporative cooling, or changes in vegetation cover) may have compensated for the increased solar energy absorption.

In terms of maximum temperature (TEMP_MAX), however, the expected relationship between lower albedo and daytime warming was more evident. In 2018, TEMP_MAX increased by +0.7427 °C overall, with larger increases for land cover 166 (+1.086 °C) and 182 (+0.809 °C). In 2019, TEMP_MAX also increased across all land covers, though slightly less than 2018. The increase in daytime temperatures, especially for land cover 166 which experienced the sharpest albedo decline, supports the hypothesis that reduced albedo contributed to amplified surface heating during peak hours.

### 5.5.2 LAI–Temperature interactions

The Leaf Area Index (LAI), representing the amount of leaf surface area per unit ground area, also decreased notably in the new model (experiment). These reductions were consistent throughout both years, with a domain-wide drop of -1.58 in 2018 and -1.02 in 2019. The decreases were particularly pronounced for land cover 182 (-1.83 in 2018, -1.87 in 2019), while land cover 166 experienced slightly smaller LAI reductions.

Reductions in LAI may reduce shading and evapotranspiration, two key mechanisms for surface cooling, especially during the daytime. This shift could have contributed to the observed increase in TEMP_MAX in the experiment simulation compared to the control. However, when examined alongside the significant decrease in minimum temperatures (TEMP_MIN), it becomes clear that LAI changes influenced both daytime and nighttime thermal behavior. For instance, the reduction in LAI did not prevent substantial nighttime cooling: TEMP_MIN decreased by -1.67 °C in 2018 and -1.22 °C in 2019. The drop was most significant for land cover 182 in the year 2018 (-2.3074 °C). The extreme temperature decrease for land cover 182 in 2018 is reasonable keeping in mind its maximum LAI decrease of -1.8336 in the year 2018, indicating a maximum decrease in density of vegetation and, hence, canopy insulation. Though LAI decline for land cover 182 was also as large in 2019 (-1.8786), the smaller marked TEMP_MIN decline (-1.4876 °C) from 2018 is attributed to inter-annual variability of energy partitioning. Specifically, the sensible heat flux decline for land cover 182 was smaller in 2019 (9.0767 W/m²) compared to 2018 (13.6599 W/m²), indicating less transport of heat away from the surface and thus less nocturnal cooling intensity (Table 5.8). It can be attributed that the 2018-2019 disparity is caused by interannual vegetation fluctuation and differing intensities of drought, with spring 2018 being significantly drier.

### 5.5.3 Combined effects and spatial variability

Jointly, the simultaneous decrease in both albedo and LAI appears to have opposite effects on temperature extremes. In the daytime, decreased albedo and LAI decrease reflection and transpiration and therefore may have increased TEMP_MAX. At night, reduced LAI allows more radiative cooling and therefore lower TEMP_MIN.

The same result is also supported by the spatial differentiation between cropland types. Land cover 182, which had higher increases in albedo and more significant decreases in LAI in 2019, had smaller increases in TEMP_MAX but also less significant decreases in TEMP_MIN, compared to land cover 166.

These results highlight the nonlinear, complex interactions between land surface processes and temperature dynamics, particularly during heatwaves. Neither the magnitude nor the direction of temperature changes can be attributed to a single factor but instead are the outcome of interacting processes like radiation balance, vegetation structure, and soil moisture processes.

## 5.6 Surface Energy Balance Analysis

Surface energy balance is of utmost significance in the management of land–atmosphere interactions, specifically under extreme heat conditions. Alterations in land surface properties—albedo, LAI, and roughness—govern the partitioning of surface energy directly. This section explores the impact of these updates through intercomparisons of old (control) and new (experiment) model simulations to the major components of energy balance: shortwave radiation, net radiation, sensible heat flux, and latent heat flux, by land cover classes of both for the whole domain and cropland-specific classes (166 and 182). The following table 4.8 presents a summary of the differences among the components of surface energy balance between old model (control) and the new model (experiment) configurations for the entire model domain and for land cover classes 166 and 182 for years 2018 and 2019.

**Table 5.8:** Differences in Surface Energy Balance Components between Experiment and Control Simulations for July 2018 and July 2019**.** The values represent the change in simulated energy fluxes (in W/m²) when using updated MODIS-derived parameters (experiment) compared to the default Ecoclimap-I values (control) in the ALARO-Surfex model. Results are shown for the full domain (no land cover mask) and for regions dominated by Ecoclimap-I land cover types 166 and 182. Positive values indicate an increase in the experiment relative to the control.

| **Variable_ Difference** | **Year** | **Overall Model** | **Land Cover 166** | **Land Cover 182** |
|---|---|---|---|---|
| Shortwave_absorbed (W/m²) | 2018 | 2.26 | 2.08 | -0.33 |
| Shortwave_absorbed (W/m²) | 2019 | 1.28 | 3.39 | -2.57 |
| Shortwave_radiation_down (W/m²) | 2018 | -4.79 | -6.05 | -4.67 |
| Shortwave_radiation_down (W/m²) | 2019 | 0.35 | 0.02 | 2.25 |
| Shortwave_radiation_up (W/m²) | 2018 | -5.75 | -7.57 | -4.03 |
| Shortwave_radiation_up (W/m²) | 2019 | -1.01 | -3.03 | 4.77 |
| Net Radiation (W/m²) | 2018 | 5.12 | 6.65 | 5.06 |
| Net Radiation (W/m²) | 2019 | 0.58 | 2.19 | -8.68 |
| Sensible Heat flux (W/m²) | 2018 | 13.14 | 21.65 | 13.66 |
| Sensible Heat flux (W/m²) | 2019 | 10.34 | 16.84 | 9.07 |
| Latent Heat flux (W/m²) | 2018 | -8.20 | -14.27 | -7.69 |
| Latent Heat flux (W/m²) | 2019 | -11.04 | -15.31 | -18.52 |

### 5.6.1 Shortwave radiation balance

#### 5.6.1.1 Shortwave radiation absorbed

For both years, the new surface parameters induced changes in shortwave radiation absorption that compare well with the observed albedo differences. Since surface albedo is directly regulating the fraction of incoming solar radiation that is returned to the atmosphere, smaller albedo means increased absorption of shortwave radiation, and vice versa.

In 2018, the simulation of the experiment showed an increase in absorbed shortwave radiation over the domain (+2.26 $W/m^2$) and for land cover type 166 (+2.08 $W/m^2$). Both are in line with the significant reduction in albedo for cropland 166 (−0.024) as shown in table 5.8, and it is implied that the updated parameters reduced surface reflectivity and increased absorption of solar energy. In contrast, for land cover type 182, the shortwave radiation absorbed reduced by a small amount (−0.33 $W/m^2$) and is in line with smaller albedo reduction (−0.012) as showing in table 4.7, representing more cautious surface reflectivity behavior.

During 2019, absorbed shortwave radiation over domains increased by +1.28 $W/m^2$ with increased positive change over land cover 166 (+3.39 $W/m^2$) and a considerable decrease over land cover 182 (−2.57 $W/m^2$). Such variable behavior again indicates alterations in surface albedo: there was a moderate reduction (−0.012) in cropland 166, while albedo over land cover 182 increased (+0.016), meaning that more solar radiation is reflected and less is absorbed.

#### 5.6.1.2 Shortwave radiation downward

For 2018, the experiment simulation showed a systematic decrease in downward shortwave radiation for the control setup over the simulation, by −4.79 $W/m^2$ at the domain level, and similarly larger values over land cover 166 (−6.05 $W/m^2$) and 182 (−4.67 $W/m^2$). Though of modest amplitude, these reductions signal for possible indirect land surface-altered feedback mechanisms like enhanced surface warming that stabilizes the atmosphere or minimal boundary layer evolution changes that could impact cloud production and radiation transport.

In 2019, heterogeneities decreased. There was a small increase of +0.35 W/m² at the domain scale with very negligible variation by type 166 (+0.02 W/m²) and a slightly higher gain over type 182 (+2.25 W/m²). These small variations can be an indicator of interactions between changed land surface properties and locally prevailing atmospheric conditions. Although the physical settings of the model were not modified in terms of radiative forcing, the novel biophysical parameters (e.g., albedo, LAI, roughness) may alter cloud cover and radiative transfer indirectly by modifying land-atmosphere coupling processes.

#### 5.6.1.3 Shortwave radiation upward

For 2018, the updated land surface parameters resulted in a net decline in upward shortwave radiation throughout the domain (-5.75 W/m²) primarily over land cover category 166 (-7.57 W/m²). This reduction is a direct consequence of the reduction in surface albedo described above, because reducing albedo leads to reduced reflectance and, consequently, reduced outgoing shortwave radiation. The decline was smaller in land cover category 182 (-4.03 W/m²), which is less severe albedo loss for this class.

In 2019, the overall model still displayed a loss of upward shortwave radiation (-1.01 W/m²), with land cover type 166 still decreasing (-3.03 W/m²), consistent with its continued albedo decline. In contrast, land cover 182 also showed a distinct enhancement of upward shortwave radiation (+4.77 W/m²), which is in very good agreement with the observed increase in albedo of this land cover type in 2019. These observations reflect the direct and intimate relationship between surface albedo and surface albedo-aspect related reflected shortwave radiation in the surface energy balance.

#### 5.6.1.4 Net radiation

Net radiation, the net of incoming and outgoing radiation, generally increased in 2018 for the whole model (5.12 W/m²) and for each of the land cover categories (166: 6.65 W/m², 182: 5.06 W/m²). It is largely because of the decrease in upward shortwave radiation due to lower albedo.

In 2019, the net radiation overall increased slightly (0.58 W/m²), and land cover type 166 increased as well (2.19 W/m²). Land cover type 182 decreased greatly in net radiation (-8.68 W/m²), showing the complex interaction of changes in shortwave and longwave radiation for this land cover type.

### 5.6.2 Sensible heat flux

Sensible heat flux, or the exchange of heat between the ground surface and the atmosphere, rose dramatically with the revised parameters during both years, compared to the control simulation.

During the year 2018, the sensible heat flux increased by 13.14 W/m², noticeably in land cover type 166 (21.65 W/m²) and land cover type 182 (13.66 W/m²). In 2019, sensible heat flux increased by 10.34 W/m² with increases for land cover category 166 (16.85 W/m²) and land cover category 182 (9.07 W/m²). Sensible heat flux increase suggests further energy was emitted as heat into the atmosphere, which likely contributed to the increase in the highest temperatures outlined in the last section.

### 5.6.3 Latent heat flux

Latent heat flux, which is the transfer of heat through evapotranspiration, decreased with the updated parameters in both years. A reduction in latent heat flux often signals drier surface conditions and contributes to warming. In 2018, the overall latent heat flux decreased by -8.2 W/m², with decreases for land cover type 166 (-14.27 W/m²) and land cover type 182 (-7.69 W/m²).

During 2019, the overall latent heat flux decreased by -11.04 W/m² with land cover type 166 and land cover type 182 reductions by -15.31 W/m² and -18.52 W/m², respectively. Decrease in latent heat flux indicates diminishing evapotranspiration that is likely related to LAI decline resulting in a decline in vegetation cover and transpiration.

### 5.6.4 Energy budget component analysis

To further visualize the impact of the updated land-use parameters on the surface energy balance for monthly averages (July 2018 and 2019), figure 5.16, illustrates the differences (New Model (experiment) - Old Model (control)) in key energy budget components for the overall model domain during the heatwave periods of 2018 and 2019.

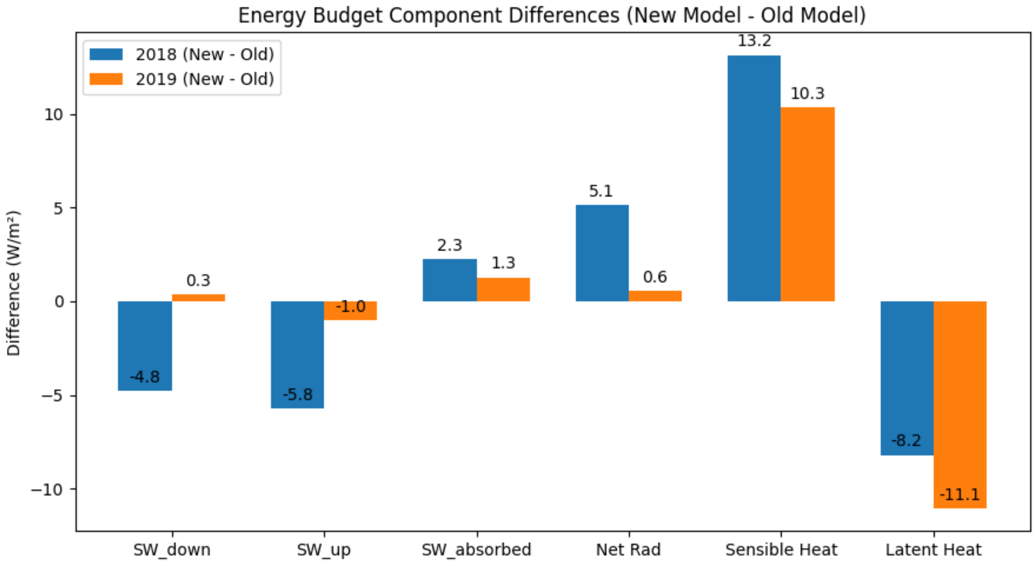


**Figure 5.16:** Different numbering from previous Energy Budget Component.

As shown in figure 5.16, shortwave radiation components have varied differently in terms of patterns. Downward shortwave radiation (SW_down) increased slightly during 2019 (approximately 0.3 W/m²) in the experiment compared to the control but, contrary to this, decreased very sharply during 2018 (approximately -4.8 W/m²). Upward shortwave radiation (SW_up) decreased in both years but decreased more sharply during 2018 (approximately -5.8 W/m²) than 2019 (approximately -1.0 W/m²). The absorbed shortwave radiation (SW_absorbed), one of the important factors for surface warming, showed an increase in both years (about 2.3 W/m² in 2018 and 1.3 W/m² in 2019), consistent with the overall decrease of albedo from the new model configuration.

Net radiation, the balance between incoming and outgoing radiation, also increased in the two years (by approximately 5.1 W/m² in 2018 and 0.6 W/m² in 2019). The increase means that the surface took in more net energy with the new land-use parameters.

Partitioning of this net radiation into different energy fluxes at the surface suggests extreme changes. Sensible heat flux, the heat that was transferred to the atmosphere, went up importantly in both the years (about 13.2 W/m² in 2018 and 10.3 W/m² in 2019). This rise implies that more of the net energy was being used to heat the air near the surface in the new model configuration.

Conversely, latent heat flux, that is, energy used for evapotranspiration, showed a decrease in both years (by about -8.2 W/m² for 2018 and -11.1 W/m² for 2019). This fall in latent heat flux suggests a decrease in rates of evapotranspiration within the new model, which might be due to the decreased values of LAI brought about by the new parameters of land-use.

The cancelling changes in sensible and latent heat fluxes are significant in understanding the impact on surface temperatures. Increased sensible heat flux likely contributed to increased maximum temperatures in the new model simulation and decreased latent heat flux implies decreased evaporative cooling from the surface.

### 5.7 Soil Moisture Analysis

Soil moisture plays a critical role in land-atmosphere interactions by influencing evapotranspiration, surface energy fluxes, and ultimately near-surface air temperatures. To assess the impact of updated land surface parameters in the new model (experiment), differences in soil moisture at two depths—1 cm (surface) and 10 cm (subsurface)—were analyzed for July 2018 and July 2019, across the entire domain and for two dominant cropland land cover types (EcoclimapI-1 classes 166 and 182).

The following table 5.9 summarizes the differences in soil moisture (New Model (experiment) - Old Model (control)) at 1 cm and 10 cm depths.

**Table 5.9:** Comparison variables differences result for the soil moisture.

| Variable Difference | Year | Overall Model | Land Cover 166 | Land Cover 182 |
|---|---|---|---|---|
| Soil Moisture (1 cm) ($m^3/m^3$) | 2018 | -0.0021 | -0.0088 | 0.0011 |
| Soil Moisture (1 cm) ($m^3/m^3$) | 2019 | -0.0048 | -0.0126 | -0.003 |
| Soil Moisture (10 cm) ($m^3/m^3$) | 2018 | 0.0043 | 0.0037 | 0.0002 |
| Soil Moisture (10 cm) ($m^3/m^3$) | 2019 | 0.0012 | -0.0009 | -0.0024 |

### 5.7.1 Surface soil moisture (1 cm Depth)

In 2018, the total change in 1 cm depth soil moisture from previous to current models was a marginal decline by -0.0021 m³/m³. Land cover type 166 decreased even more by -0.0088 m³/m³, and land cover type 182 increased by 0.0011 m³/m³. In 2019, decline in soil moisture at 1 cm depth was larger overall (-0.0048 m³/m³). Land cover type 166 again had the highest reduction (-0.0126 m³/m³), and land cover type 182 also decreased (-0.003 m³/m³). These trends suggest that LAI declines were the dominant factor in controlling surface soil moisture trends, particularly at 1 cm depth. Transpiration and shading reductions increase surface drying and sensible heat flux by reducing it. This effect is more pronounced at shallow depths like 1 cm, where soil moisture responds highly to short-term meteorological conditions and evapotranspiration rates.

Figure 5.17 illustrates the temporal evolution of soil moisture at 1 cm and 10 cm depths for the overall model domain during July 2018. The shaded areas represent the difference between the old model (control) and the new model (experiment) model configurations. At the 1 cm depth, the new model generally shows slightly lower soil moisture content throughout the month compared to the old model. Figure 5.18 shows the same for July 2019. Similar to 2018, the new model tends to simulate lower soil moisture at 1 cm depth for most of the heatwave period in 2019. The magnitude of the difference varies over time, suggesting a dynamic response to the evolving meteorological conditions and land surface interactions.

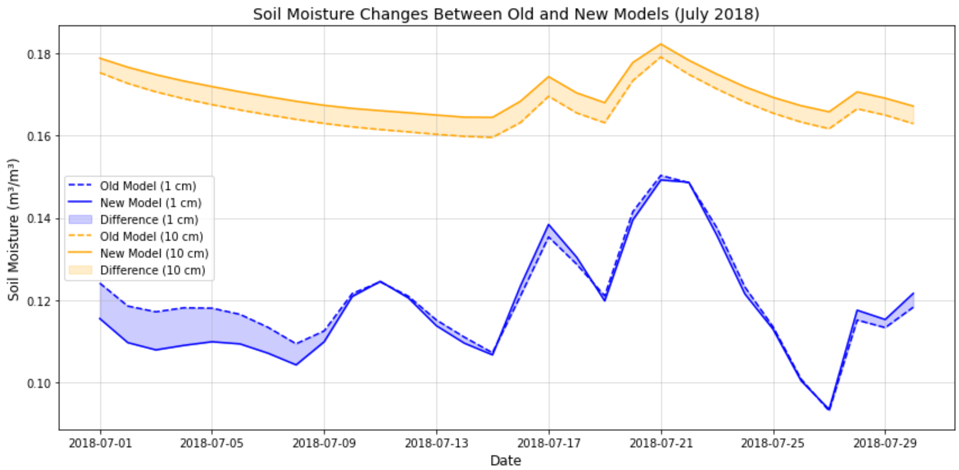


**Figure 5.17:** Temporal evolution of soil moisture at 1 cm and 10 cm depths for 2018.

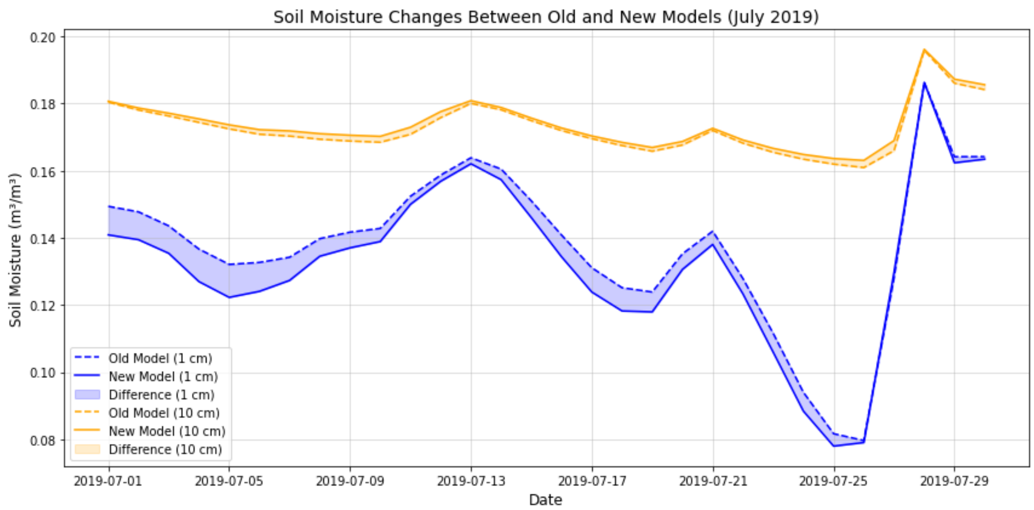


**Figure 5.18:** Temporal evolution of soil moisture at 1 cm and 10 cm depths for 2019.

These trends are visually confirmed in figure 5.19, which depict time series of soil moisture changes at 1 cm depth for July 2018 and 2019. In both years, the new model (experiment) consistently simulated lower shallow soil moisture compared to the old model (control). This drying effect contributed to reduced evapotranspiration and exacerbated daytime heating biases (TEMP_MAX).

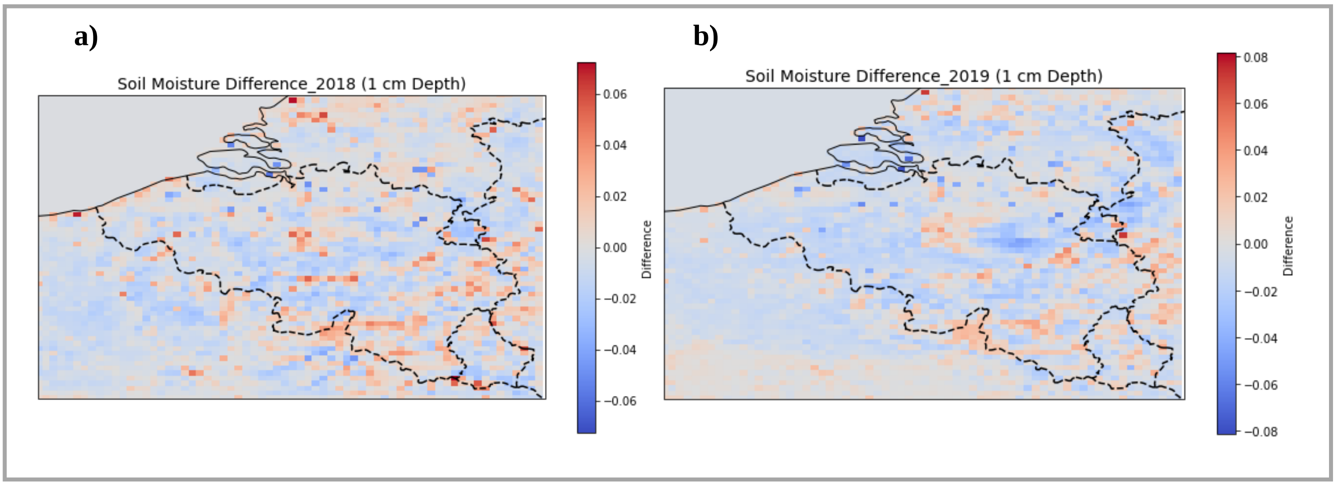


**Figure 5.19: a)** Soil moisture (1 cm) ($m^3/m^3$) difference_2018_July and b**)** Soil moisture (1 cm) ($m^3/m^3$) difference_2019_July.

### 5.7.2 Subsurface soil moisture (10 cm Depth)

At the 10 cm depth, the changes in soil moisture between the two model configurations show a different pattern. In 2018, the overall change was a slight increase by 0.0043 $m^3/m^3$. Land cover type 166 also saw a slight increase (0.0037 $m^3/m^3$), whereas land cover type 182 saw an extremely slight change (0.0002 $m^3/m^3$). In 2019, the overall change at 10 cm depth was a slight increase (0.0012 $m^3/m^3$). However, land cover type 166 reduced a little bit (-0.0009 $m^3/m^3$), and land cover type 182 reduced too (-0.0024 $m^3/m^3$).

Referring back to figures 5.17 and 5.18, variations at the 10 cm depth are generally less pronounced than at the 1 cm depth. At this depth, the new model in 2018 simulates somewhat greater soil moisture for most of the month, indicating that deeper soil layers retained more moisture despite surface drying. This suggests that the updated land-use parameters may have improved the representation of soil moisture dynamics at deeper layers, particularly during heatwave conditions. For 2019, the 10 cm depth variation is less regular in sign and magnitude throughout the month. This variability may result from more dynamic precipitation and atmospheric conditions that year or possibly due to differences in initial soil moisture and vegetation activity early in the season.

Soil moisture variations in spatial patterns at depth 10 cm are illustrated in figure 5.20. The figure illustrate that increased deeper soil moisture holding was greater in central Belgium in 2018. However, in 2019, local drying trends occurred, as an indication of interannual changes in soil water patterns.

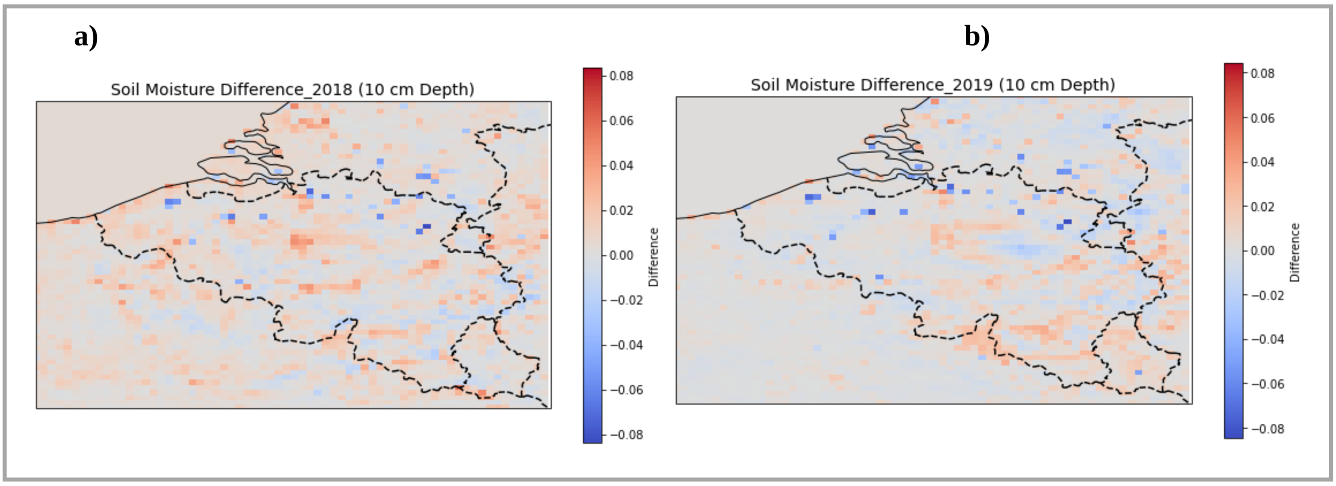


**Figure 5.20: a)** Soil moisture (10 cm) ($m^3/m^3$) difference 2018_July and **b)** Soil moisture (10 cm) ($m^3/m^3$) difference 2019_July.

# 6. DISCUSSION

This study analyzed the impact of incorporating observed land-use properties in the ALARO-Surfex model on heatwave simulation in Belgium in July 2018 and 2019. The result highlights the complex relationship between land surface parameters (LAI, albedo, roughness), surface energy balance components (sensible heat flux, latent heat flux, net radiation), soil moisture status, and their combined influences on temperature processes during heatwaves. The assessment verifies that revision of land-use parameters has significant implications for model performance, with significant improvements in some areas and unexpected degradations in others.

## 6.1 Impact of Land-Use Updates on Temperature Biases

### 6.1.1 Improvements in average temperatures (TEMP_AVG)

The new model demonstrated a significant improvement in the simulation of mean temperatures (TEMP_AVG), particularly in reducing random as well as systematic errors. Domain-average Mean Absolute Error (MAE) decreased from 2.04 °C in 2018 to 1.74 °C, while Mean Absolute Bias (MAB) improved from 1.62 °C to 1.24 °C. Similar, but less extreme, decreases were observed in 2019. All of these are evidence that the updated land-use parameterization is a better reflection of the overall thermal conditions during heatwaves.

The faster advance in 2018 over 2019 can be ascribed in part to differences in the nature of the two heatwaves. While 2018 was marked by protracted dryness and intense solar radiation, the 2019 heatwave was shorter in duration but more intense in maximum temperature (van der Wiel et al., 2020). This would have caused differences in the sensitivity of the surface energy balance to variations in land surface properties. At heatwave conditions, accurate simulation of vegetation cover (LAI) and surface reflectance (albedo) is required for accurate partitioning of the energy fluxes into sensible and latent heat. The new parameters, derived from satellite observations, must have been assisting in simulating these processes realistically, highlighting the significance of realistic land surface description at heatwaves. Minor variations in surface qualities can create enormous imbalances in thermal dynamics, especially under conditions of extremity.

These upgrades were particularly robust in land cover types dominated by agriculture (166 and 182). This highlights the importance of incorporating observed land-use properties into regional climate models, especially over agricultural areas, which are relatively dynamic and prone to abrupt alterations by human activity such as irrigation and crop rotation. Previous studies have shown that regions of crops are under-sampled in climate models due to heterogeneity and sensitivity to short-term change (e.g., Seneviratne et al., 2010). Our findings align with this literature and emphasize the need for more detailed and dynamic parameterization of crop regions.

### 6.1.2 Degradation in maximum temperatures (TEMP_MAX)

Although average temperatures improved, TEMP_MAX performance worsened in 2018 and 2019, particularly over cropland pixels. MAE worsened from 1.79 °C to 2.07 °C in 2018, with a shift in Mean Absolute Bias from 0.22 °C to 1.16 °C—a consistent overestimation of daytime highs.

This decline is likely linked to surface energy partitioning shifts. Reduced albedo in croplands (−0.024 in 2018 for class 166) resulted in higher shortwave absorption. In combination with reduced LAI (−1.60), which lowered evaporative cooling, the model simulated increased sensible heat flux (+21.65 W/m² for class 166) and reduced latent heat flux (−14.27 W/m²). These findings agree with Wilson et al. (2012), where they demonstrated that reduced vegetation and increased solar absorption can contribute to increased daytime temperatures.

This overestimaiton suggests that while realism is added by observed land-use inputs, they can also compound errors unless they are coupled with adaptive surface resistance or irrigation schemes. The severe heatwave conditions in both years—especially 2019, further stress-test the model's capacity to simulate extremes.

### 6.1.3 Improvements in minimum temperatures (TEMP_MIN)

In contrast to the performance for TEMP_MAX, the new model significantly enhanced its simulation of nighttime minimum temperatures (TEMP_MIN). In 2018, domain-average MAE decreased from 2.52 °C to 1.54 °C, and MAB dropped from 2.27 °C to 0.33 °C. Similar upgrades were observed in 2019. These results suggest that the new model better captures nocturnal land-atmosphere coupling processes, which are essential to accurately estimate the effects of heat stress. Some parameters most likely accounted for the upgrades, the improved simulation of soil moisture in the new model, particularly at the deeper layers (SM_3, +0.0043 $m^3/m^3$ in 2018 for crop type 166), most likely increased soil heat capacity. This allows the soil to store more daytime heat and release it more slowly during the night, moderating nighttime cooling and improving TEMP_MIN simulations. Besides, correlation analysis showed a moderate positive correlation between TEMP_MIN and 10 cm depth soil moisture (SM_3), which supports this explanation. These findings refer to the enhanced ability of the new model to capture nocturnal cooling procedures that are of crucial relevance to the assessment of heatwave impacts on vulnerable individuals. Previous studies emphasized the role of nighttime temperatures to enhance heat stress, particularly for elderly and urban populations (e.g., Fischer & Schär, 2010).

## 6.2 Surface Energy Balance Response to Land Surface Updates

The updated land surface characteristics induced substantial alterations in the surface energy balance, as evidenced by significant changes in radiative and turbulent fluxes.

### 6.2.1 Albedo and shortwave radiation absorption

Satellite-retrieved albedo values input produced a reduction in surface reflectivity, primarily in 2018 (-0.019), that led to an enhancement in absorbed shortwave radiation (+2.26 $W/m^2$). This negative relationship is strong and forms a fundamental part of the land surface energy budget (Wilson et al., 2012; Li et al., 2016). However, the thermal response to albedo perturbation was not uniformly warming across the domain.

Although the diminution in albedo typically translates to more solar energy absorption and subsequently more surface warming, the observed changes in temperature, especially TEMP_MIN, were less apparent. In other cases, minimum temperatures declined despite higher energy absorption, which suggests a buffer by other variables such as evapotranspiration and available soil moisture. These results highlight the complexity of land-atmosphere interactions, where the feedback to a single variable like albedo is buffered by coupling with vegetation and hydrology (Seneviratne et al., 2010).

Surprisingly, in 2019 albedo increased above type 182 land cover and decreased above type 166. Although the two opposite trends occurred, temperature biases still existed in the two cases, particularly for TEMP_MAX. This indicates that albedo alone cannot account for the observed thermal changes. Instead, the effect of meteorological conditions such as cloud cover, radiation regimes, and phenology of vegetation comes into play in regulating the net available energy at the surface (Ma et al., 2024).

### 6.2.2 Sensible and latent heat flux

The partitioning of net radiation into sensible and latent heat fluxes differed greatly in the new simulations. The 2018 simulation had a +13.14 $W/m^2$ increase in sensible heat flux, indicating more energy was being transferred into the atmosphere as heat. This likely contributed to the daytime temperature (TEMP_MAX) overprediction, especially in cropland areas where reduced LAI and drier soils diminished evaporative cooling.

The contribution of soil moisture constraints in augmenting SHF cannot be overstated. Soil moisture at 1 cm depth (SM_1) reduced by -0.0021 $m^3/m^3$ during the 2018 heatwave, which intensified the latent-to-sensible heat flux transition. This is consistent with studies by Fischer et al. (2007), where they concluded that soil moisture deficits experienced during heatwaves enhance surface warming through reduced evaporative cooling. For cropland 166, where soils are loamy with intermediate water-holding capacities, the combined low LAI and high soil moisture led to +21.65 $W/m^2$ SHF increases further exacerbating TEMP_MAX biases. In contrast, at the opposite extreme, for cropland 182, with higher clay content and deeper root zones, there was enhanced retention of moisture (+0.0011 $m^3/m^3$) that dampened SHF increases to +13.66 $W/m^2$. This identifies the influence of vegetation cover type and soil texture in modulating land-atmosphere feedback during heatwaves.

Simultaneously, latent heat flux decreased by -8.20 W/m², indicating less energy used by evapotranspiration processes. This decline can partially be attributed to lower LAI values, which reduce canopy transpiration, and by restricted soil moisture availability during heatwave periods. These findings agree with previous research showing that lower vegetation cover and dry soils have the consequence of elevating sensible heat fluxes, thereby enhancing surface warming (Fischer et al., 2007; Li et al., 2016).

Soil moisture also controls this partitioning by imposing a boundary condition on the energy availability. Surface soils dry rapidly under heatwaves, suppressing latent heat flux and increasing the proportion of energy to sensible heating.

The observed increases in sensible heat flux and reductions in latent heat flux highlight the critical role of land surface properties in modulating near-surface temperatures. These findings underscore the importance of accurate land-use parameterization for developing heatwave mitigation strategies, such as urban cooling initiatives and irrigation planning.

### 6.3 Impact of Land Surface Updates on Cropland Types 166 and 182

It exhibited various responses to new land surface parameters between the two predominant cropland classes in Belgium: Ecoclimap-I classes 182 (temperate pastures) and 166 (temperate crops). They express alterations in crop phenology, farming management practices, and soil properties governing land-atmosphere interaction during heatwaves.

#### 6.3.1 Definitions and characteristics of cropland types

Cropland 166 (Temperate Crops), which typically includes annual crops such as wheat, barley, and maize, which are intensively tilled with alternating planting and harvesting seasons. These crops have shallow rooting depths (0.5–1.5 m) and are also subject to soil water stress, particularly in flowering and grain-filling stages (Faggian, 2015). The soils in such a location are loamy with moderate water retention capacity. While cropland 182 (Temperate Pastures), the land cover type comprises perennial pastures and mixed forage crops, less intensively managed and with deeper root systems (1–2 m depth). Pastures possess higher leaf area index (LAI) during the summer as a result of growth throughout the year, enhancing evapotranspiration and soil water storage (Seneviratne et al., 2010). The soils are rich in clay, which has higher water-holding capacity compared to cropland 166.

### 6.3.2 Mechanistic explanations for observed differences

#### 6.3.2.1 Albedo and energy partitioning

166 Cropland had a larger albedo reduction (-0.024 in 2018) compared to Cropland 182 (-0.012), leading to higher absorption of shortwave radiation and solar heating during daytime (Table 9). This is in agreement with studies by Wilson et al. (2012), who found that bare soil exposure after harvest in annual crops lowers albedo and increases sensible heat flux. Cropland (182) had higher cover levels, which minimized the fluctuations in albedo.

#### 6.3.2.2 LAI and evaporative cooling

The reduction in LAI was more pronounced in cropland 182 (-1.83 in 2018), while this class showed better nighttime cooling (TEMP_MIN reduced by -2.31°C) due to higher residual soil moisture (SM_1: +0.0011 $m^3/m^3$) and latent heat flux (LHF: -7.70 $W/m^2$). This suggests that deeper-rooted pasture sustained evapotranspiration longer during drought periods, as also found by Hirschi et al. (2011). 166 Cropland, having lower LAI and soil water, experienced increased daytime warming (TEMP_MAX increased by +1.09°C) due to reduced shading and evaporative cooling.

#### 6.3.2.3 Soil moisture dynamics

The 10 cm cropland 166 soil layer contained slightly more water (+0.0037 $m^3/m^3$) in 2018, perhaps due to reduced evapotranspiration from the preceding crop senescence. This was not sufficient to negate day heating as shallow-rooted crops could not access deeper soil reserves. Cropland (182) utilized deeper soil water, buffering temperature extremes (Table 11).

### 6.3.3 Crop-Specific responses to heat and drought

The overestimation of maximum temperatures (TEMP_MAX) in cropland 166 aligns with findings by Li et al. (2016), which highlight how heatwaves amplify temperature biases in regions characterized by low Leaf Area Index (LAI) and soil moisture. In such areas, the lack of plant cover and low ground moisture decrease evaporative cooling and consequently increase daytime warming. Irrigation, but not replicated in this study, might be able to mitigate such effects, as Cui et al. (2023) demonstrated. On the other hand, the increased simulation of minimum temperatures (TEMP_MIN) for field 182 is due to the "buffering" effect of permanent vegetation, having greater humidity and soil moisture content. This trend, to which Napoly et al. (2017) referred, indicates the effect of vegetation structure on night-time cooling as well as the importance of land cover type in temperature dynamics during heatwaves.

### 6.4 Disaster Risk Reduction and Climate Adaptation Strategies

Heatwaves are increasingly recognized as one of the most significant climate-related hazards, posing risks to human health, agricultural productivity, energy systems, and urban infrastructure (IPCC, 2021; Caluwaerts et al., 2020). The findings of this study demonstrate the potential of incorporating observed land-use properties into regional climate models like ALARO-SURFEX to improve the accuracy of heatwave simulations. These advancements have direct implications for disaster risk reduction (DRR) and climate adaptation strategies, particularly in densely populated urban areas and agriculturally productive regions such as Belgium.

#### 6.4.1 Heatwave risk Assessment and early warning Systems

Effective disaster risk reduction begins with good risk estimation, founded on good climate models to predict extreme heat events. New land-use parameter advances in minimum temperature (TEMP_MIN) simulation highlight the importance of upper-level modeling in calculating exposed populations and areas. For instance, model outputs' high-resolution heat maps can be utilized to inform early warning systems by enabling stakeholders to issue timely warnings during heatwaves (UNDRR, 2015). Early warning systems play a critical role in reducing exposure and vulnerability, particularly among elderly people, individuals with existing illnesses, and low-income households who are likely to lack access to cooling facilities (WHO, 2023).

Moreover, the deterioration in maximum temperature (TEMP_MAX) simulations observed is further evidence that there is a need for further advancements in modeling techniques to assist in ensuring that all aspects of heatwaves' dynamics are represented well. Enhancing these constraints would enhance early warning systems, with the potential to save lives and assist in reducing economic losses over episodes of extreme heat.

### 6.4.2 Urban planning and infrastructure resilience

Cities are most susceptible to heatwaves due to the urban heat island (UHI) effect, which enhances intense temperatures in cities (Oleson et al., 2015). The findings of this study are useful for urban planners to use in decision-making on planning heat-resilient cities. For example, increasing vegetative cover—represented by higher Leaf Area Index (LAI) values—can alleviate surface temperatures through promoting shading and evapotranspiration. Similarly, applying reflective surfaces (higher albedo) over pavements and rooftops can potentially reduce solar radiation absorption and thereby mitigate the impacts of UHI (Wang et al., 2021).

The advanced simulation of dynamics of sensible heat flux (SHF) further emphasizes the integration of land surface features in urban planning models. Identification of urban grids with SHF can help planners aim interventions such as planting green cover, efficient water use, and developing energy-efficient infrastructure. Such interventions, apart from enhancing urban heatwave resilience, also contribute to overall sustainability goals, including reducing carbon emissions and conserving water resources.

### 6.4.3 Agricultural adaptation and water resource management

Agricultural crops are particularly susceptible to heatwaves, which can lead to crop failure, yield loss, and water requirement for irrigation (Lobell et al., 2011). The findings of this study, particularly the enhanced representation of soil moisture dynamics, have practical implications for agricultural adaptation strategies. For instance, the presence of adequate root zone moisture (as represented by the vertical agreement between SM_1 and SM_3) plays a significant role in preventing heat stress for crops during excessive heat (heatwaves).

Still another sector that would need improved heatwave simulations is water resources management. The decrease in TEMP_MAX simulations, linked to improved sensible heat flux, makes integrated water resources management plans more essential. Decision-makers could then make informed decisions on water-saving infrastructure investments, promote efficient irrigation, and develop drought-resistant crops. These are initial steps towards food security and reducing heatwave-associated socioeconomic impacts on rural communities.

### 6.4.4 Policy implications and stakeholder engagement

The inclusion of observed land use data into regional climate models has enormous policy impacts for disaster risk reduction and climate adaptation. Policymakers can utilize the improved model outputs to guide evidence-based policy formulation for investment in early warning, community resilience, and cooling infrastructure. For example, precise temperature maps can be utilized to guide the siting of cooling centers to vulnerable and exposed urban communities.

Stakeholder engagement is key in translating scientific findings into successful policies. Multistakeholder forums, such as the European Climate Adaptation Platform (Climate-ADAPT), facilitate the sharing of knowledge between researchers, policymakers, and practitioners to ensure that adaptation is founded on up-to-date scientific insight (EEA, 2021). This study points towards the importance of including observed land-use data in regional climate models, highlighting the need for sustained investment in Earth observation systems and data-exchange initiatives.

# 7. CONCLUSION

## 7.1 Conclusion

This study investigated the impact of incorporating satellite-retrieved land-use properties into the ALARO-Surfex model on the simulation of heatwaves in Belgium during July 2018 and 2019. The study sought to examine how the updation of significant land surface parameters—Leaf Area Index (LAI), albedo, and roughness—impacts the ability of the model to simulate temperature dynamics, surface energy balance, and soil moisture variations during extreme heat events.

The results of this study depict the complex and sometimes counterintuitive effect of the revision of land-use parameters in regional climate models. While the incorporation of satellite-derived data resulted in improvement in the simulation of mean (TEMP_AVG) and minimum (TEMP_MIN) temperatures, it also resulted in the degradation of simulations of maximum temperature (TEMP_MAX).

Especially, the new scheme resulted in a reduction in Mean Absolute Error (MAE) and Mean Absolute Bias (MAB) of mean temperatures and thus enhanced overall thermal representation. Enhanced minimum temperature simulations result in greater precision in representing nighttime cooling processes, which is needed to represent heatwave-related heat stress. Such improvements are due to soil moisture, LAI, and radiative flux being represented better within the new scheme.

The study, however, showed a strong overestimation of maximum temperatures in the updated model. The bias was caused by changes in surface energy balance due to increased sensible heat flux and reduced latent heat flux resulting from reduced albedo and LAI in some areas. These changes reveal that the revised model, while it improved some features of the simulation, introduced biases in the surface partitioning of energy, which led to an overestimation of daytime warming.

The analysis of spatial and land cover change emphasized the importance of land cover heterogeneity in climate modeling at the regional scale. The different types of land cover, i.e., dominant crop fields (type 166) and crop types (type 182), reacted differently to the land-use parameter updates. This necessitates accurate and high-resolution data for land cover and parameterizations capable of capturing the unique behaviors and dynamics of different surface types.

Cross-validation with observation data at the ICOS Lonzée station overall supplemented the results on the entire domain, demonstrating improved simulation of minimum temperatures and the deterioration in simulation of the maximum temperatures. These discrepancies among station-specific outputs and the entire-domain means reinforce challenges in the process of validation for models as well as effects due to the vicinity of site conditions on performance in models.

Finally, this study illustrates that incorporating land-use features from satellite observations in regional climate models can fortify and destabilize different aspects of heatwave simulation. The outcome highlights adopting an equitable approach in model design relative to the optimal simulation of land surface processes, energy balance, and land surface heterogeneity for the enhancement of overall credibility and reliability of regional climate models for simulating severe weather conditions.

## 7.2 Implications for Disaster Management and Risk Reduction

The findings of this study have significant implications for disaster management, particularly concerning heatwave risk mitigation and climate adaptation policy. Sound heatwave simulations play a vital role in facilitating early warning systems, emergency preparedness planning, and urban planning strategies to reduce exposure and vulnerability to severe heat.

Improved minimum temperature (TEMP_MIN) simulations provide actionable insight to guide public health responses to heatwaves. For example, reliable overnight cooling forecasts can be utilized to target locations where the elderly and chronically sick may be at higher risk. Similarly, better representations of soil moisture dynamics provide valuable information for agricultural adaptation planning, including planning irrigation and planting drought-tolerant crop varieties.

Simultaneously, the overestimation of extreme temperatures (TEMP_MAX) highlights the need for further model sophistication to the extent that every aspect of heatwave mechanisms is adequately captured. Addressing these deficiencies would render the early warning system more reliable and allow anticipatory actions such as the provision of cooling centers and public health warnings to be taken.

Urban planners can apply the results of research in designing heat-resilient cities using practices such as increased vegetation, reflective surfaces, and water efficiency. For instance, higher Leaf Area Index (LAI) levels can lower surface temperatures by causing shading and evapotranspiration, and reflective materials (higher albedo) can reduce absorption of solar radiation, thereby alleviating urban heat island effects.

### 7.3 Future Work

Based on the findings of this study, several avenues for future research can be pursued to further improve the accuracy of heatwave simulations in regional climate models:

- **Improved Land Surface Parameterizations:**

  Improved land surface parameterization is needed to represent the dynamic interaction among vegetation, soil water content, and atmospheric fields. Improved simulations of heatwaves can be more credible through such improvements, thus facilitating disaster management interventions. For instance, high-fidelity descriptions of crop response to heat and dryness can be applied to inform agricultural adaptation, e.g., by optimizing the timing of irrigation and the planting of drought-resistant crops.

- **Long-Term Climate Change Projections:**

  This study focused on heatwave simulations for two specific years (2018 and 2019). Future research could extend the analysis to longer time periods and investigate the impact of land-use change on heatwave trends under future climate change scenarios. This would involve integrating projected changes in land cover, vegetation dynamics, and anthropogenic activities into the model to assess their combined effects on heatwave intensity and frequency.

- **Coupled Modeling:**

  A more comprehensive approach would involve coupling the regional climate model with other Earth system components, such as the hydrological model and the urban canopy model. This would allow for a more integrated representation of the interactions between the land surface, atmosphere, and urban areas, potentially leading to more accurate simulations of heatwave dynamics. For instance, hydrological models can improve predictions of water scarcity during heatwaves, while urban canopy models can enhance assessments of urban heat island effects.

## REFERENCES


**Andres-Anaya, P., Sanchez-Aparicio, M., Del Pozo, S., Lagüela, S., Hernández-López, D., & Gonzalez-Aguilera, D. (2024).** A new methodology for estimating surface albedo in heterogeneous areas from satellite imagery. Applied Sciences, 14(1), 75. https://doi.org/10.3390/app14010075

**Berckmans, D., De Troch, R., Giot, O., Deckmyn, A., Hamdi, R., & Termonia, P.** (2017). Reinitialized versus continuous regional climate simulations using ALARO-0 coupled to the land surface model SURFEXv5. Geoscientific Model Development, 10, 223–238. https://doi.org/10.5194/gmd-10-223-2017

**Berckmans, J.** (2018). Modelling land-atmosphere interactions: Impact of near future land use and climate change over Western Europe (Doctoral dissertation, University of Antwerp).

**Caluwaerts, S., Hamdi, R., Top, S., Lauwaet, D., Berckmans, J., Degrauwe, D., Dejonghe, H., De Ridder, K., De Troch, R., Duchêne, F., Maiheu, B., Van Ginderachter, M., Verdonck, M.-L., Vergauwen, T., Wauters, G., & Termonia, P.** (2020). The urban climate of Ghent, Belgium: A case study combining a high-accuracy monitoring network with numerical simulations. Urban Climate, 31, 100565. https://doi.org/10.1016/j.uclim.2019.100565

**Christensen, J. H., Carter, T. R., Rummukainen, M., & Amanatidis, G.** (2007). Evaluating the performance and utility of regional climate models: The PRUDENCE project. Climatic Change, 81(S1), 1–6. https://doi.org/10.1007/s10584-006-9211-6

**Cui, F., Hamdi, R., Kuang, W., Yang, T., He, H., Termonia, P., & De Maeyer, P**. (2023). Interactions between the summer urban heat islands and heat waves in Beijing during 2000–2018. Atmospheric Research, 291, 106813. https://doi.org/10.1016/j.atmosres.2023.106813

**Dee, D. P., Uppala, S. M., Simmons, A. J., Berrisford, P., Poli, P., Kobayashi, S., ... & Vitart, F.** (2011). The ERA-Interim reanalysis: Configuration and performance of the data assimilation system. Quarterly Journal of the Royal Meteorological Society, 137(656), 553–597. https://doi.org/10.1002/qj.828

**Didan, K.** (2015). MOD13A2 MODIS/Terra Vegetation Indices 16-Day L3

Global 1km SIN Grid V006. NASA EOSDIS Land Processes Distributed Active Archive Center. Accessed 2024-11-15 from https://doi.org/10.5067/MODIS/MOD13A2.006

**EEA** (European Environment Agency). (2021). *Adapting to climate change in Europe: 2021 update.* Climate-ADAPT. https://climate-adapt.eea.europa.eu/en

**Faggian, P.** (2015). Climate change projections for Mediterranean region with focus over Alpine Region and Italy. Journal of Environmental Science and Engineering B, 4, 482–500. https://doi.org/10.17265/2162-5263/2015.09.004

**Fang, H., et al.** (2013), Characterization and intercomparison of global moderate resolution leaf area index (LAI) products: Analysis of climatologies and theoretical uncertainties, J. Geophys. Res. Biogeosci., 118, 529–548, https://doi.org/10.1002/jgrg.20051.

**Fischer, E. M., Seneviratne, S. I., Vidale, P. L., Lüthi, D., & Schär, C.** (2007). Soil moisture–atmosphere interactions during the 2003 European summer heat wave. Journal of Climate, 20(20), 5081–5099. https://doi.org/10.1175/JCLI4288.1

**Giorgi, F and L. O. Mearns,** 1999: Introduction to special section: Regional climate modeling revisited. J. Geophys. Res., 104, 6335– 6352.

**Giorgi, F., & Gutowski, W. J.** (2015). Regional climate modeling: Status and perspectives. Annual Review of Environment and Resources, 40, 467–490. https://doi.org/10.1146/annurev-environ-102014-021217

**Giot, O., De Troch, R., Hamdi, R., Deckmyn, A., & Termonia, P. (**2014). Impact of using the surface scheme SURFEX within ALARO-0 for the ERA-INTERIM high-resolution dynamical downscaling over Belgium. 3rd Lund Regional-scale Climate Modelling Workshop Proceedings, 101–102.

**Gorelick, N., Hancher, M., Dixon, M., Ilyushchenko, S., Thau, D., & Moore, R.** (2017). Google Earth Engine: Planetary-scale geospatial analysis for everyone. Remote Sensing of Environment. https://doi.org/10.1016/j.rse.2017.06.031

**Hersbach, H., Bell, B., Berrisford, P., Hirahara, S., Horányi, A., Muñoz-Sabater, J., ... & Thépaut, J. N.** (2020). The ERA5 global reanalysis. Quarterly Journal of the Royal Meteorological Society, 146(730), 1999–2049. https://doi.org/10.1002/qj.3803

**Hirschi, M., Seneviratne, S., Alexandrov, V. et al** (2011). Observational evidence for soil-moisture impact on hot extremes in southeastern Europe. Nature Geosci 4, 17–21 https://doi.org/10.1038/ngeo1032

**Integrated Carbon Observation System (ICOS).** (2023). ICOS Atmospheric Station – Lonzée (BE-Lon). Belgium. Retrieved from https://www.icos-cp.eu

**IPCC** (2021). Climate Change 2021: The Physical Science Basis. https://www.ipcc.ch/report/ar6/wg1/

**Jin, Y., Schaaf, C. B., Woodcock, C. E., Gao, F., Li, X., Strahler, A. H., Lucht, W., & Liang, S.** (2003). Consistency of MODIS surface bidirectional reflectance distribution function and albedo retrievals: 2. Validation. Journal of Geophysical Research: Atmospheres, 108(D5), 4159. https://doi.org/10.1029/2002JD002804

**Karin van der Wiel et al** 2020 Environ. Res. Lett. 15 034050 https://doi.org/10.1088/1748-9326/ab7668

**Karin van der Wiel** ***et al*** 2020 *Environ. Res. Lett.* **15** 034050. https://doi.org/10.1088/1748-9326/ab7668

**Kornhuber, K., Coumou, D., Vogel, E., et al.** (2019). Amplified Rossby waves enhance risk of concurrent heatwaves in major breadbasket regions. Nature Climate Change, 10, 48–53. https://doi.org/10.1038/s41558-019-0637-z

**Kotlarski, S., Keuler, K., Christensen, O. B., Colette, A., Déqué, M., Gobiet, A., ... & Wulfmeyer, V.** (2014). Regional climate modeling on European scales: A joint standard evaluation of the EURO-CORDEX RCM ensemble. Geoscientific Model Development, 7(4), 1297–1333. https://doi.org/10.5194/gmd-7-1297-2014

**L.W. Davis, & P.J. Gertler**, Contribution of air conditioning adoption to future energy use under global warming, Proc. Natl. Acad. Sci. U.S.A. 112 (19) 5962-5967, https://doi.org/10.1073/pnas.1423558112 (2015).

**Li, D., T. Sun, M. Liu, L. Wang, and Z. Gao,** 2016: Changes in Wind Speed under Heat Waves Enhance Urban Heat Islands in the Beijing Metropolitan Area. J. Appl. Meteor. Climatol., 55, 2369–2375, https://doi.org/10.1175/JAMC-D-16-0102.1

**Lobell, David & Schlenker, Wolfram & Costa-Roberts, Justin.** (2011). Climate Trends and Global Crop Production Since 1980. Science (New York, N.Y.). 333. 616-20. 10.1126/science.1204531.

**Lucas-Picher, P., Boberg, F., Christensen, J. H., & Berg, P**. (2013). Dynamical downscaling with reinitializations: A method to generate fine-scale climate datasets suitable for impact studies. Journal of Hydrometeorology, 14(4), 1159–1174. https://doi.org/10.1175/JHM-D-12-063.1

**Ma, B., Ma, Y., Ma, W., Xie, Z., Han, C., & Wang, B**. (2024). Estimating the daily mean blue-sky land surface albedo on the Tibetan Plateau using convolutional neural network. International Journal of Digital Earth, 17(1). https://doi.org/10.1080/17538947.2024.2431621

**Masson, V., J. Champeaux, F. Chauvin, C. Meriguet, and R. Lacaze,** 2003: A Global Database of Land Surface Parameters at 1-km Resolution in

Meteorological and Climate Models. J. Climate, 16, 1261–1282, https://doi.org/10.1175/1520-0442(2003)16<1261:AGDOLS>2.0.CO;2

**Masson, V., Le Moigne, P., Martin, E., Faroux, S., Alias, A., Alkama, R., Belamari, S., Barbu, A., Boone, A., Bouyssel, F., Brousseau, P., Brun, E., Calvet, J.-C., Carrer, D., Decharme, B., Delire, C., Donier, S., Essaouini, K., Gibelin, A.-L., Giordani, H., Habets, F., Jidane, M., Kerdraon, G., Kourzeneva, E., Lafaysse, M., Lafont, S., Lebeaupin Brossier, C., Lemonsu, A., Mahfouf, J.-F., Marguinaud, P., Mokhtari, M., Morin, S., Pigeon, G., Salgado, R., Seity, Y., Taillefer, F., Tanguy, G., Tulet, P., Vincendon, B., Vionnet, V., and Voldoire, A.** (2013): The SURFEXv7.2 land and ocean surface platform for coupled or offline simulation of earth surface variables and fluxes, Geosci. Model Dev., 6, 929–960, https://doi.org/10.5194/gmd-6-929-2013

**Myneni, R., Knyazikhin, Y., Park, T.** (2015). MCD15A3H MODIS/Terra+Aqua Leaf Area Index/FPAR 4-day L4 Global 500m SIN Grid V006. NASA EOSDIS Land Processes Distributed Active Archive Center. Accessed 2024-11-15 from https://doi.org/10.5067/MODIS/MCD15A3H.006

**Napoly, A., Boone, A., Samuelsson, P., Gollvik, S., Martin, E., Seferian, R., Carrer, D., Decharme, B., & Jarlan, L.** (2017). The interactions between soil–biosphere–atmosphere (ISBA) land surface model multi-energy balance (MEB) option in SURFEXv8 – Part 2: Introduction of a litter formulation and model evaluation for local-scale forest sites. Geoscientific Model Development, 10, 1621–1644. https://doi.org/10.5194/gmd-10-1621-2017

**NASA LP DAAC.** (2024). MODIS/Terra Vegetation Indices (MOD13A2). https://lpdaac.usgs.gov/products/mod13a2v006/

**O Batelaan, F De Smedt, L Triest,** Regional groundwater discharge: phreatophyte mapping, groundwater modelling and impact analysis of land-use change, Journal of Hydrology, Volume 275, Issues 1–2, 2003,Pages 86-108, ISSN 0022-1694, https://doi.org/10.1016/S0022-1694(03)00018-0.

**Perkins-Kirkpatrick, S. E., & Lewis, S. C.** (2020). Increasing trends in regional heatwaves.NatureCommunications,11,3357.https://doi.org/10.1038/s41467-020-16970-7

**Rauscher, S. A., Coppola, E., Piani, C., & Giorgi, F.** (2010). Resolution effects on regional climate model simulations of seasonal precipitation over Europe. Climate Dynamics. 35(4), 685-704. /https://doi.org/10.1007/s00382-009-0607-6.

**Redon, E., Lemonsu, A., and Masson, V.** (2020): An urban trees parameterization for modeling microclimatic variables and thermal comfort conditions at street level with the Town Energy Balance model (TEB-SURFEX v8.0), Geosci. Model Dev., 13, 385–399, https://doi.org/10.5194/gmd-13-385-2020

**Román, M. O., Schaaf, C. B., Lewis, P., Gao, F., Anderson, G. P., Privette, J. L., et al**. (2010). Assessing the coupling between surface albedo derived from MODIS and the fraction of diffuse skylight over spatially characterized landscapes. Remote Sensing of Environment, 114(4), 738–760. https://doi.org/10.1016/j.rse.2009.11.014

**Royal Meteorological Institute of Belgium (MeteoBelgique).** (2024). Belgian Climate Grid. Retrieved from https://www.meteo.be

**Rummukainen, Markku.** (2010). State-of-the-art with regional climate model. Wiley Interdisciplinary Reviews: Climate Change. 1. 82 - 96. https://doi.org/10.1002/wcc.8

**Schaaf, C. B., Gao, F., Strahler, A. H., et al**. (2002). First operational BRDF, albedo and nadir reflectance products from MODIS. Remote Sensing of Environment, 83(1–2), 135–148. https://doi.org/10.1016/S0034-4257(02)00091-3

**Schaaf, C., Wang, Z.** (2015). MCD43A3 MODIS/Terra+Aqua BRDF/Albedo Daily L3 Global - 500m V006. NASA EOSDIS Land Processes Distributed Active Archive Center. Accessed 2024-11-15 from https://doi.org/10.5067/MODIS/MCD43A3.006

**Seneviratne, S. I., Corti, T., Davin, E. L., Hirschi, M., Jaeger, E. B., Lehner, I., Orlowsky, B., & Teuling, A. J.** (2010). Investigating soil moisture–climate interactions in a changing climate: A review. Earth-Science Reviews, 99(3-4), 125–161. https://doi.org/10.1016/j.earscirev.2010.02.004

**Seneviratne, Sonia & Lüthi, Daniel & Litschi, Michael & Schär, C.** (2006). Land-atmosphere coupling and climate change in Europe. Nature. 443. 205-9. https://doi.org/10.1038/nature05095

**Smet, Geert & Termonia, Piet & Deckmyn, Alex.** (2012). Added economic value of limited area multi-EPS weather forecasting applications. Tellus A. 64. https://doi.org/10.3402/tellusa.v64i0.18901

**Stewart, I. D., and T. R. Oke,** 2012: Local Climate Zones for Urban Temperature Studies. Bull. Amer. Meteor. Soc., 93, 1879–1900, https://doi.org/10.1175/BAMS-D-11-00019.1

**SURFEX Land Cover Classification** (2024): https://www.umrcnrm.fr/surfex/spip.php?article219

**Termonia, P., Fischer, C., Bazile, E., Bouyssel, F., Broˇzkov´ a, R., B´enard, P., Joly, A.,** 2018. The ALADIN System and its canonical model configurations AROME CY41T1 and ALARO CY40T1. Geosci. Model Dev. 11 (1), 257–281. https://doi.org/10.5194/gmd-11-257-

2018.

**Teuling, A. J., et al.** (2010). Contrasting response of European forest and grassland energy exchange to heatwaves. Nature Geoscience, 3(10), 722–727. https://doi.org/10.1038/ngeo950

**Top, S.** (2018). The impact of land cover on the urban heat island and its simulation: A case study using the MOCCA network in Ghent (Master's thesis, Ghent University). https://lib.ugent.be/catalog/rug01:002508620

**UNDRR** (United Nations Office for Disaster Risk Reduction). (2015). *Sendai Framework for Disaster Risk Reduction 2015–2030.*

**Van Heerwaarden, Chiel & Arellano, J. & Teuling, R..** (2010). Land-atmosphere coupling explains the link between pan evaporation and actual evapotranspiration trends in a changing climate. Geophysical Research Letters 2010 (2010) 37. 37. https://doi.org/10.1029/2010GL045374.

**Wang, J., Chen, Y., Liao, W. et al**. (2021). Anthropogenic emissions and urbanization increase risk of compound hot extremes in cities. Nat. Clim. Chang. 11, 1084–1089 https://doi.org/10.1038/s41558-021-01196-2

**WHO (World Health Organization).** (2023). A framework for the quantification and economic valuation of health outcomes originating from health and non-health climate change mitigation and adaptation action. ISBN 978-92-4-005791-3

**Wilson, T., Meyers, T., Kochendorfer, J., Anderson, M., & Heuer, M.** (2012). The effect of soil surface litter residue on energy and carbon fluxes in a deciduous forest. Agricultural and Forest Meteorology, 161, 134–147. https://doi.org/10.1016/j.agrformet.2012.03.011

**Xue Y, Janjic Z, Dudhia J, Vasic R, De Sales F** (2014) A review on regional dynamical downscaling in intraseasonal to seasonal simulation/prediction and major factors that affect downscaling ability. Atmos Res 147:68–85. https://doi:10.1016/j.atmosres.2014.05.001

**Zscheischler, J., Westra, S., van den Hurk, B. J. J. M., et al.** (2018). Future climate risk from compound events. Nature Climate Change, 8(6), 469–477. https://doi.org/10.1038/s41558-018-0156-3

**Zsebeházi, G., & Mahó, S. I.** (2021). Assessment of the urban impact on surface and screen-level temperature in the ALADIN-Climate driven SURFEX land surface model for Budapest. Atmosphere, 12(6), 709. https://doi.org/10.3390/atmos12060709

**Zsebeházi, G., & Szépszó, G.** (2020). Modeling the urban climate of Budapest using the SURFEX land surface model driven by the ALADIN-

Climate regional climate model results. IDŐJÁRÁS/Quarterly Journal of the Hungarian Meteorological Service, 124(2), 191–207. https://doi.org/10.28974/idojaras.2020.2.3

# APPENDICES

## APPENDIX A: SUPPLEMENTARY FIGURES TO CHAPTER 4

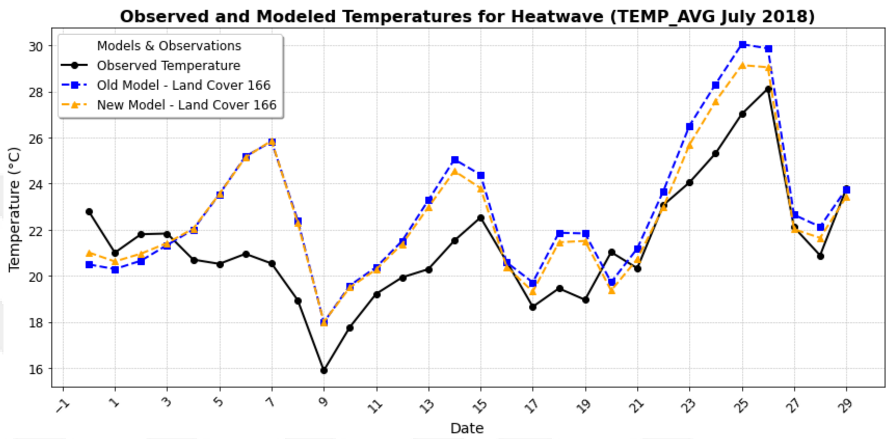


**Figure A.1:** Average Temperatures °C Time series Applying Land Cover Type 166 for the Heatwave 2018.

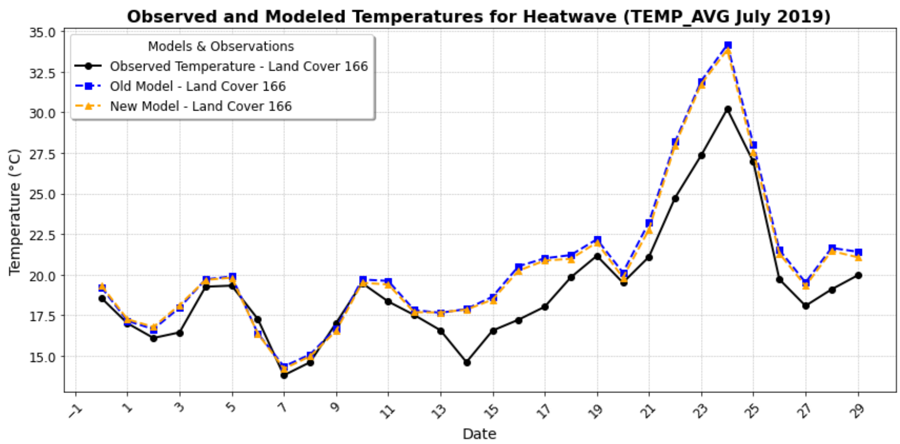


**Figure A.2:** Average Temperatures °C Time series Applying Land Cover Type 166 for the Heatwave 2019.

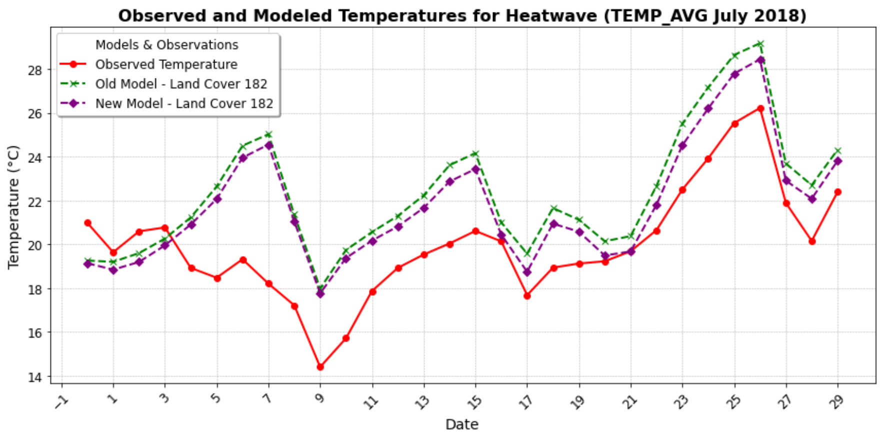


**Figure A.3:** Average Temperatures °C Time series Applying Land Cover Type 182 for the Heatwave 2018.

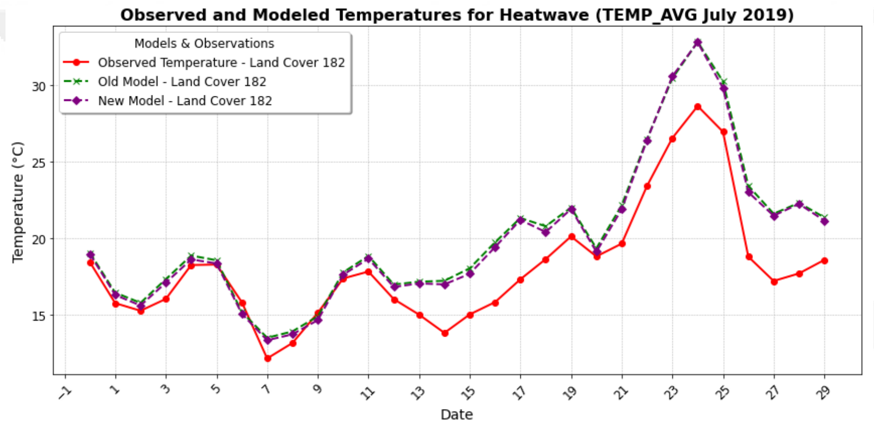


**Figure A.4:** Average Temperatures °C Time series Applying Land Cover Type 182 for the Heatwave 2018.

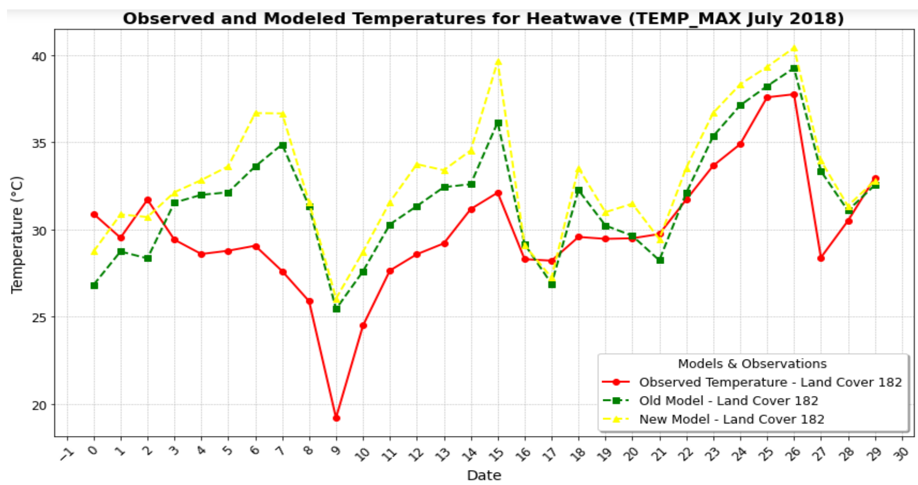


**Figure A.5:** Maximum Temperatures °C Time series Applying Land Cover Type 182 for the Heatwave 2018.

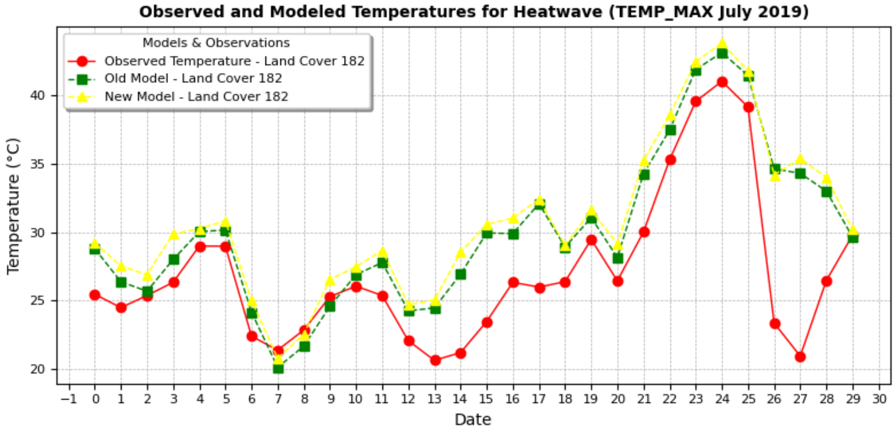


**Figure A.6:** Maximum Temperatures °C Time series Applying Land Cover Type 182 for the Heatwave 2019.

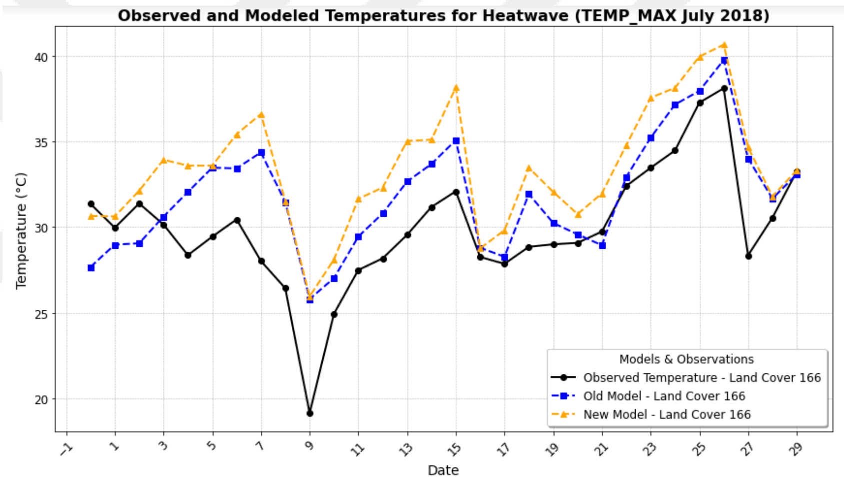


**Figure A.7:** Maximum Temperatures °C Time series Applying Land Cover Type 166 for the Heatwave 2018.

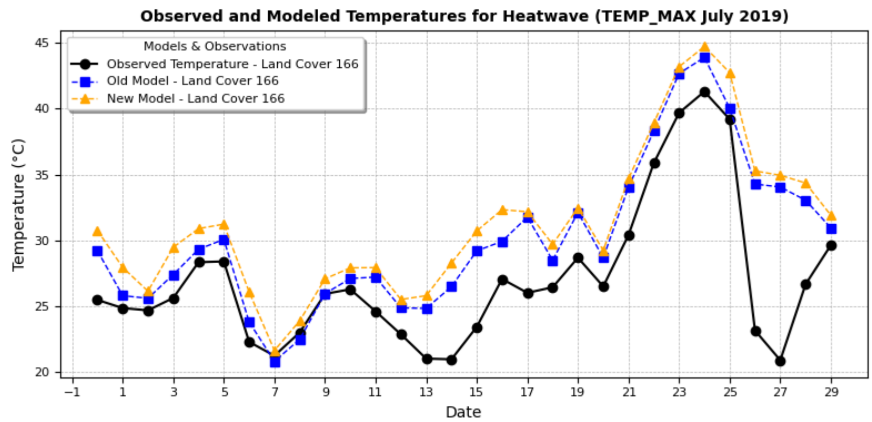


**Figure A.8:** Maximum Temperatures °C Time series Applying Land Cover Type 166 for the Heatwave 2019.

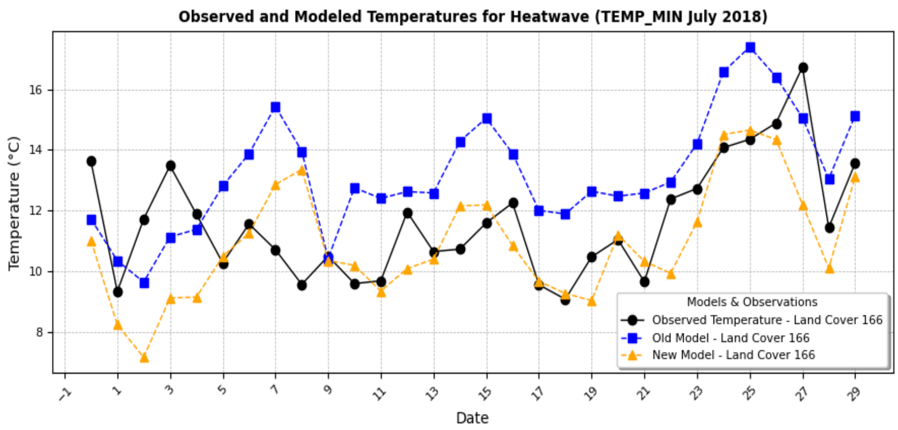


**Figure A.9:** Minimum Temperatures °C Time series Applying Land Cover Type 166 for the Heatwave 2018.

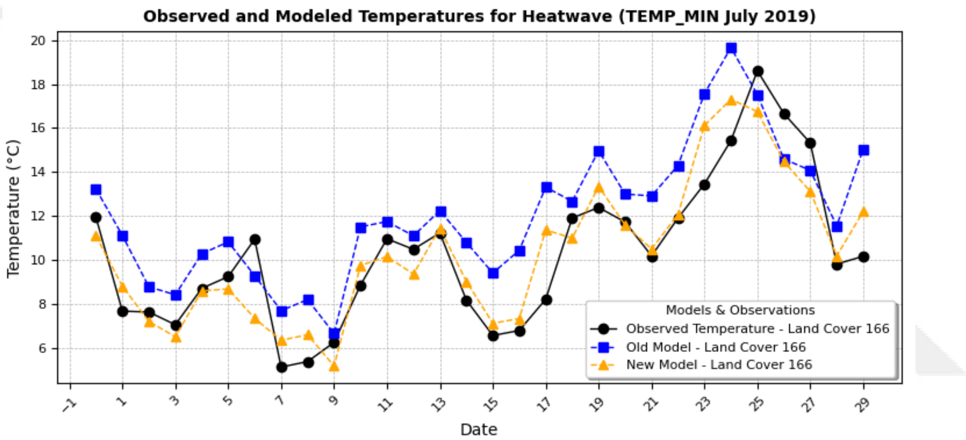


**Figure A.10:** Minimum Temperatures °C Time series Applying Land Cover Type 166 for the Heatwave 2018.

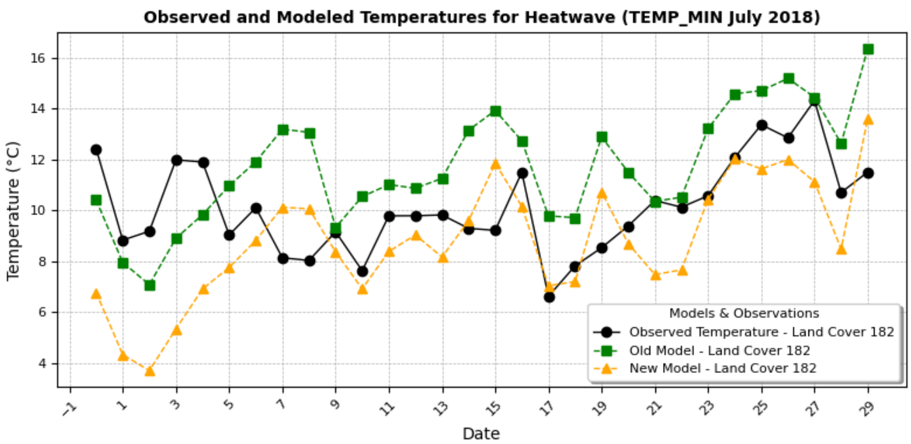


**Figure A.11**: Minimum Temperatures °C Time series Applying Land Cover Type 182 for the Heatwave 2018.

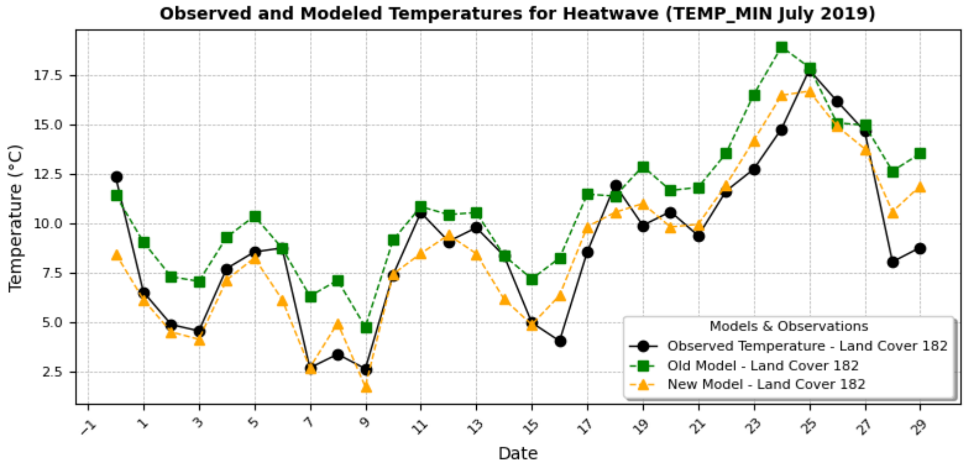


**Figure A.12:** Minimum Temperatures °C Time series Applying Land Cover Type 182 for the Heatwave 2019.

## CURRICULUM VITAE

**NAME SURNAME:** Sajjad Riyadh Shinjar Alghezi

**EDUCATION:**

- **B.Sc.:** 2018, University of Wasit, Faculty of Engineering, Department of Civil Engineering

**OTHER PUBLICATIONS, PRESENTATIONS AND PATENTS:**

- **Alghezi, S**., & Zülfikar**, A.** (2025, May). Seismic hazard assessment of Kahramanmaraş region: Analysis of earthquake sources and probabilistic seismic risk. In Proceedings of the 4th International Graduate Research Symposium (IGRS’25) (pp. 1050–1056). İstanbul Technical University.